1992

Raman, surface-enhanced Raman scattering and infrared studies of phthalocyanines: Thin films and Langmuir-Blodgett monolayers.

Doriano. Battisti
University of Windsor

National Library of Canada
Acquisitions and Bibliographic Services Branch
395 Wellington Street
Ottawa, Ontario
K1A 0N4

Bibliothèque nationale du Canada
Direction des acquisitions et des services bibliographiques
395, rue Wellington
Ottawa (Ontario)
K1A 0N4

Your file Votre référence

Our file Notre référence

NOTICE

The quality of this microform is heavily dependent upon the quality of the original thesis submitted for microfilming. Every effort has been made to ensure the highest quality of reproduction possible.

If pages are missing, contact the university which granted the degree.

Some pages may have indistinct print especially if the original pages were typed with a poor typewriter ribbon or if the university sent us an inferior photocopy.

AVIS

La qualité de cette microforme dépend grandement de la qualité de la thèse soumise au microfilmage. Nous avons tout fait pour assurer une qualité supérieure de reproduction.

S'il manque des pages, veuillez communiquer avec l'université qui a conféré le grade.

La qualité d'impression de certaines pages peut laisser à désirer, surtout si les pages originales ont été dactylographiées à l'aide d'un ruban usé ou si l'université nous a fait parvenir une photocopie de qualité inférieure.

Canada

Raman, Surface Enhanced Raman Scattering and Infrared Studies of Phthalocyanines: Thin Films and Langmuir-Blodgett Monolayers

BY

DORIANO BATTISTI

A Dissertation

Submitted to the Faculty of Graduate Studies through the Department of Chemistry and Biochemistry in partial fulfillment of the requirements for the Degree of Doctor of Philosophy at The University of Windsor

1992

ISBN 0-315-78861-5

Canada

ABSTRACT

Raman scattering of thin films, and surface enhanced {resonance} Raman scattering(SE{R}RS), mostly of Langmuir-Blodgett(LB) monolayers are interpreted for various phthalocyanine derivatives. SERS and SERRS are reported for phthalocyanines transferred to silver and gold island films and silver coated tin spheres. The Raman data were complemented with the infrared(IR) data and the vibrational assignment of the phthalocyanine was attempted. The Raman spectra of vanadyl phthalocyanine sublimed as an ultra thin film onto reflecting surfaces are reported. Energy transfer and enhanced absorption was observed in a two component system composed of one LB of a perylene derivative and one LB of zinc tetra-*tert*-butylphthalocyanine. The LB technique was applied to control the coverage on the surface in the investigation of SERRS of vanadyl tetra-*tert*-butylphthalocyanine and surface coverage dependence. SERRS, IR, ultraviolet-visible(uv-vis) spectroscopy were used to characterize stable green and blue forms of lanthanide bisphthalocyanine complexes. SERRS was applied to investigate the interaction of nitrogen dioxide and one LB of metal-free tetra-*tert*-butylphthalocyanine, copper tetra-*tert*-butylphthalocyanine and ytterbium(and lutetium) bisphthalocyanines. UV-VIS spectroscopy was also valuable in the investigation of nitrogen dioxide and the phthalocyanine derivatives.

DEDICATION

To my wife Carmela, our parents and our brothers

ACKNOWLEDGEMENTS

During the course of almost five years it becomes very easy to realize that there was good will from many people. The excellent supervision and encouragement from Dr. R. Aroca led to interesting and dedicated work. His weekly group meetings kept us sharp and "up with the times". I am also grateful to my labmates past and present(C. A. Jennings, K. Akers, F. Martin, U. Guhathakurta, Dr. E. Clavijo, E. Johnson, and J. Souto). They have always provided a good working relationship and challenging discussions. I would also like to express my thanks to our collaborators. They include Drs. G. J. Kovacs, Dr. A. M. Hor, Dr. R. O. Loutfy at the Xerox Research Centre of Canada, Drs. T. Tomilova and E. Luk'yanets at the Organic Intermediate and Dyes Institute, Moscow, and Dr. A. Tsivadze at the Institute of General and Inorganic Chemistry Academy of Science, Moscow. The technical staff at the University of Windsor is also acknowledged. They include Mr. M. Fuerth and Mr. J. Olsen from the Department of Chemistry and Biochemistry, Mr. J. Robinson form the Department of Mechanical Engineering and Mr. W. Grewe from the Department of Physics.

Finally I would like to thank my "human catalysts", Carmela for her constant support and understanding, and our parents (Ferruccio, Maria, Angelo) and brothers (Roberto, Alessandro, Carlo).

TABLE OF CONTENTS

LIST OF TABLES

LIST OF FIGURES

LIST OF ABREVIATIONS

A	depolarization factor
Ag-Sn spheres	Silver coated tin spheres
bend	bending
CCD	charge coupled device
CuPc	copper phthalocyanine
CuPcTTb	copper terta-*tert*-butylphthalocyanine
d	metal molecule separation
def.	deformation
EPR	electron paramagnetic resonance
E_{op}	electric field of P-polarized light
E_{os}	electric field of S-polarized light
ϵ	dielectric constant of metal
ϵ_o	dielectric constant of medium
FT	Fourier Transform
FTIR	Fourier Transform Infrared
H_2Pc	metal free phthalocyanine
$HoPc'_2$	holmium octa-*tert*-butylbisphthalocyanine
IR	infrared
LB	Langmuir-Blodgett
LL	laser line
Ln	lanthanide

$LnPc_2$	lanthanide bisphthalocyanine
$LnPc^t_2$	octa-*tert*-butlybisphthalocyanine of lanthanide element
$LuPc_2$	lutetium bisphthalocyanine
$LuPc^t_2$	lutetium octa-*tert*-butylbisphthalocyanine
m	medium intensity
ML	monolayer
N_o	number of molecules spread on subphase
$NdPc^t_2$	neodymium octa-*tert*-butylbisphthalocyanine
NOX	$[2NO_2\ (gas) \leftrightarrow N_2O_4\ (gas)]$
NO_2	nitrogen dioxide gas
MPc	metallated phthalocyanine
PBDC	N'octyl,N-isobutyl-3,4:9,10-perylene-bisdicarboximide
Pc	phthalocyanine ligand
P-polarization	electric field parallel to the plane of incidence
PP	P-polarized incident field, and P-polarized scattered field
PS	P-polarized incident field, and S-polarized scattered field
PT	P-polarized incident field, and total scattered collection
r	radius of metal particle
r_s, r_p	Fresnel coefficient for S-polarized and P-polarized light
RS	Raman spectrum
RRS	resonance Raman spectrum
s	strong intensity

SEM	scaning electron microscopy
SCE	standard calomel electrode
SERS	surface enhanced Raman scattering
SERRS	surface enhanced resonance Raman sacttering
S-polarization	electric field perpendicular to the plane of incidence
SP	S-polarized incident field, and P-polarized scattered field
SS	S-polarized incident field, and S-polarized scattered field
ST	S-polarized incident field, and total sacattered collection
sh	shoulder
SP	surface plasmon
t-butyl	*tert*-butyl
tb	*tert*-butyl
TEM	transmission electron microscopy
uv-vis	ultraviolet-visible
v	very
VOPc	vanadyl phthalocyanine
VOPcTTb	vanadyl tetra-*tert*-butylphthalocyanine
w	weak intensity
$YbPc_2$	ytterbium bisphthalocyanine
ZnPcTTb	zinc tetra-*tert*-butylphthalocyanine
λ	wavelength
Φ	angle of incidence

CHAPTER 1: Introduction

The intention of this chapter is to provide a general introduction regarding the molecular structure, the properties, and the potential applications of a class of organic molecules known as phthalocyanines(Pcs). They are unique molecules that find their place in many areas of science. Their origin begins in the synthetic laboratory and their science becomes enriched by the study of their structural and physical properties. Notably, the Pc structure resembles that of haemoglobin and chlorophyll.

Phthalocyanine Discovery

The name phthalocyanine, from the Greek naphtha (rock-oil) and cyanide(dark blue) and its structure, was first proposed by Linstead and his students in 1933-1934.[1-4] They synthesized a new class of highly coloured and unusually stable organic compounds. Metallated phthalocyanines(MPc) were first produced in the reaction of heating o-cyanobenzamide or phthalonitrile with iron, copper, magnesium and other metals. The metal free phthalocyanine or di hydrogen phthalocyanine(H_2Pc) was however first identified in 1907 as a product in the preparation of o-cyanobenzamide from phthalamide and acetic acid.[5] The first X-Ray crystal studies by Roberston on nickel phthalocyanine, copper phthalocyanine(CuPc) and platinum phthalocyanine showed that the metal and the four isoindole groups were contained in one plane.[6-9] In air, most Pcs are extremely stable and begin to show signs of degradation at temperatures of 400-500 °C. In vacuum, temperatures in excess of 900 °C are required to decompose Pc[10]. The high stability of Pc towards light/heat, acid/alkalies is attributed to the coordination of the metal with the four pyrrole nitrogen atoms and

the conjugated π system.

Applications of Phthalocyanine

Pcs are insoluble in water and organic solvents. This makes them suitable for commercial applications in areas such as electrophotography, dyes, and xerography. In 1987 it was estimated that 16 million pounds of Pc blue toner and two million pounds of green toner were produced in the United States at a commercial value of about ten dollars per pound[11]. Phthalocyanines have also been used as stains in histology[12]. The lack of toxicity in Pcs has extended their use as dyes in food colouring, contact lenses and polypropylene sutures. Thin films of H_2Pc are stable against moderate temperatures, oxidation, humidity and were reported as "write-once" media for optical data storage.[13] Vanadyl phthalocyanine was also reported as a potential candidate for optical data recording.[14]

Pc, like many organic pigments, has a small band gap. They have been fabricated into photovoltaic devices where a Pc thin film is commonly sandwiched between two dissimilar electrodes. In the photovoltaic effect light is absorbed by the organic layer, which leads to exciton creation and dissociation at the surface and eventually to charge separation and transport.[15] The photovoltaic activity in Pc devices has led to potential Pc based solar cells.[16-21] The photoactivity was influenced by the molecular organization within the film. For example, the crystalline phase of vanadyl *tert*-butylphthalocyanine, denoted as phase(II), was more effective in photogeneration than phase(I), which was classified as polycrystalline.[20] Along the same context, sublimed films of titanyl phthalocyanine showed two distinct phases.

Those films with an absorption at 820 nm were better photoconductors than those with the absorption band centred at 720 nm.[21]

Investigations in Pcs as catalysts for the reduction of molecular oxygen to water have also been reported.[22] The reaction was highly exothermic and could apply to fuel cells. Cobalt tetrasulfophthalocyanine chemically bound to a titanium dioxide surface has been reported to show photocatalytic activity.[23] In the latter work, excitation at 366 nm (in the bandgap of titanium) produced hydrogen peroxide in an oxygen saturated solution and hydrogen peroxide depletion in the absence of oxygen. Electroanalytical studies on chemically modified carbon electrodes of cobalt phthalocyanine showed sensitive limits to the detection of sugars(1-5 nmol), oxalic acid(0.3 pmol), and various α-keto acids(< 1 nmol).[24,25]

A recent interest in Pc is in their use as chemical sensors for gases. Chapter 7 is devoted to this area, and our results on the chemical interaction of nitrogen dioxide and various Pc will be presented in that section.

Three books have been written about Pcs which cite the journal and patent literature.[11,26,27] Recently, another book was published which extensively accounts for the properties and applications of Pc.[28] The monographs in the latest book are detailed, and suggest that the science of Pc has not been exhausted.

Molecular Phthalocyanine Structure

In Figure 1 the structures of H_2Pc and MPc are presented where the basic Pc unit consists of four isoindole groups joined by meso-bridged nitrogen atoms. The aromatic core or macrocycle is composed of 18 π electrons which leads to intense

Figure 1.1 Molecular structure of metal free phthalocyanine(H_2Pc) and metal(M) coordinated phthalocyanine(MPc). The pyrrole nitrogen(1), and meso-bridged nitrogen(2) are also depicted.

H_2Pc

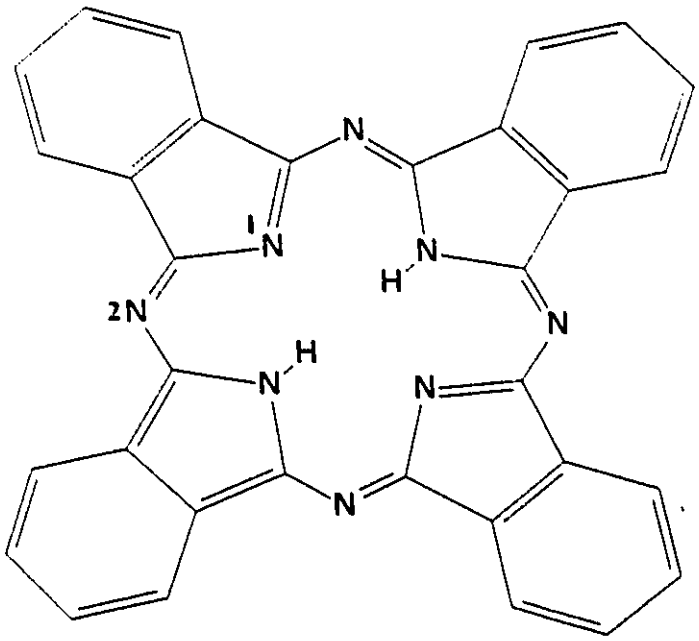

MPc

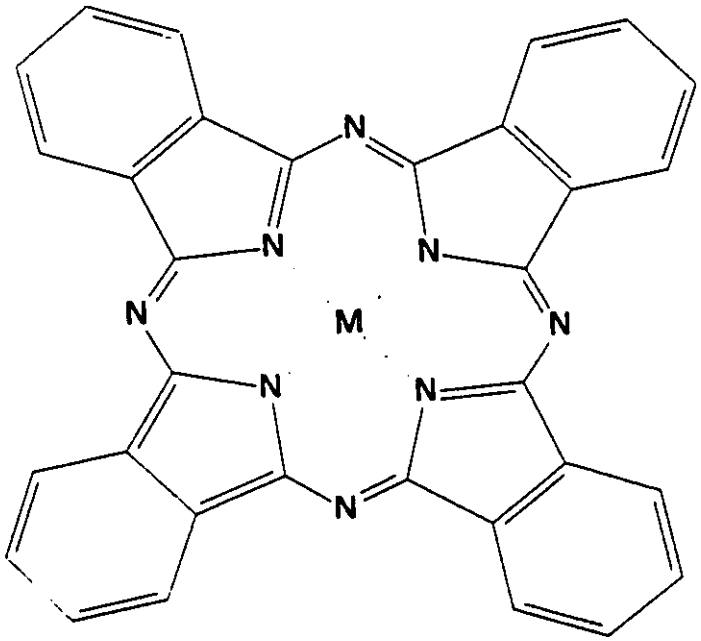

Figure 1.1

absorption. A molar absorptivity in the order of 10^5 ($Lcm^{-1}mol^{-1}$) is typical for Pc in the red region of the visible absorption spectrum. Substitution on the benzene rings of Pc leads to substituted phthalocyanines and the organic synthesis of these complexes has been reviewed by Leznoff.[29] The metal and the interaction of the π system with the substituents on the benzene rings are significant in Pc redox chemistry. For example,in octacyanophthalocyanine complexes of Zn and Cu, the electron withdrawing cyano groups reduce the electron density on the ligand.[30] At present, seventy-six different metals form complexes with Pc. They include Group 1-15, transition elements and all the members in the lanthanide and actinide blocks.[11]

Crystallographic data for most metal phthalocyanines reveal that the macrocycle is planar and that the bond between the carbon and pyrrole nitrogen is larger by (about 0.038 Å in the **6** form of CuPc) than the bond formed between the carbon and meso-bridging nitrogen atom. For CuPc in the **6**-phase the mean displacement of the carbon and nitrogen atoms is 0.03 Å above or below the macrocycle. The metal in CuPc is bonded to all four pyrrole nitrogen with a mean bond length of 1.935 Å.[31] The average C-N bond length is 1.347 Å, which gives a bond order of ca. 1.5 and supports the extensive π conjugation in the central macrocycle.[31] The cavity formed by the four isoindole nitrogen atoms is approximately a square with a length of 2.7 Å. In D_{4h} complexes of Pc[i.e., MPc(M=Cu, Zn, Fe)], the metal is symmetrically positioned inside the cavity. Cations of Pb and Sn are, however, too large to fit into the cavity. They form four coordinated complexes with C_{4v} molecular symmetry.[32] In passing, it is also

interesting to note that the electrical conductivity in crystals of triclinic PbPc and monoclinic PbPc differed by eight orders of magnitude.[33] Five coordinate square pyramidal complexes have also been observed in such molecules as chlorogallium phthalocyanine(ClGaPc), and chloroaluminium phthalocyanine.[34] In these complexes, the Group III element was coordinated to the four pyrrole nitrogen and to the chlorine atom. In the square pyramidal complex of vanadyl phthalocyanine(VOPc) the VO^{2+} cation sits 0.575 Å above the ring and vanadium is coordinated to the pyrrole nitrogens.[35] Six coordinated tetragonal complexes have been synthesized. These include molecules like $SnPcCl_2$ [36] and $PcCo(picoline)_2$ [37]. The planarity of the macrocycle is destroyed in molecules that show seven and eightfold coordination. In the superphthalocyanine(SPc) as in $SPcUO_2$ there are five isoindole groups joined by meso bridged nitrogen atoms, and the entire macrocycle is distorted from planarity due to the large angle strain within the molecule.[38] The coordination geometry for the uranium atom approximates a pentagonal bipyramid. Bisphthalocyanines have been documented. In these structures, the metal cation is eightfold coordinated to two Pc rings. X-ray crystal data for bis(phthalocyanato)tin(IV)[39], bis(phthalocyanato)uranium(IV)[40], and bis(phthalocyanato)neodymium(III)[41] show that the rings are rotated approximately 45° with respect to one another. The separation between the two rings is about 2.8 Å. All of the lanthanide elements form dimeric phthalocyanine complexes and further discussion is presented in Chapter 6 where our optical spectroscopic data are presented.

Polymorphs of Phthalocyanine

Another well known structural property of Pc in the solid state is polymorphism. It results from the different stacking of the molecules along a certain direction. Polymorphs also have unique physical properties as observed in the different electrical conductivities of triclinic and monoclinic PbPc.[33] It is known that Pcs form columnar stacks with the macrocyle inclined to the axis of the stack. For example, the normal on the Pc molecule forms an angle with the b axis of the crystal of 26.5° and 45.8° in the α and the δ form of CuPc respectively.[31,42]

The polymorphic form is dependent on the method of preparation. The α-form is normally produced by dissolving the Pc complex in concentrated sulfuric acid and precipitating it out with a large amount of cold water.[43] A pressure dependent phase change was reported for thin films of CuPc[43], where the α-form was produced at sublimation pressures up to 13.3 Pa, while the δ-phase required higher sublimation pressure. Polymorphs of Pc also give different X-ray diffraction patterns, infrared(IR) and visible absorption spectra. Their solution spectra are, however, identical.

In high vacuum(10^{-7} -10^{-8} Pa), the α-form is produced for thin films of MPc prepared at room temperature.[44] Conversion from $\alpha \rightarrow \delta$ form required heating to temperatures of 300 °C. Mindorff et al. reported that annealing the α form of H_2Pc to produce the δ form was, however, irreversible.[45] Vapours of alcohol can also produce the $\alpha \rightarrow \delta$ transformation in ZnPc.[46] Sidorov and Kotlyar observed new IR bands at 780, 877, 1100 and 1173 cm^{-1} in the spectra of the δ-form of MPc.[47]

Spectral characterization of α, β, χ(produced by milling the α-form) polymorphs of H_2Pc showed distinct differences in the visible, near-infrared and infrared spectra.[48] Changes in the infrared were observed in the 700-800 cm^{-1} and in the N-H region. The red shift in the N-H stretching frequency observed only in the β form was attributed to intermolecular hydrogen bonding which could weaken the N-H stretching bond.

Electronic Spectra of Phthalocyanine

A recent overview of the optical properties of Pc has been published by Stillman and Nyokong.[49] The absorption spectra of Pc derivatives have received considerable attention. The vapour absorption or "unperturbed" spectra in a series of MPc contained 5 characteristic bands denoted as: Q(ca.660 nm), B(ca.320 nm), N(ca. 275 nm), L(ca. 245 nm) and C(ca. 210nm).[50] The N, L, and C bands are not always resolved in the solution spectra. The Q and B(or Soret) bands are the main absorption bands in Pc and arise from as π-π^* ($a_{1u}\rightarrow e_g$ in D_{4h}) and π-π^*($a_{2u}\rightarrow e_g$ in D_{4h}) transitions respectively. The energy diagram for CuPc(D_{4h} point symmetry) is shown in Figure 1.2. Their assignment is mostly based on the theoretical and experimental work by Gouterman and coworkers.[52,53] In D_{4h}, the a_{1u} is the highest occupied molecular orbital(HOMO) and the e_g is the lowest unoccupied molecular orbital(LUMO).

They classify the absorption spectra of Pc derivatives to one of five groups. The first type of spectrum is denoted to the distinct absorption features seen in metal free phthalocyanine(D_{2h}) or its derivatives. For these Pcs, the Q-band is seen as two intense bands(Q_x and Q_y). The two weaker absorptions which are also observed in the

Figure 1.2 Molecular orbitals of CuPc. Taken from Reference 51.

Energy Diagram of CuPc

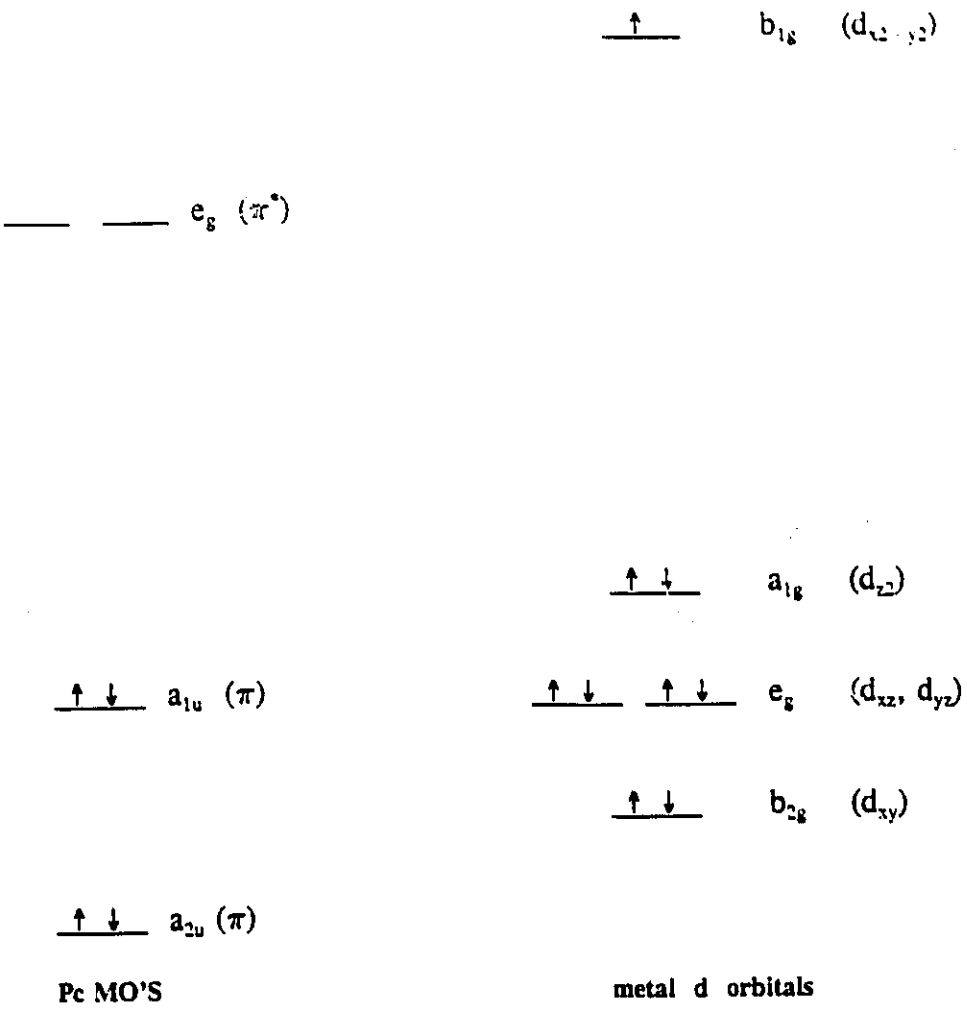

Figure 1.2

Q-band envelope were considered as vibrational overtones of the Q_x and Q_y.[54] The two component Q band is attributed to the lower symmetry in D_{2h}, i.e., to the splitting of the degenerate e_g when the symmetry is lowered from $D_{4h} \rightarrow D_{2h}$. Distinct transition moments were observed by Lyons et al. in the polarized absorption spectrum of H_2Pc crystals.[55] Deprotonation in metal free phthalocyanine gives an absorption spectrum similar to that found in Pc complexes of D_{4h} symmetry.

The second type of absorption spectra is given to Pc complexes with D_{4h} symmetry in which only π-π^*(B, and Q bands) are observed. The spectra may contain a weak vibronic band{Q(0,1)} at the high energy end of the Q band.[50] The third type of spectra contains an additional band(assigned to a charge transfer transition) in between the Soret and Q-band. As an example, reduction of CoPc with borohydride gave a new band at 467 nm, which was assigned to a metal-ligand charge transfer band based on the magnetic circular dichroism spectrum.[56] The fourth type of spectra is assigned to Pc complexes that show dimerization or higher order associations in solution.

This phenomenon is characterized by a new band appearing near the high energy side of the Q-band as the dye concentration is increased. Aggregation can be diminished in solvents that give better dye solubility since greater solvation of the monomer would reduce the dye-dye interactions. Alternatively, solvents with high dielectric constants were reported to reduce the dye-dye interaction. For example the dimerization constant of 4,4',4'',4'''-tetraoctadecylsulfonamidopthalocyaninecopper(II)(CuPc-X_4) in benzene was smaller

than in carbon tetrachloride,[57] and the dimerization constant of CuPc-X_4 was lower in tetrahydrofuran than in benzene.[58] The degree of association was also shown to be dependent on the metal cation(M=Mg, Co, Zn, Bi, Cu, Ni, Pd, Pt) in a series of tetrakis(cumylphenoxy)-phthalocyanine complexes.[59]

In dimeric silicon phthalocyanine, the Q and B bands are blue shifted with respect to the monomer.[60] The shift in the electronic bands was attributed to the exchange interaction(or exciton coupling) of the transition moment of one ring with the transition moment on the other ring. In the dipole approximation, the coupling is proportional to the dot product of the transition moments of the two chromophores and inversely proportional to the cube of the separation distance.[61] For *translational equivalent* molecules, the exciton theory predicts a displacement of the absorption band relative to that of the free molecule. A blue-shifted and a red shifted band are expected for parallel and in-line transition moments respectively.[62] For *translational inequivalent* molecules exciton coupling leads to a splitting of the optical transition, known as Davydov splitting. The magnitude of the splitting is a measure of the interaction energy. For molecules with molar extinction coefficients larger than 10^4($Lcm^{-1}mol^{-1}$) Davydov splitting in the order of 10^3-10^6 cm^{-1} may be expected and may account for band broadening, especially in the solid state.[61] Lever et al. have reported exciton splitting of the order of 2300 cm^{-1} in metal free binuclear phthalocyanines.[54]

The last type of absorption spectra pertains to Pc in the solid state, where the normally narrow absorption bands in the solution spectra are seen as broad bands.

Davidson noted that in MPc(M= H_2, Mg, Fe, Co, Cu, Zn), prepared as thin solid films, the splitting and broadening of both Q and Soret bands could be attributed to a vibronic effect; however, Davydov splitting was not ruled out.[63] This report also showed that the N band was the most sensitive to metal substitution. Thin film preparation also has been reported to affect the spectral position and shape of the Q Band. For example, in thin films of ClGaPc, the prismatic block phase was grown under slow rates of evaporation and the platelet block phase was formed at higher evaporation rates.[64]

Outline of Thesis

The work that remains is divided into chapters. Chapter 2 describes the experimental techniques and the instrumentation used to prepare Pc into thin solid films and Langmuir-Blodgett(LB) films. In this thesis, normal Raman scattering, surface enhanced Raman scattering(SERS), infrared, and ultraviolet-visible spectra were used to characterize Pc molecules. The majority of the work was related to the characterization of phthalocyanine LB films using SERS. A small review of SERS theory is given in Chapter 3. It accounts for the enhancing properties of the SERS substrate. Chapter 4 begins with a review of the Raman spectra of Pc. The vibrational characterization is presented for vanadyl phthalocyanine thin films adsorbed onto a halide crystal and reflecting substrates. Infrared and SERS data for vanadyl tetra-*tert*-butylphthalocyanine and zinc tetra-*tert*-butylphthalocyanine is also discussed in Chapter 4. The chapter closes with the observation of energy transfer between one LB monolayer of a perylene derivative and one LB layer of a

phthalocyanine complex transferred to a SERS substrate. The effect of surface coverage on surface enhanced resonance Raman scattering of vanadyl tetra-*tert*-butylphthalocyanine is addressed in chapter 5. Here the LB technique was used to control surface coverage. Chapter 6 is dedicated to the vibrational characterization and electronic spectra of the blue and the green forms of rare earth bisphthalocyanines. An application of SERS is described in Chapter 7, where the high sensitivity of SERS was used to monitor the reversible adsorption of nitrogen dioxide on a single monolayer of various Pc derivatives. The general conclusions of this thesis follow in Chapter 7.

CHAPTER 2: Instrumentation and Experimental Techniques

Vacuum Evaporator Apparatus

Thin solid films of Pc, substrates for Surface Enhanced Raman Scattering (SERS), and smooth metal films were prepared in traditional and "in house built" vacuum evaporation systems[1,2] composed of some factory purchased electronic components. The commercial components used to monitor pressure include Balzers IKR 020 cold cathode gauge, Balzers TPR 010 Parani gauge, and Balzer pressure gauge control. The power source used to control the current to the boat for resistive heating was the Balzers BSV 080 glow discharge/evaporation control unit. Edwards E2M2/E2M5 rotary vacuum pumps and an Edwards diffusion pump were employed to obtain high vacuum. Film thickness and the rate of evaporation were monitored by an Inficon XTC single film monitor/controller with a standard 6 MHz gold coated quartz sensor. Film thickness is reported as mass thickness.

The basic working principle behind the apparatus was to convert the material to the gaseous phase by supplying heat of vaporization, and to control the rate at which the gaseous atoms or molecules condense onto the substrate. In the high vacuum regime(10^{-4}-10^{-3} Pa), the mean free path of particles was large enough to ensure that the evaporant moved to the substrate. High vacuum also reduced the possibility of contamination to the substrate by residual gases. The rate of evaporation and the thickness of the film were carefully monitored in order to reproduce the desired film. These parameters were important to duplicate the SERS substrates with a near constant plasmon absorption profile. For metal films the rate of

evaporation was easily controlled ca. ±0.1 nm/s. The rate of sublimation for Pc molecules was however more difficult. Even after degassing for 10-15 minutes, the best controllable rate was ca. ±0.5 nm/s for Pc derivatives. Thin films of Pc and metal films were prepared in separate systems to avoid contamination to the SERS substrates.

The main components in the evaporator are illustrated in Figure 2.1. The baffle(b) valve separated the working chamber from the high vacuum compartment. The high vacuum chamber was composed of a liquid nitrogen cold trap(6) and a diffusion pump(7) with Santovacs 5 diffusion pump oil. Valves(V) were used to isolate and evacuate the working and high vacuum chambers. The pressure gauge control module recorded the pressure at gauges P_1(Parani) and P_2(cold cathode). In our evaporator, high vacuum of $2x10^{-4}$ Pa was obtained within one hour of operation. The sample holder(1) was a modified heater that was attached to the top flange of the evaporator. A VARIAC was used to control the voltage to the heater(maximum temperature 250 °C) when the substrate was to be heated. A type K(NiCr-NiAl) thermocouple was positioned permanently within the heater and near the surface of the substrate. It was used to record the temperature at the substrate. The manually operated shutter(3) masked the substrate from the evaporant but not the crystal oscillator(2). This arrangement allowed the control of the rate of film growth before opening the shutter and depositing the material on the substrate. A boat(4) was used to contain the material that was to be deposited as a film. It was fastened to a set of electrodes(5) or posts. The posts were also connected by a set of cables to the high

Figure 2.1 Schematic of vacuum evaporator

substrate holder(1), crystal oscillator sensor(2), shutter(3), boat(4), posts(5), cold trap(6), diffusion pump(7), baffle valve(b) valves(V), Parani vacuum gauge(P_1), cold cathode gauge(P_2)

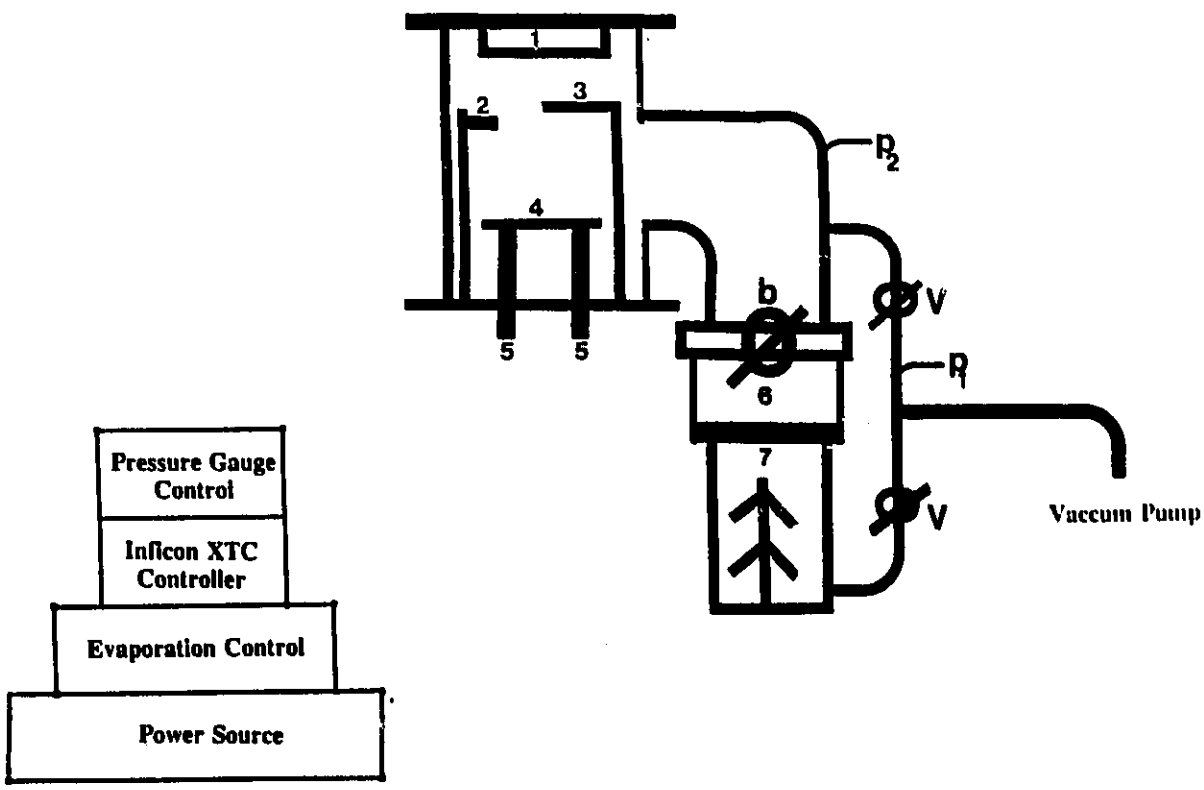
1
2
3
4
5
5
b
6
7
V
V
Vaccum Pump
Pressure Gauge Control
Inficon XTC Controller
Evaporation Control
Power Source

Figure 2.1

power source or transformer, which delivered current to the boat for resistive heating. The transformer delivered high current by stepping down the voltage (4, 8, or 16V) in the secondary. The rate of evaporation/sublimation was controlled by adjusting the amount of current that flowed through the boat. In the preparation of metal films, the XTC Inficon controller was programmed with the constants provided by the manufacturer. In the fabrication of organic thin films of Pc a Z-ratio of unity, and a sample density of 1.5 gcm^{-3} were selected.

Calibration of film thickness was periodically checked by the procedure outlined in the XTC Technical Manual. The film thickness calibration correction would be in terms of the tooling factor which required the determination of film thickness by an alternative method. In our case, thick films of Ag(ca. 150 nm) or Au were sent to the Xerox Research Centre of Canada where the thickness was determined by the stylus method.

All boats used in the vacuum evaporation apparatus were purchased from R. D. Mathis Company(Long Beach California). Tantalum boats(ME10-.005 Ta) were used for the sublimation of Pc materials. In evaporation of silver and tin, tantalum boats(S9A-.005 Ta) were utilized; however evaporation of gold required tungsten boats(S9A-.005 W). Both silver and tin shots (99.999% purity) were obtained from Johnson and Matthey Aesar Group(Toronto). A gold(99.99%) rod was purchased from Aldrich. These metals were used in the preparation of SERS substrates and smooth metal films.

Thin films of Pc were formed onto Corning 7059 glass slides and halide

crystals suitable for transmission infrared spectroscopy. The glass substrates were used as supplied by Corning(Danville, Virginia). Thin solid films of phthalocyanine were made from i) VOPc, tetra-*tert*-butylPcM(M=VO, Zn),$LnPc_2$(Ln=Yb, Lu) and ii) $LnPc_2$(Ln= Pr, Nd, Sm, Eu, Gd, Tb, Dy Ho, Er, Tm). Samples denoted i) were supplied by Dr. Kovacs, and Dr. R. O. Loutfy from the Xerox Research Centre of Canada. Those designated ii) were supplied by Dr. A. Y., Tsivadze at the Institute of General and Inorganic Chemistry Academy of Science, Moscow.

Langmuir Trough and Langmuir-Blodgett Films

Introduction

Irving Langmuir is mostly credited for the work on insoluble monomolecular films at the liquid-gas interface. Among other findings, he showed that the cross sectional area(.21-.25 nm^2) of palmitic acid, stearic acid and cerotic acid were very similar regardless of the length of the hydrocarbon chain.[3] His findings confirmed that a monomolecular film was formed on the subphase and that the carboxyl groups were in contact with the subphase, while the hydrocarbon tails were packed vertically above the subphase. Katherine Blodgett, who was Langmuir's coworker, reported the first successful transfer of a monomolecular film of stearic acid and calcium stearate to a glass slide.[4,5] The transfer of the Langmuir monolayer at the liquid-gas interface to a solid support is known as the Langmuir-Blodgett or LB technique.[6-12] A detailed description of Langmuir monolayers and LB films is found in the following sections. A new book devoted to LB films was recently written. It accounts for the renewed interest in the field and includes chapters devoted to monolayer properties and their

molecular structure, LB film deposition, LB characterization and properties, spectroscopy of complex monolayers, multilayers and monolayers of biomolecules, and potential applications of LB films.[13]

Researchers are attracted to LB films because film thickness and molecular orientation can be precisely controlled. For example Kuhn, studied the dependence of energy transfer between acceptor and donor molecules separated by monolayers of arachidic acid of known thickness.[14] Others may have interests in LB forming materials because they can be transferred at near ambient temperature and pressure, unlike the conditions used to form films by evaporation or sublimation. It is believed that size reduction offered by the LB technique could lead to an era of organic supermolecular electronics.[15] Studies on the electrical conductivity in LB films showed that electrical conduction is related to the structure and to the arrangement of molecules.[15] It is expected that ultra thin films of organic molecules should respond more positively to external stimuli than conventional evaporated thin films. For example, diffusion transport in films is thickness dependent and it is remarkably fast at molecular thicknesses.[16] The field of LB films is also interdisciplinary and involves elements of physical chemistry, physics, chemical engineering and material science. As an example, our group has collaborations with industrial and academic institutes of organic chemistry who synthesize Pc and perylene derivatives for possible applications in LB film technology. Our current LB research interests are in the preparation of LB films of phthalocyanine and perylene derivatives, and their optical spectroscopic characterization by surface enhanced Raman scattering. Swalen has reviewed various

other optical techniques that can be used to study LB films.[17,18]

As the number of novel molecules(like Pc) increase in LB technology, further research will be required in the areas of substrate selectivity, interpretation of the isotherm, optimal conditions for good monolayer transfer, and the evaluation of LB structure on the solid support. Some of the latest research in LB films of mostly fatty acids has certainly revealed important results. For example, investigation in LB of cadmium stearate and stearyl alcohol has shown that the transfer ratio was heavily dependent on the contact angle and the surface pressure.[19] Defects with a diameter of 10 nm were observed in cadmium arachidate LB films by the atomic mass microscope.[20] Leisieur et al. have noted that defects might be important for diffusion processes.[21] Another important proposal was that the orientation of docosanoic acid on the subphase was not preserved during transfer to the formvar coated copper grid.[22]

LB Instrumentation

The main components of the LB trough were purchased from Brinkmann Instruments. They include a film balance or Langmuir trough and a central unit that controls the velocity and direction of the moving barrier. The barriers and trough are coated with Teflon. A Lauda Filmlift FL-1 film deposition device is simply a programable stepper motor that allows the substrate to enter and leave smoothly the liquid-gas interface during the transfer of the Langmuir monolayer. The temperature of the subphase was maintained with the Lauda refrigerating model RM6 circulator. In our set up the film balance rests on stone plate placed on the top of a sand filled table(similar to that used to support a micro analytical balance). The heavy table

Figure 2.2 Schematic illustration of the Langmuir film balance and other LB accessories

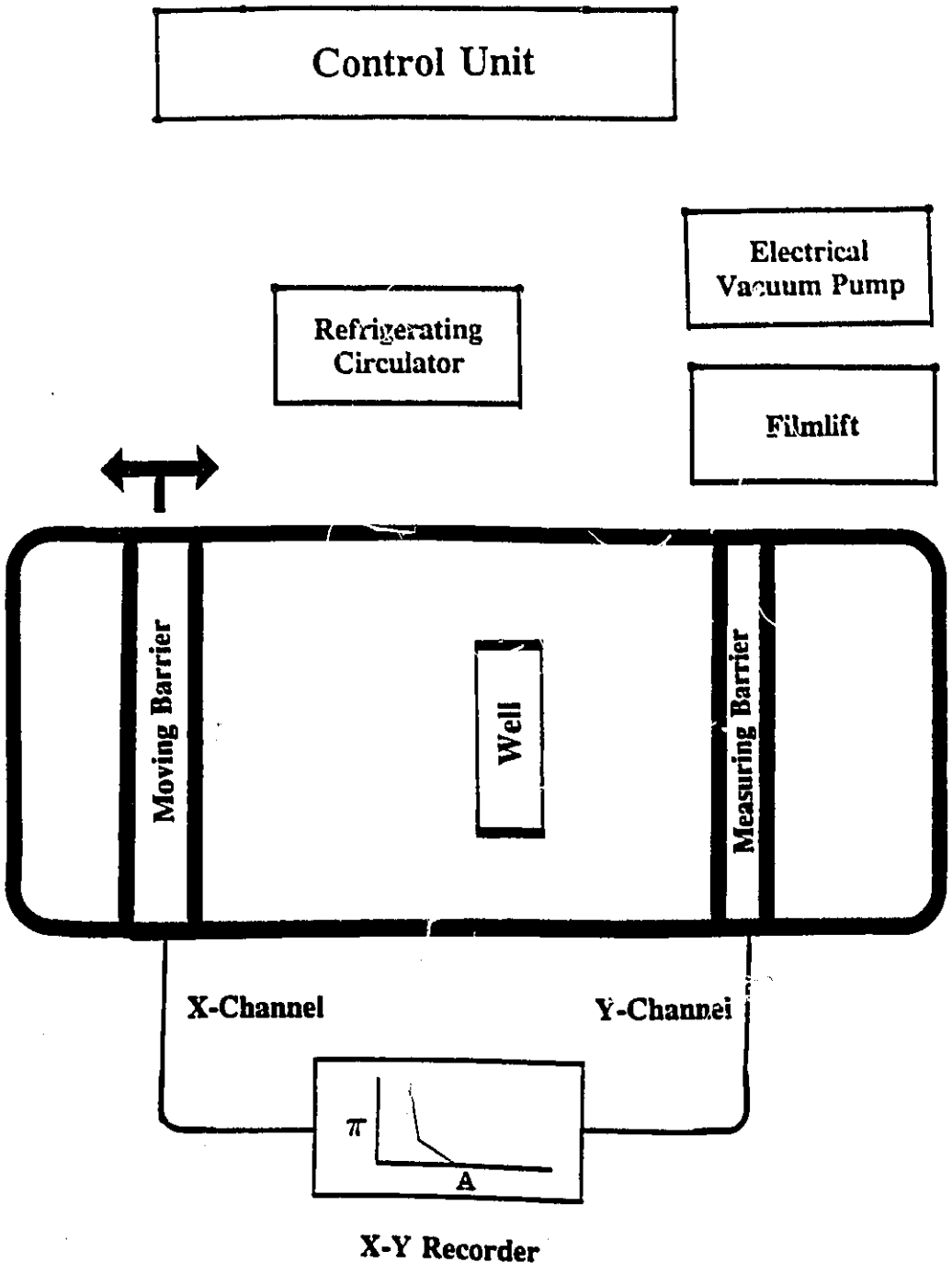
Control Unit
Electrical Vacuum Pump
Refrigerating Circulator
Filmlift
Moving Barrier
Well
Measuring Barrier
X-Channel
Y-Channel
π
A
X-Y Recorder

Figure 2.2

adequately damped the natural vibrations within the room. The entire trough was protected from airborne contaminants by a Plexiglass box. Figure 2.2 illustrates the basic components of the Langmuir-Blodgett trough.

The film balance, control unit, and XY recorder are used to determine experimentally the isotherm of surface pressure(π) versus molecular area(A) of the Langmuir film. The moving barrier can move either towards(compression) or away(expansion) from the fixed barrier. The surface pressure was measured by the electronic displacement transducer on the measuring barrier and fed into the Y channel of the HP 7015B XY recorder. The signal generating the area/molecule was fed into the X channel of the recorder. The Lauda Filmlift FL-1 device was used to secure the substrate and move it up and down through the liquid-gas interface in the region of the well. The substrate was fastened to the magnetic arm of the filmlift by a metallic clip.

Langmuir Monolayers and Langmuir-Blodgett Technique

In the "classical" formation of a Langmuir monolayer, the *amphiphile* is dissolved in a volatile organic solution and a known number of molecules are spread with a syringe onto a aqueous subphase in the region enclosing the moving and the measuring barrier. The amphiphile is a long chain fatty acid which contains a hydrophilic(carboxylic acid) group and a hydrophobic(saturated hydrocarbon) part. The subphase can affect the properties of amphiphile, and the effect can be observed in the isotherm. For example pH, ions, and temperature dependence were observed

in the Π-A measurements of heneicosanic acid[23], behenic acid[24] and pentadecanoic acid[25]. To the right of the measuring barrier the subphase is clean and to the left of the barrier the subphase contains the floating amphiphiles. The molecules are mechanically compressed by advancing the moving barrier towards the measuring barrier. The rate of compression is described by units of (area/number of molecules)/time). The area(in nm^2) and time(in s) quantities are respectively the total area and the time the moving barrier takes to sweep through a designated surface area on the subphase. In our system the moving barrier sweeps through an area of 562 $X10^{14}$ nm^2 during π-A measurements. The measuring barrier records surface pressure(Π) as the difference in surface tension:

$$\Pi = \gamma_o - \gamma \qquad (2.1)$$

where γ_o is the surface tension of the subphase and γ is the surface tension in the presence of the amphiphile.

At the surface pressure of 0 mN/m(milli-Newton $meter^{-1}$) the amphiphiles are independent of each other and their orientation is determined by their interaction with the subphase. At low surface pressure the molecules at the liquid-gas interface may be modelled as a two dimensional gas.[8] As the molecules are compressed together, they form a monomolecular film that passes through phase transitions(i.e., gas→liquid→solid). The liquid phase of fatty acids and phospholipids can be further characterized by liquid-expanded and liquid-condensed phases.[24] Phase transitions in the isotherm are seen as

plateaus at different surface pressures. Fluorescence probes and fluorescence imaging microscopy have been used to study phase behaviour in monolayers.[24] X-ray reflectivity data for a monolayer of arachidic acid on the subphase has shown that as the monolayer was compressed from the liquid→solid phase, the tail of the fatty acid formed a tilt angle(with respect to the surface normal) which varied from 30° to 0°. In the solid phase the tails were all parallel and vertically upwards.[26]

The monolayer can be compressed until the collapse pressure where the molecules in the solid phase are expelled from the two dimensional arrangement and forced into a three dimensional phase. The collapse pressure is revealed in the isotherm when the surface pressure suddenly drops. Transfer of the Langmuir layer to a solid support is made at constant surface pressure well below the collapse pressure.

The last step in the LB technique is the transfer of the monolayer(held at constant surface pressure) from the liquid-gas interface to a solid substrate. A feedback loop between the surface pressure transducer and the moving barrier maintains the monolayer at constant surface pressure. The transfer cycle may begin with the substrate in air or in the subphase. In the latter case the substrate is lowered into the subphase before monolayer spreading and compression. The monolayer is transferred to a substrate by slowly(a few mm/s) raising and lowering the substrate vertically through the liquid-gas interface. The Langmuir layer results in X, Y,or Z deposition. The notation X, and Z are used to describe the transfer of the Langmuir layer during the downstroke and upstroke of the substrate respectively. In Y deposition, the monolayer is deposited as the substrate is lowered into and raised from the subphase. As each monolayer is

Figure 2.3 Schematic of the Langmuir-Blodgett film processes.

Langmuir-Blodgett(LB) Film Making

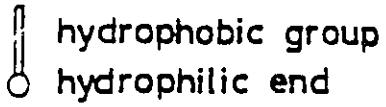

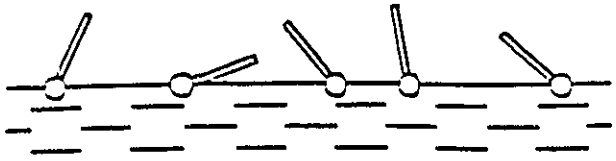

a) Transfer of Molecules to subphase

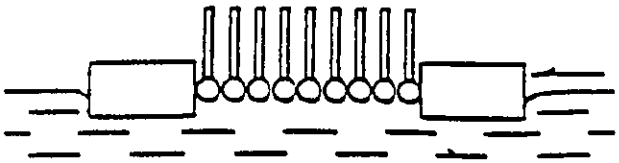

b) Compression of Molecules

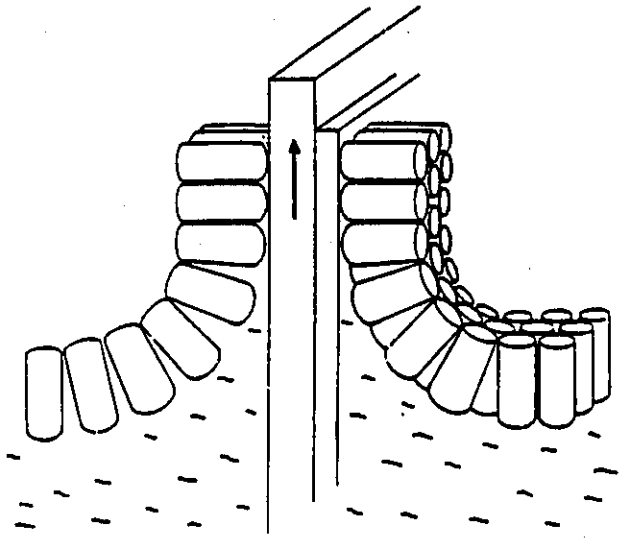

c) LB Film Transfer
(X,Y,Z) Deposition

Figure 2.3

transferred to the substrate the film thickness should increase linearly. This condition can be checked with optical measurements such as ellipsometry, and absorption spectroscopy(UV-Visible, Infrared). Figure 2.3 summarizes the basic steps in LB film making.

Calibration of the Film Balance for Isotherm Data Acquisition

With the trough covered with the subphase, the surface pressure or Y-axis of the isotherm is calibrated by simulating a surface pressure($\Pi = mg/l_{eff}$) along the measuring barrier with a calibration weight of mass(m). The quantity **g** and $\mathbf{l_{eff}}$ refer to the acceleration due to gravity and the effective length of the measuring barrier. In our system, the calibration weight is used to simulate a surface pressure of 37.7 mN/m. The F-scale potentiometer on the control unit is used to bring the signal generated by the calibration weight to 37.7 surface pressure units. Zero surface pressure is manually set by taring the signal of the Y-channel. The surface pressure transducer in the Lauda trough is capable of recording surface pressure in the range of 0-100 mN/m.

The calibration of the area per molecule or X-axis of the isotherm is based on the calibration area of 5.62 $X10^{16}$ nm^2 and 8.64$X10^{16}$ molecules(i.e., A-scale=750). The A-scale is used to enter the number of spread molecules on the subphase. When the moving barrier is in the fully expanded position, the largest area per molecule is 0.65 nm^2/molecule(i.e., 5.62 $x10^{16}$ nm^2/8.64 $x10^{16}$ molecule). The moving barrier does not go to 0 area since it will damage the measuring barrier. The closest distance between the moving barrier and the measuring barrier is 0.5 mm. At this position the area enclosed

between the two barriers is 1.07 x10^{14} nm^2. Based on 8.64 X 10^{16} molecules this area marks .0124 nm^2/molecule(i.e. 0.65 *1.07/562) position. The zero adjustment on the recorder is used to set the .0124 nm^2/molecule mark and the A-corrector potentiometer on the control unit is used to set the 0.65 nm^2 mark. Lauda conveniently supplies isotherm chart paper whose X-axis is divided into 65 scale units. Trough calibration is only required for Π-A measurements.

When the trough is calibrated, a predetermined number of molecules can be spread onto the subphase for isotherm determination. With the moving barrier in the fully expanded position, the number of molecules spread onto the subphase is observed and fed into the A-scale potentiometer. Lauda supplies tables that list the A-scale setting corresponding to the number of molecules delivered to the subphase. Five scales for area/molecule are supplied by Lauda to accommodate small and large molecules. The possible scales(in units of nm^2) are: a) 0→0.26, b) 0→0.65, c) 0→1.625, d) 0→3.25, and e) 0→6.50. In Figure 2.4 the experimental isotherm of arachidic acid is shown. The arachidic acid molecules were spread from a chloroform solution onto the subphase(pH= 5.5) maintained at 20 °C. The three phases are also shown where the gas, liquid and solid states are characterized when the surface pressure is in the region, 0, 0-25, 25-50 mN/m respectively. Extrapolation of solid phase to Π→0 mN/m gave a limiting area of 0.22 nm^2 which corresponds to the cross-sectional area of the carboxylic group. The results and the profile of the isotherm were in excellent agreement with other fatty acids like stearic acid for which a limiting area of 0.22 nm^2 was reported.[27]

Figure 2.4 Surface pressure versus molecular area isotherm for arachidic acid measured in our laboratory.

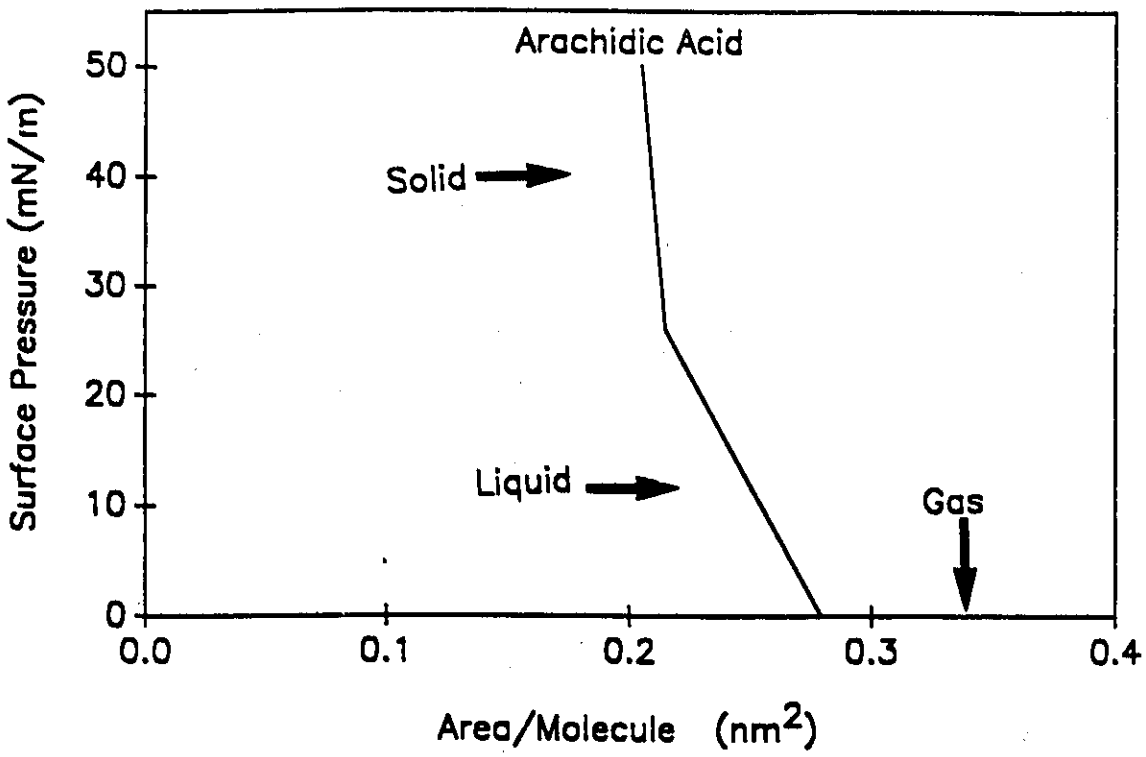
Arachidic Acid
Solid
Liquid
Gas
Surface Pressure (mN/m)
50
40
30
20
10
0
0.0
0.1
0.2
0.3
0.4
Area/Molecule (nm^2)

Figure 2.4

In House Fabrication of Langmuir-Blodgett Monolayers

This section describes the general method and the materials used to form monolayers and their transfer to solid supports.

Materials

Phthalocyanine, and perylene derivates were spread from chloroform, benzene or toluene. The solvents were HPLC grade and obtained from Aldrich. Underivatized Pcs are insoluble in organic solvents and can not be spread onto the subphase. The solubility of tetra-*tert*-butyl substituted phthalocyanines and rare earth bisphthalocyanines is, however, adequate and these molecules were transferred as monolayers and multilayers by the LB technique. In this work LB films and spectroscopic studies of i) tetra-*tert*-butylPcM(M=2H, Zn, VO), $LnPc_2$(Ln=Yb, Lu), N-octyl,N-isobutyl-3,4:9,10-perylene-bis-dicarboximide(PBDC), ii) tetra-*tert*-butylPcM(M=Cu), LnL_2 L=tetra-*tert*-butylPc Ln=(lanthanide element), were considered. Purified compounds designated i)→ii) were supplied by Dr. G. J. Kovacs and Dr. R. O. Loutfy (Xerox Research Centre of Canada), and Dr. E. A. Luk'yanets and Dr. L. Tomilova(Institute of Organic Intermediates and Dyes, Moscow, USSR), respectively. The tetra-*tert*-butylPc derivatives were easily dissolved in organic solvents, and solutions in the concentration range of $2\text{-}3\times10^{-4}$ M were used. The $LnPc_2$ molecules however have limited solubility and solutions of 0.5-1 $\times10^{-4}$ M were prepared by sonication. Arachidic acid was purchased from Aldrich.

Trough Cleaning

The trough was thoroughly cleaned prior to work. The water used to clean the trough was of the same grade as that used in monolayer fabrication. The water was double

distilled(the second distillation was from a Barnstead Sybron unit) and filtered by a Milli-Q Plus(Millipore) portable unit. The resistivity of the water measured by the Milli-Q Plus unit was 18 MΩcm. The pH of the water was 5.5 not adjusted.

The cleaning procedure was extensive and involved wiping the Teflon coated trough with a Kimwipe or lens paper wetted with Aldrich HPLC grade acetone. Contrad 70(Canlab) soap was mixed with cleaning water and poured into the trough. The moving barrier was activated and the soapy solution was forced back and forth to aid in the dissolution of possible contaminants. The cleaning solution was then suctioned off with an electrical vacuum pump. The soap was completely rinsed from the trough by repeating the cycle of adding clean water and removing it with the vacuum pump.

Following cleaning, the subphase was delivered to the trough and the desired subphase temperature($\pm$ 0.5°C) was maintained by the refrigerating circulator unit. Prior to monolayer spreading, the moving barrier was swept from the fully compressed limit to the expanded limit. This mechanical movement was used to clean the liquid-gas interface before spreading the monolayer.

Preparation of Monolayers

The procedure for monolayer spreading and compression was similar for all molecules. The molecules were dissolved in either chloroform, toluene or benzene and a volume of solution was spread with a 0.1 ml Hamilton syringe. The volume of solution was dependent on the molar concentration and the number of molecules that were to be delivered to the subphase. For isotherm acquisition the exact number of molecules was predetermined. The number of molecules spread to form a monolayer to be transferred

as LB film was, however, based on the dimensions of the substrate and the compressibility of the molecule. This was a trial and error process and the goal was to form a monolayer(at constant surface pressure) with enough surface area that would facilitate transfer as an LB film.

The compression rate[($5.62X10^{16}$ nm^2/N_o)/time] during isotherm acquisition was dependent on the number of molecules(N_o) and the time(in s) necessary for the moving barrier to sweep through the area of $562X10^{14}$ nm^2. The time element was dependent of the velocity of the moving barrier. For LB films, the trough was operated in constant surface pressure mode. Here the moving barrier would advance until the desired surface pressure was reached. The monolayer was maintained for approximately 30 minutes at constant surface pressure before it was transferred to the solid support. In all cases the Lauda Filmlift FL-1 device was set to transfer the substrate at a rate of 4.8 mm/min. For LB multilayers a pause time of three minutes elapsed before the substrate passed through the upstroke/downstroke cycle.

Langmuir-Blodgett Substrates

Monolayers were transferred to Corning 7059 glass slides and Surface Enhanced Raman Scattering(SERS) substrates. The Corning slides were cleaned when monolayers were transferred to glass by the method described by Möbius and Bücher.[7] The glass slides were placed in hot chromosulfuric acid maintained at 110 °C. After two hours in the cleaning solution, the slides were copiously rinsed with double distilled Milli Q water and placed in a NaOH(Aldrich) solution(pH 11) for 12 hours. The resulting slides were

Figure 2.5 SERS substrates, SEM of Ag-Sn spheres(A), TEM of 10 nm Ag(B) and 4 nm Au(C)

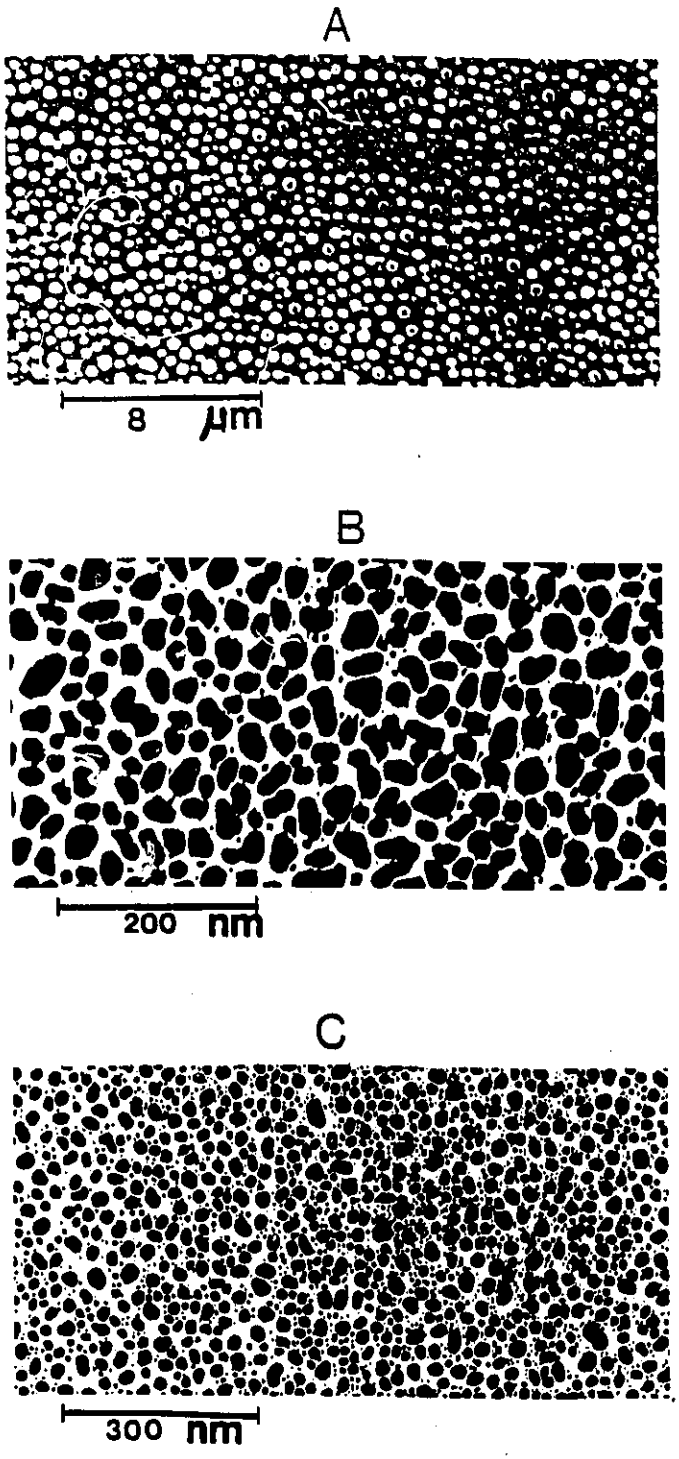

Figure 2.5

hydrophilic. A hydrophobic surface was achieved by further treating the slides in a 5%(w/v) solution of dichlorodimethylsilane(Aldrich) in chloroform for fifteen minutes. These slides were then rinsed in methanol and finally water.

Three different SERS substrates were formed by evaporating high purity metal onto untreated Corning 7059 glass slides. Silver and gold island films were formed by evaporating 10 nm Ag or 4 nm Au at a rate of 0.1 nm/s onto a glass slide maintained at 220 °C. The SERS substrate was allowed to return to room temperature before removing it from the evaporator. The third SERS substrate is designated as silver coated tin spheres(Ag-Sn spheres), and the preparation involved a two step process.[28] In the first step 100 nm of Sn was evaporated at a rate of 0.5 nm/s onto a glass substrate maintained at 120 °C. Murr has shown that Sn formed hemispherical island films when the temperature of the substrate was kept between 81-131 °C.[29] In the second step, the substrate is allowed to cool to room temperature, and 100 nm of Ag is evaporated at a rate of 0.5 nm/s onto the tin spheres.

Surface morphology of the SERS substrates was observed with the electron microscope. Transmission micrographs of Ag and Au islands were recorded on a JEOL CX100 EM operated at 100 KV. These samples were prepared by securing a type-B carbon substrate(J.B. EM Services Inc., Quebec) onto the glass substrate before metal evaporation. A scanning electron microscope(SEM) was, however, used to record the surface features of Ag-Sn spheres. The substrate in this case was directly observed with the Nanolab7 SEM operating at 15 KV. The electron micrographs from the metal substrates are given in Figure 2.5.

Figure 2.6 Absorption spectra of Au and Ag island films

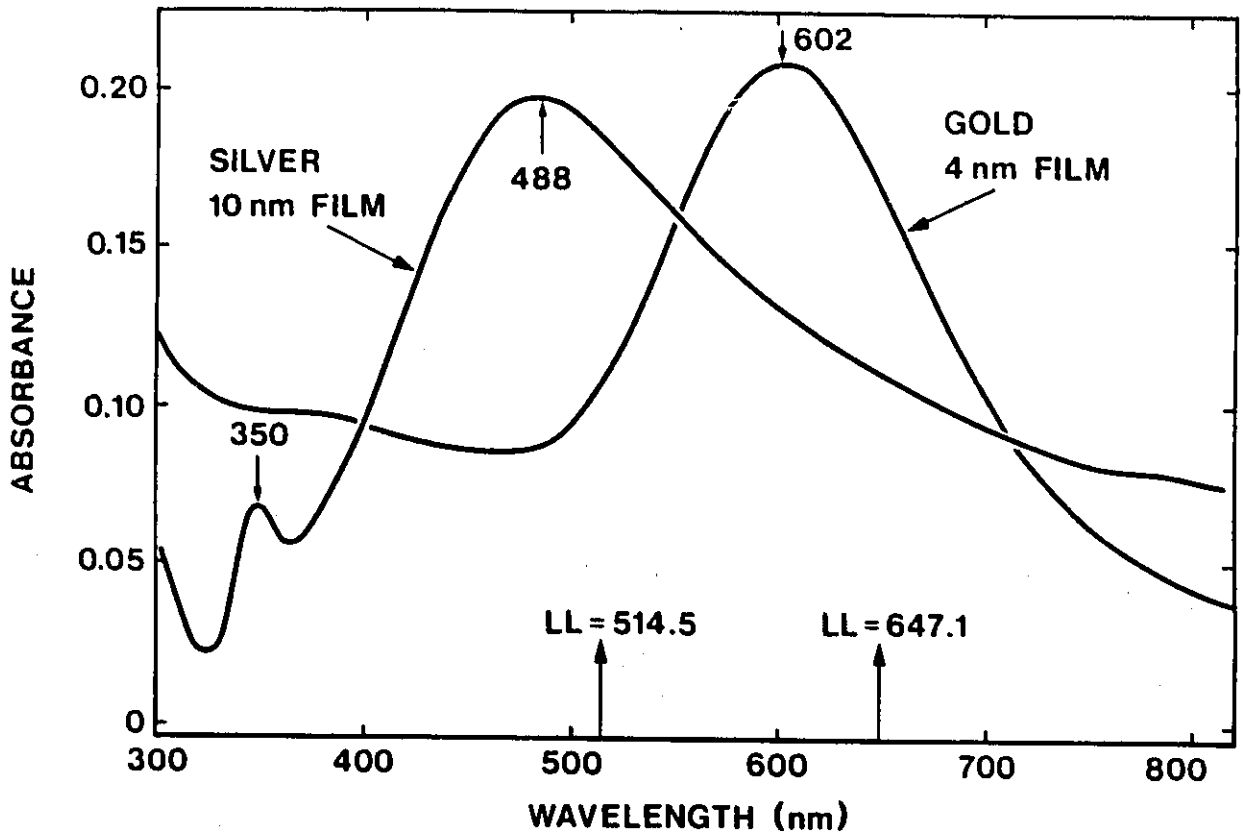
602
0.20
SILVER
10 nm FILM
488
GOLD
4 nm FILM
0.15
ABSORBANCE
0.10
350
0.05
LL = 514.5
LL = 647.1
0
300
400
500
600
700
800
WAVELENGTH (nm)

Figure 2.6

Figure 2.7 Absorption spectrum of Ag-Sn spheres. The spectrum was taken in reflection mode.

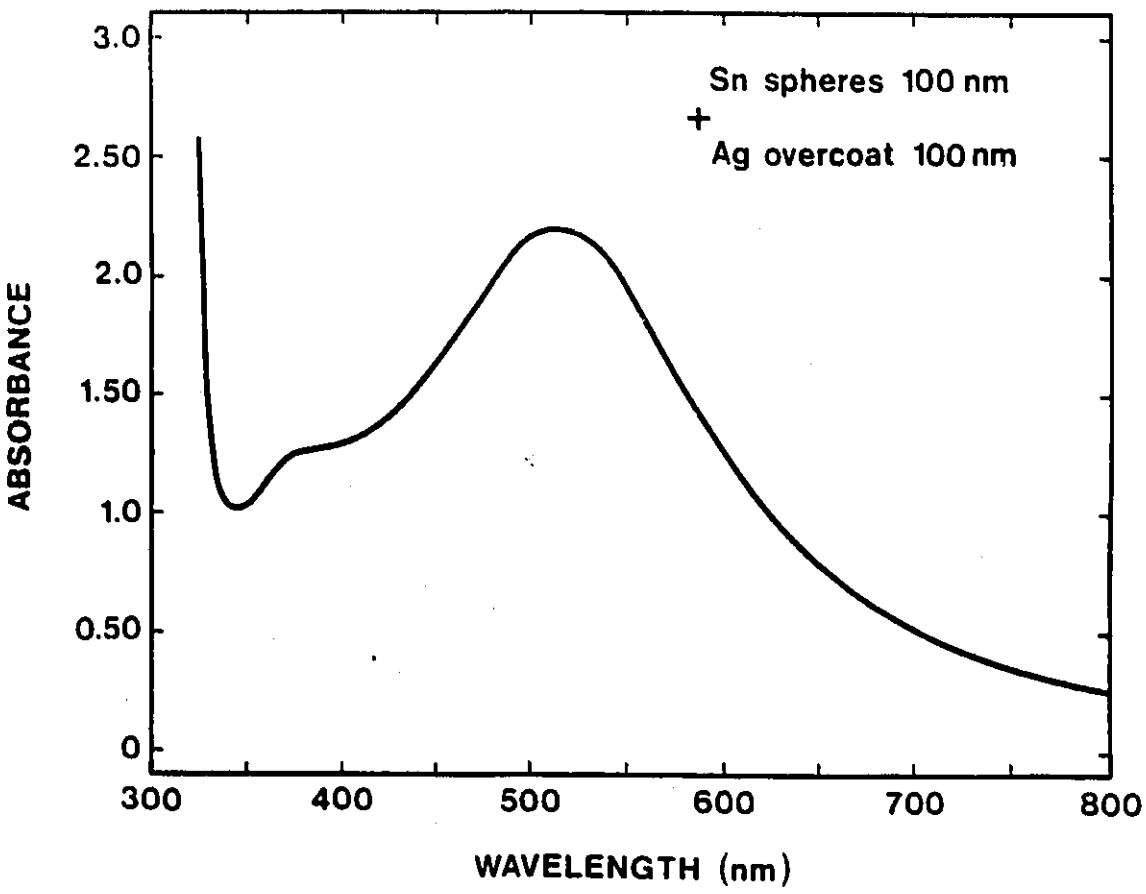
Sn spheres 100 nm
+
Ag overcoat 100 nm
ABSORBANCE
3.0
2.50
2.0
1.50
1.0
0.50
0
300
400
500
600
700
800
WAVELENGTH (nm)

Figure 2.7

Figure 2.6 represents typical absorption spectrum taken from the island films. The 488 nm and 514.5 nm laser lines(LL) from the Ar^+ laser were in full resonance with the plasmon absorption of the Ag island film. The Au island film, however, had an absorption in the red spectral region and excitation with the 647.1 nm laser line of the Kr^+ laser was required for surface plasmon resonance. The plasmon absorption profile for Ag-Sn spheres is shown in Figure 2.7. All three laser lines can be used to excite plasmon resonances in this structure since the broad plasmon absorption encompasses both blue and red spectral regions.

Raman Instrumentation

Raman data were collected by a Spex 1403 spectrometer interfaced to an IBM computer(XT). The spectrometer was situated on an optical table. The software was written in our laboratory and has been described elsewhere.[30] The program "Raman" was used to move the pair of holographic gratings(1800 grooves/mm) and register the inelastic scattering. Photons were detected by a thermoelectrical and water cooled Hamamatsu R928 multialkali photomultiplier and observed with conventional photon counting electronics. The program "Raman" generated a data file that could be retrieved by a second program "Ramplot" to manipulate and plot the Raman spectrum. Spectra Calc software produced by Galactic Industries is currently being used instead of Ramplot.

The 488 and 514.5 nm radiation from a Spectra-Physics model 164 Ar^+ laser and the 647.1 nm and 676.4 nm lines from a Spectra-Physics model 2020 Kr^+ were used for Raman excitation. Optical filters supplied from Spectra-Physics were used to remove

plasma lines. The incident laser light was plane polarized by a polarization rotator(Spectra-Physics model 310-21). Scattered light was passed through a scrambler before passing through the entrance slit of the spectrometer to ensure similar sensitivities towards light polarized in different directions. Components of scattered Raman light could also be selected by placing a polarization analyzer in between the collecting optics and the scrambler.

The 90° collection geometry used in the Raman experiments is shown in Figure 2.8. Porto's notation was used to describe the direction and polarization of incident and scattered electric field vectors.[31] In our laboratory illumination was along the positive Z-axis, observation was along the X-axis and the sample was placed along the Y-axis. The plane of incidence was the ZX plane. Incident light and scattered light was polarized either parallel(P) or perpendicular(S) to the incident plane. The analyzer was rotated to collect S or P scattered light. Four combinations were therefore possible and they are written as:

$$\begin{aligned} &Z(YY)X = SS \\ &Z(YZ)X = SP \\ &Z(XY)X = PS \\ &Z(XZ)X = PP \end{aligned} \qquad (2.2)$$

The symbols outside the parenthesis are the propagation directions for incident light(i.e., Z) and scattered light(i.e., X). The first and second terms in parenthesis refer to the polarization of the electric field of incident(i.e., X, Y) and scattered(i.e., Y, Z) light respectively. The notations SS, SP, PP ,PS are equivalent to the Cartesian description of incident polarized light(first letter) and scattered polarized

Figure 2.8 A schematic representation of the 90° scattering geometry. The film is illuminated at 60° incident angle. Polarization of incident and scattered light leads to four polarization combinations(SS,SP,PP,PS) The four letter notation used by Porto(Bottom)

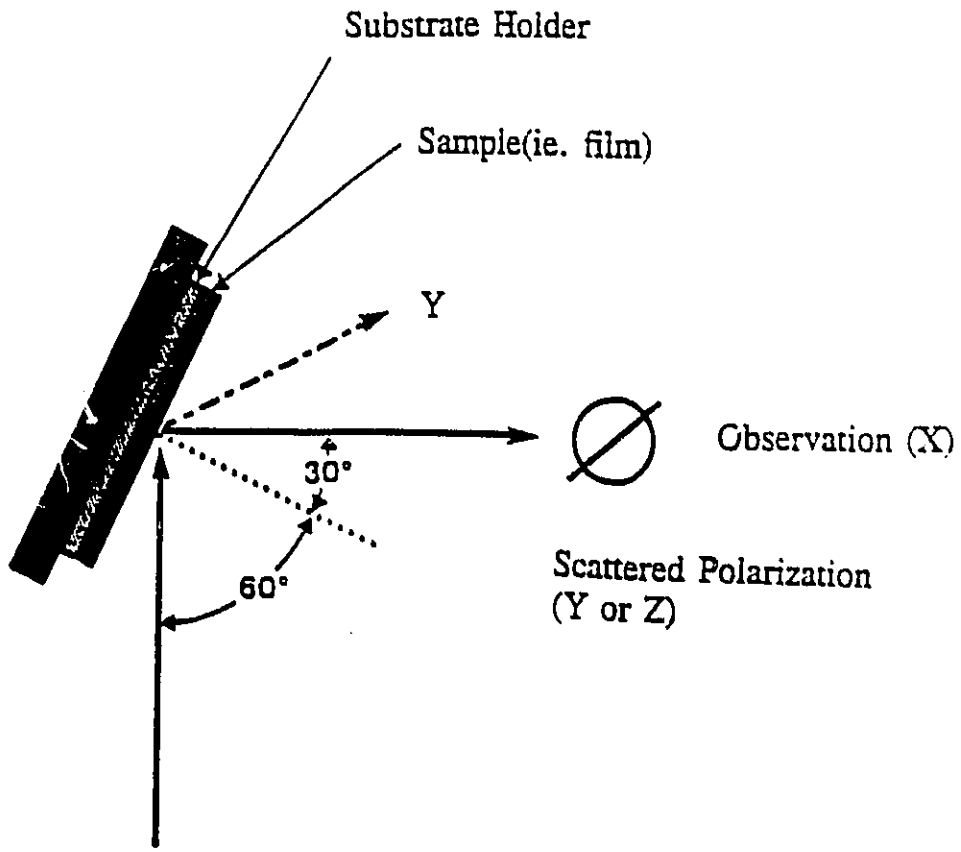

Porto's Notation

Z(YY)X = SS

Z(YZ)X = SP

Z(XY)X = PS

Z(XZ)X = PP

Figure 2.8

light(second letter). In the special case where the crystal is orientated so that its axes are collinear with the space fixed axis, the element of the polarizability tensor is the quantity in parenthesis described by the Porto notation. As an example, the SS spectrum would be dominated by bands that contain the a_{yy} Raman component. When the analyzer was not used, total(T) polarization was collected and the polarization in the Raman spectra was described as ST or PT.

The depolarization(ρ) ratio[32,33] of the 218(E) cm^{-1} or 314(F_2) cm^{-1} bands of CCl_4 was used to calibrate S and P electric fields. It can be shown the $\rho = I_{SP}/I_{SS}$, where I is the integrated band intensity in the SS and SP spectra. A value of $\rho = 0.75$ was obtained for the non totally symmetric bands of CCl_4 with proper calibration. The CCl_4(Aldrich spectroscopic grade) was contained in a quartz cell and used daily for frequency calibration of the spectrometer. Occasionally the accuracy of the spectrometer was inspected with a capillary of distilled indene(Aldrich).

An XYX-positioner was used to secure and align the sample. A cold cell, or a spinning cell could be attached to the XYX-positioner. The spinning cell was always used for LB samples to prevent thermal decomposition. The typical spectral bandpass and laser power(at the sample) were 5 cm^{-1} and 50 mW respectively.

Fourier Transform Infrared(FTIR) Instrumentation

Transmission spectra were collected with a Nicolet 5DX FTIR and Bomem DA3 FTIR spectrophotometer. The Bomem files were imported to Spectra Calc software for spectral manipulations. Infrared spectra were routinely recorded in the region of 400-4000 cm^{-1}.

UV-VIS Absorption Instrumentation

Ultraviolet-visible(uv-vis) absorption spectra were recorded on a HP 8450 diode array and Response spectrophotometer. The files generated by the Response instrument were imported to Spectra Calc for spectral manipulations.

Electrochemistry Instrumentation

Spectroelectrochemical data were obtained with a PAR Model 175 universal programmer and a PAR Model 174A polarographic analyzer. During electrochemical cycling, uv-vis spectra were obtained and stored every 1.2 s on an HP Model 8450A uv-vis spectrometer. This work was conducted by Carol Jennings at Xerox Research Centre of Canada.

CHAPTER 3: Raman Scattering on Metal Surfaces

Introduction

In the classical application of vibrational spectroscopy, both infrared(IR) absorption and Raman scattering(RS) were applied to explore molecular structure in the gas, liquid and solid state through the appearance of group characteristic frequencies.[1-3] Group theory shows that both methods are complimentary and especially powerful when used together for studies in molecular structure.[4,5] For example, in centrosymmetric molecules a vibrational mode is either Raman or IR active. The character table contains the components that give rise to infrared(via the change in dipole moment) and Raman(via the polarizability derivative tensor) activity. Raman scattering has always been more challenging than IR absorption because the cross section in RS is about 10^{-10} smaller than in IR. In many cases the luminescence from the substrate or from impurities within sample could unfavourably swamp out the Raman signal.

Raman instrumentation has, however, improved with better detection instrumentation and a larger selection of laser lines that could be used to record resonance Raman spectra(RRS). Selecting or "tuning" a laser line into resonance with an electronic transition in the molecule gives rise to resonance Raman scattering(RRS) and enhanced intensity of certain bands. In particular, the Raman modes that are related to the electronic transition are greatly enhanced as much as 10^2-10^6 fold.[6] The selectivity in RRS is derived from the localization of the electronic transition to one part of the molecule. For example, in the RRS of Fe(II)-α-diimine

complexes the charge is localized in the skeletal region and only the skeletal modes were enhanced.[7] Topics in RRS have been thoroughly reviewed by Behringer[8] and Rousseau[9] et al.

The most recent interest in Raman spectroscopy includes detection and analysis at the sub monolayer[10] level. Instrumentally, a new development is Fourier transform[11,12] (FT)[10] Raman spectroscopy with near IR laser sources(Nd:YAG operating at 1.064 μm). The current Raman detection systems have significantly advanced over the photomultiplier tubes used in conventional Raman detection.[10] For example, non resonance Raman spectra were recorded with charge coupled device(CCD) multi-channel detection for a Langmuir layer on the subphase.[13] Prior to the recent developments of CCD detectors, other experimental Raman techniques were developed and applied to problems in surface science. Greenler was the first to consider a minor enhancement in the Raman intensity for a molecule near a highly reflecting surface.[14] Raman spectroscopy of adsorbed molecules on surfaces further flourished after the initial report of Fleischmann and coworkers who first observed intense Raman scattering from pyridine adsorbed on a roughened silver electrode.[15] Their findings led to the development of a new technique that incorporated a roughened *surface* to *enhance* the *Raman scattering*(SERS) of molecules. For molecules adsorbed or near a rough metal surface the SERS intensity was significantly greater than the normal Raman scattering. For carbon monoxide adsorbed on vapour deposited Ag, an enhancement of 10^6 was observed for the adsorbed layer.[16] Hexter et al. noted an enhancement factor of 10^4 for pyridine on Ag electrodes. Their

calculations were based on the surface area of the roughened electrode and the band intensities of liquid(991 cm^{-1}) and adsorbed(1006 cm^{-1}) pyridine.[17]

The current consensus is that Raman scattering and surface enhanced Raman scattering(SERS) are two vibrational techniques, among several others, that may be used to probe the structure at the interface that exists in electrochemical(solid-liquid interface), heterogeneous catalytic(solid-gas interface) and other systems(i.e., solid-solid interface).[18] The vibrational spectrum of the adsorbates is the fingerprint that gives details about the chemical bonds and their geometry at the interface.[19] Chemical reactivity at metal surfaces is also relevant to possible applications of SERS. Ackers and coworkers have applied SERS to identify the surface intermediates in the Ag catalysed reaction of ethylene and oxygen to form ethylene oxide.[20] In the same context, the product in the chemical reaction of imidazole(a corrosion inhibitor) on silver sols was identified in the SERS spectra.[21] The application of SERS to biological systems has been recently reviewed.[22] Raman scattering is one of the most important tools for in situ vibrational studies at surfaces.[18]

SERS Theory

The observation of intense Raman scattering of pyridine in the electrochemical experiment described by Fleischmann et al. was originally attributed to the increase in the surface area that occurred during the oxidation-reduction cycle.[15] Creighton et al.[23] and Van Duyne et al.,[24] however, showed that the growth in surface area by electrochemical cycling could not significantly account for the strong Raman signals

of adsorbed pyridine. They proposed an increase in the Raman scattering cross section for the adsorbed molecules on the electrode surface. Various models were collected and published in the first book dedicated to surface enhanced Raman scattering.[25] About 572 SERS papers were cited by Seki in 1986.[26] They include SERS from molecules adsorbed onto colloids(Ag, Au, Cu, Pt, Rh, Na, K), electrodes(Ag, Au, Cu, Cd, Hg, TiO_2), and island films(Ag, Au, Cu, Ni, Pd, Ti, Li, Na, In, Co, NiO). An essential feature of all SERS were the protrusions and bumps at the surface which gives rise to surface roughness. For colloids and island films the metal domains can be approximated as spheres and spheroids respectively. The size of the particles are not homogeneous and smaller or comparable to the wavelength of the exciting laser line. The particle shape is also important, and it can be described by the aspect ratio defined by **a/b** where **a** and **b** are respectively the lengths of the semi-major and semi-minor axis. Prolate spheroids have $a/b > 1$, while oblate spheroids have $a/b < 1$. Particle where $a/b = 1$ are spheres.

The common opinion is that SERS is an electromagnetic effect. The extent of the chemical contribution to the total SERS effect can be examined case by case.[27] Mechanisms that amplify the electric field at the molecule are considered electromagnetic while those that strengthen the polarizability derivative tensor are termed chemical or electronic. The chemical effect is commonly associated with resonant excitation into the charge transfer(CT) band of the metal-molecule complex.[27-30] Chemical enhancement is therefore restricted to molecules directly at the surface. For pyridine adsorbed onto silver island the excitation profile for the 1010

cm^{-1} band confirmed significant chemical enhancement when the laser line was tuned in resonance with charge transfer band which was well outside the surface plasmon resonance.[31] Otto et al. note that chemical enhancement on coldly deposited metal films originates from adatoms of atomic scale roughness. They support their claim in experiments where no Raman signals were observed upon annealing the film.[32] The adatoms were supposedly destroyed upon heating.

The electromagnetic(EM) effect is attributed to resonant excitation of the collective conduction electrons or surface plasmons(SP) modes that are present on rough metal surface. The SP act to concentrate the incident field at the surface of the metal particles.[33] An essential requirement for EM effects is the surface roughness which helps produce radiative SP that can couple to the exciting laser line and participate in the Raman emission.[33,34] For an isolated sphere(with dimensions less than the incident wavelength), the electric field that is produced inside a sphere, by a laser line of electric field E_o and frequency w is given by[35]:

$$E_{in:\,x,y,z} = \frac{1}{1 + [\epsilon(w)/\epsilon_o - 1]A_{x,y,z}} E_{ox,y,z} \qquad (3.1)$$

where $\epsilon(w)$ and ϵ_o are the complex dielectric constants of the metal particle and the surrounding medium respectively. The depolarization factor(A) in 3.1 is an integral and completely shape dependent(i.e., A=.333 sphere, A=.17356 prolate(a/b=2) and size independent.[35] Resonance is achieved when:

$$\epsilon_o + \quad [\mathrm{Re}\{\epsilon(w)\} - \epsilon_o]A = 0 \qquad (3.2)$$

For a sphere the SP resonance occurs when the real part $\mathrm{Re}\{\epsilon(w)\}$ of the dielectric constant equals $-2\epsilon_o$. The imaginary part($\mathrm{Im}\{\epsilon(w)\}$)of the complex dielectric constant is related to SP damping and prevents 3.1 from reaching infinity. A small $\mathrm{Im}\{\epsilon(w)\}$ component would therefore minimizes damping of the SP.[36] In the visible region excitation of the SP are fulfilled by Ag, Cu, Au, alkali metals.[37] For this reason most investigation of SERS have been with the coinage metals.

The SP are localized on isolated bumps and do not propagate along the film surface.[35] The field E_{ins} will give rise to a electric field outside (E_{out}) the sphere, which is always greater the E_o. The displacement vector D can be used to relate E_{out} to E_{ins}. The boundary conditions require that the normal displacement vector $D^{\perp}=\epsilon(w)E^{\perp}_{ins}=\epsilon_o E^{\perp}_{out}$ and that the tangential displacement electric vector $E^{\parallel}_{out} = E^{\parallel}_{ins}$.[35]

The Raman emission is also enhanced by the metal particle. The Raman dipole oscillating at w_s polarizes the metal particle and uses it as an antenna to amplify its Raman radiation.[35,37,38] The overall SERS enhancement therefore results from amplification of both incident and scattered fields. The electromagnetic enhancement in SERS decays as the molecule is separated from the surface. For a molecule located a distance(d) from a sphere(radius r) the SERS intensity[39] is proportional to $[r/(r + d)]^{12}$. For a monolayer the SERS dependence with distance[39] is proportional to $[r/(r + d)]^{10}$.

A number of SERS experiments have demonstrated good evidence for EM

enhancement. The predicted exponential decay was demonstrated in a series of experiments that used spacer layers of arachidic acid monolayers to control precisely the distance from the metal particle.[40,41] The experimental dependence of the Raman signal on the aspect ratio(or depolarization factor) and on the dielectric constant of the surrounding media was also in agreement with electromagnetic predictions.[42] The authors showed that by changing the parameters A and ϵ_o the SP resonance moved but that the maximum enhancement coincided with the shifted SP resonance. Further evidence of EM enhancement was observed in the excitation profiles of carbon monoxide on vapour deposited Ag(SP in the red spectral region) and colloidal Ag(SP in the blue spectral region).[43] For both substrates the excitation profile peaked in the vicinity of the surface plasmon resonance. The interested reader should consult the excellent reviews by Aroca et al.[34], Moskovits[33], and Chang[35] for additional details in surface enhanced Raman spectroscopy.

SERS Spectra:Physisorption, Chemisorption and Depolarization

The interaction between the metal particle and the adsorbate is revealed in the SERS spectrum. Chemisorption is observed when new bonds are formed between the adsorbate and the surface(i.e., formation of a surface complex). The surface could lower the symmetry of the molecule, which could lead to new band(s) and shifts in band frequency and relative intensity. Chemisorption is also restricted to adsorbates directly in contact with the metal. For example, chemisorption was observed by the presence of a strong band assigned to Ag-N or Ag-O frequency of the metal-molecule complex.[44] The authors also showed that the surface complex was not formed when

the molecules(deposited as a LB layer) were separated from the surface by a spacer layer of arachidic acid.

For molecules physisorbed onto a SERS substrate, the spectrum shows no change in the vibrational bands or their relative intensity. The SERS spectrum is almost identical to the normal Raman spectrum. The signal to noise ratio is, however, greater in the SERS spectrum. There is no extensive metal-molecule interaction that would alter the molecular electronic distribution and the polarizability derivative tensor.[34] Thus for physisorbed species, chemical enhancement can be excluded and the dominate enhancement is from electromagnetic mechanism.

SERS spectra are also depolarized and cannot be used to obtain molecular orientation. The surface roughness features scramble both the incident field into three orthogonal components and the net orientation of the adsorbed molecules.[45]

Tailoring Metal Island Films in SERS

Electromagnetic enhancement is observed to peak when the laser line is tuned into resonance with surface plasmons absorption band. Several investigations have considered optimal conditions to maximize SERS. Koh et al. used Si particles(whose size could be varied) as an underlayer to roughen the silver surface.[46] They reported an optimal groove depth of 10 nm for the Si layer. Others have controlled the rate of deposition[47,48], the mass thickness[48,49] and the temperature of the substrate during the formation of metal island films. The width and maximum absorption of the SP are related to the shape, size and inter particle spacing and can be varied by changing the deposition conditions.[50,51] Film preparation is normally controlled to give

reproducible surface morphology and surface plasmon resonances. For example the 647.1 nm laser line was outside the SP absorption(maximum centred at 480 nm) in the 2.5 nm Ag island film but in full resonance with the SP of a 9.5 nm film.[48] Recently a substrate (formed by evaporating 20 nm metal film at a rate of 0.1nm/s to a glass slide maintained at 200 °C) showed SERS activity in the near-infrared.[52]

The combination of SERS(in resonance with the localized SP) and RRS(in resonance the molecular electronic absorption) gives optimal enhancement and sensitivity. The double resonance effect leads to surface enhanced resonance Raman Scattering(SERRS).

Minor Raman Enhancement on Reflecting Surfaces

A minor Raman enhancement(6-10) is predicated for molecules adsorbed onto "smooth surfaces" of highly reflecting metals.[33] The nomenclature smooth surfaces has been used to describe films that do not support radiative plasmon modes. The original treatment was given by Greenler et al.[14] and later expanded by Moskovits.[53] The surface changes the illuminating field on the molecule and the inelastic scattering from the Raman dipole. As shown in Figure 3.1 the molecule is excited by an incident field($E_{o\infty}$ or E_{op}) and a reflected field($r_sE_{o\infty}$ or r_pE_{op}). The magnitude of the reflected field is calculated from the Fresnel coefficients(r_s, r_p) of s and p polarized light. The resultant electric electric field components at the surface are given by[53]:

$$\begin{aligned} E_x &= (1 + r_s)E_{o\infty} \\ E_y &= (r_p - 1)\mathrm{Cos}\Phi E_{op} \\ E_z &= (1 + r_p)\mathrm{Sin}\Phi E_{op} \end{aligned} \qquad (3.3)$$

where the s and p are the electric fields polarized normal and parallel to the plane of incidence(ZY). The Fresnel coefficients relate the amplitude of the reflected(ref.) beam to the incident beam. In vacuum[54]:

$$r_s = (E_s \text{ ref.})/(E_{os}) = \frac{\text{Cos}\Phi/\epsilon^{1/2} - (1 - \text{Sin}^2\Phi/\epsilon)^{1/2}}{\text{Cos}\Phi/\epsilon^{1/2} + (1 - \text{Sin}^2\Phi/\epsilon)^{1/2}} \qquad (3.4)$$

$$r_p = (E_p \text{ ref.})/E_{op}) = \frac{\text{Cos}\Phi - (1/\epsilon - \text{Sin}^2\Phi/\epsilon^2)^{1/2}}{\text{Cos}\Phi + (1/\epsilon - \text{Sin}^2\Phi/\epsilon^2)^{1/2}}$$

where Φ is the angle of incidence to the normal on the surface and ϵ is the complex dielectric constant of the metal. On a metal surface, a phase shift of 180° occurs for the s-polarized reflected field for all angles of incidence and $r_s \rightarrow -1$.[55] The p-polarized reflected field is, however, in phase and changes to 180° at high angles of incidence. In the limit of a good reflector $r_p \rightarrow +1$ and the reflected field reinforces the incident field. The calculations for Ag, Au, and Cu metals show that the normal component(E_z) of p-polarized light and an incident angle of 50°-70° produces enhanced fields.[10,34] Figure 3.2 depicts the square of the electric field on a reflecting surface as a function of the incident angle.

The inelastic light that reaches the detector is also increased by the light that is reflected from the surface as shown in Figure 3.1. The surface selection rules have been developed for polarized incident and scattered light. The predicated intensity patterns for the four polarized Raman spectra are[53]:

$$
\begin{aligned}
SS \quad & \alpha \mid a_{xx}(1 + r_s)(1 + r_s') \mid^2 \\
SP \quad & \alpha \mid a_{yx}(1 + r_s)(1 - rp')\mathrm{Cos}\Phi' + a_{zx}(1 + r_s)(1 + r_p')\mathrm{Sin}\Phi' \mid^2 \qquad (3.5) \\
PP \quad & \alpha \mid \{a_{yy}(1 - r_p)\mathrm{Cos}\Phi + a_{yz}(1 + r_p)\mathrm{Sin}\Phi'\}(1 - r_p')\mathrm{Cos}\Phi' \\
& + \{a_{zy}(r_p - 1)\mathrm{Cos}\Phi + a_{zz}(1 + r_p)\mathrm{Sin}\Phi\}(1 + r_p')\mathrm{Sin}\Phi' \mid 2 \\
PS \quad & \alpha \mid a_{xy}(r_p - 1)(1 + r_s')\mathrm{Cos}\Phi + a_{xz}(1 + r_p)(1 + r_s')\mathrm{Sin}\Phi \mid^2
\end{aligned}
$$

where the primes indicated the quantities for the scattered fields and a_{ij} are the polarizability derivatives tensor components for the normal coordinate. For molecules adsorbed on a good reflecting surface, the PP spectrum is expected to be the most intense and dominated by bands that transform as a_{zz}.

Figure 3.1 Excitation and scattering for a molecule(O) placed above a smooth surface. Incident and reflected beam are represented by 1 and 2 respectively.

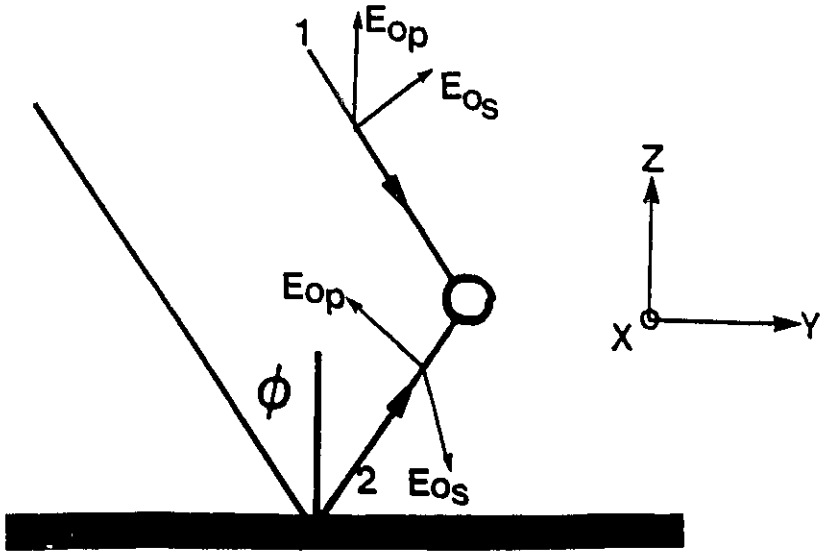

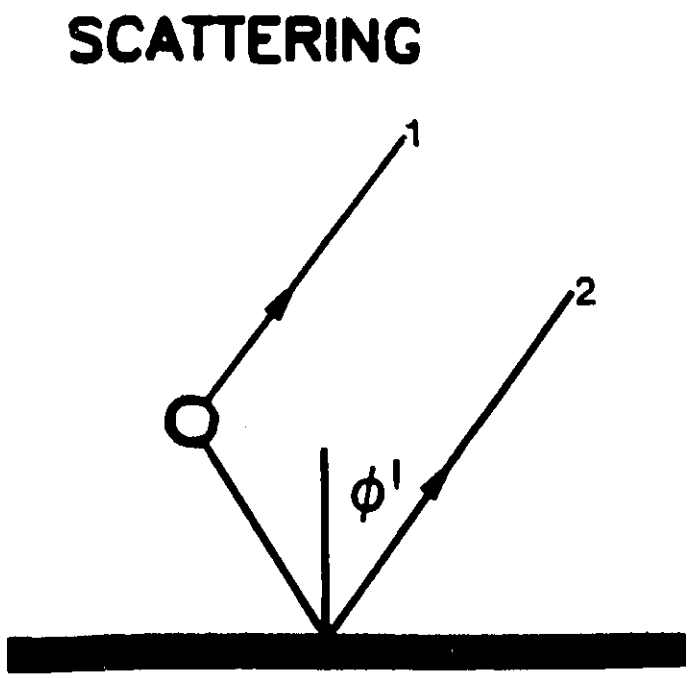

Figure 3.1

Figure 3.2 The square of the field components as a function of the angle of incidence and with 514.5 nm excitation for In and Ag.
(E^2_x- ▲, E^2_y- O, E^2_z- ●)

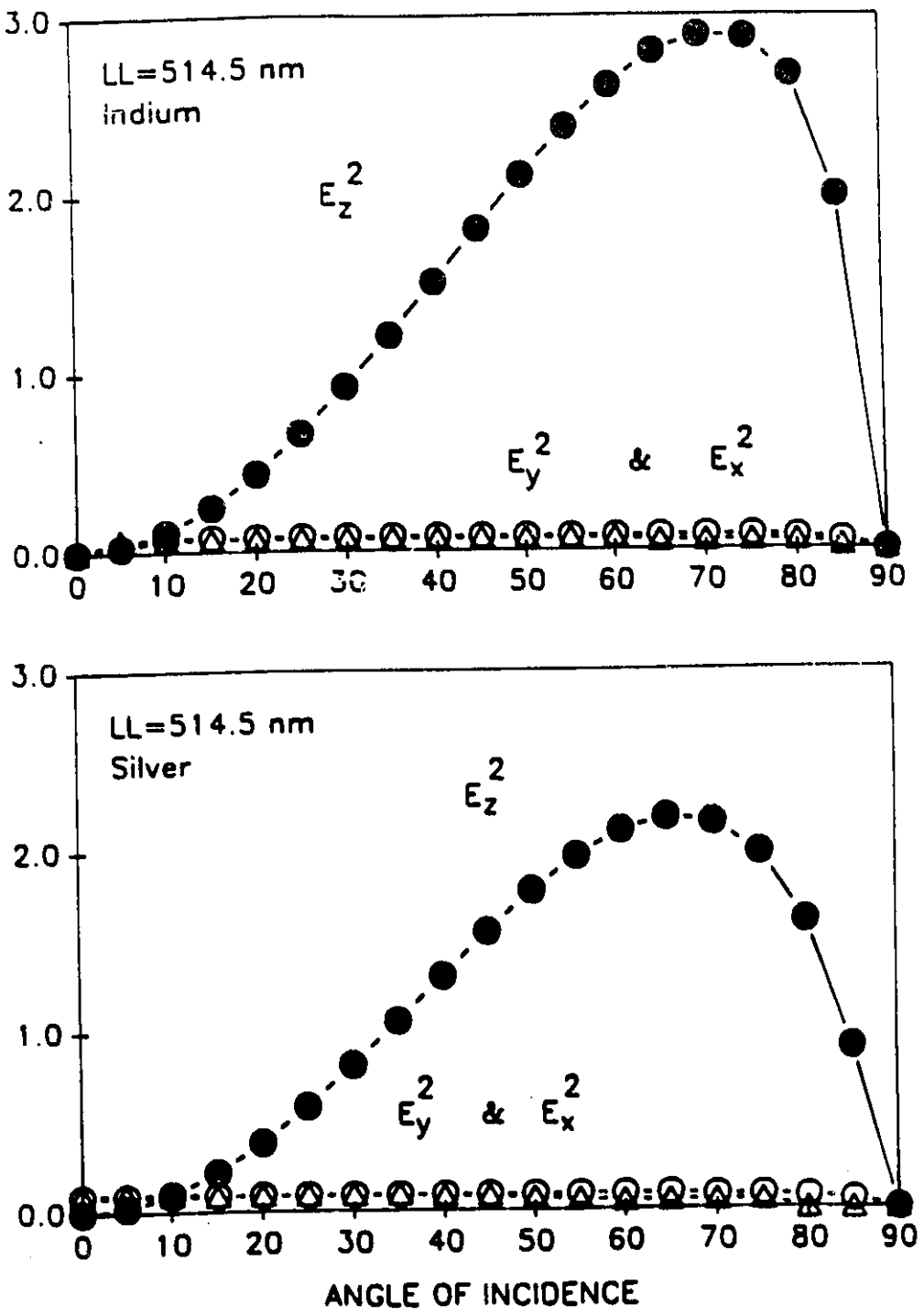
3.0
2.0
1.0
0.0
LL=514.5 nm
Indium
E_z^2
E_y^2 & E_x^2
0 10 20 30 40 50 60 70 80 90
LL=514.5 nm
Silver
E_z^2
E_y^2 & E_x^2
ANGLE OF INCIDENCE

Figure 3.2

CHAPTER 4: Vibrational Spectroscopy of Phthalocyanine

Introduction

Routinely vibrational spectroscopy is primarily used to identify functional groups in a molecule through the appearance of "fingerprint" frequencies which are characteristic of the structural units. The normal coordinate analysis(NCA) of molecules is, however, pursued for the assignment of 3N-6(or 3N-5 for a linear molecule) fundamental vibrational modes to internal coordinates. For small molecules the NCA could be solved on a microcomputer; however, for unsubstituted Pc where $N \geq 57$(as in MPc,or H_2Pc) the problem becomes very complex and is normally solved on a main frame computer. A NCA of copper phthalocyanine was recently published for the totally symmetric modes.[1] The authors noted that the A_{1g} modes were heavily coupled. Following the theory of characteristic vibrational frequencies, bands of phthalocyanine were identified using the subunits or model compounds that were structurally related to Pc for which the vibrational assignment was known. These would include such molecules as benzene[2], indole[3], pyrrole[4] and porphyrin[5]. This strategy has been used by our laboratory.

Jennings[6] has tabulated and compared modes of the $H_2Pc(\alpha, \beta, \chi)$, MPc(M= Mg, VO, Cu, Zn, Sn, Pb), and ClMPc(M=Al, Ga, In) to the model compounds. Her data are comprehensive and were used to generate the characteristic frequencies of Pc as shown in Table 1. The Raman spectra and further detailed vibrational assignments of various Pc molecules have been published by our group.[7-16] The macrocycle bands are associated with the inner ring of Pc, which is composed of the sixteen alternating

Table 4.1 Characteristic Raman Bands of Phthalocyanine

Pc Shift (cm^{-1})	Pc Assignment	Model Compound:Raman Shift(cm^{-1}) Assignment
160- 184	isoindole ring, deformation	
204- 219	isoindole ring, deformation	
221- 245	isoindole ring, deformation	224 (indole)
447	isoindole ring, deformation	423 (indole)
479- 486	isoindole ring, deformation	
511- 517	isoindole ring, deformation	
540- 566	isoindole ring, deformation	
564- 606	benzene	606 (benzene)
678- 683	macrocycle breathing	670 (porphyrin)
720- 730	C-H out of plane	
743- 755	macrocycle stretching	751 (porphyrin)
780- 804	macrocycle stretching	795 (porphyrin)
827- 847	macrocycle stretching	
1007-1013	C-H	
1024-1040	C-H	1038 (benzene)
1072-1082	C-H	
1102-1114	C-H	
1138-1147	pyrrole, ring breathing	1148 (pyrrole)
1150-1200	C-H	1150 (benzene), 1178(benzene)
1212-1230	C-H	
1306-1312	C-H	1326 (benzene)
1337-1343	pyrrole ring, stretching	1384 (pyrrole)
1393-1408	isoindole ring, stretching	1412 (indole)
1427-1436	isoindole ring, stretching	
1447-1464	isoindole ring, stretching	1455 (indole)
1457-1471	isoindole ring, stretching	
1480-1484	isoindole ring, stretching	
1506-1527	CN pyrrole or CC pyrrole	
1520-1550	CN aza group	1534 (indole)
1580-1610	benzene	1585 (benzene), 1606(benzene)

carbon and nitrogen atoms. The Raman spectra of Pcs have also been reported by others.[17-19] Weak Raman bands due to the coordination of the metal to the pyrrole nitrogens have been observed in the 230-256 cm^{-1} spectral region.[8,11,13,14] The metal-nitrogen assignment has been more extensively studied in the far infrared.[20-21] The symmetry assignment of totally and non totally symmetric modes is given by the symmetry species and their activity in the IR, Raman and polarized Raman spectra. For example, for a D_{2h} Pc (i.e., H_2Pc) the A_g modes would be IR inactive and the SS Raman polarized spectrum would be dominated by A_g bands. The non totally symmetric modes (i.e., B_{1g}, B_{2g}, B_{3g}) would be observed with large relative intensity in the SP spectrum. The resonance Raman(RR) spectra of Pc are due to Herzberg-Teller[22] scattering since both totally symmetric and non totally symmetric modes are enhanced and no overtone progressions are observed in the RR spectra.[12] Herzberg-Teller scattering is normally observed for molecules where the ground and the excited state have similar geometries, as in the porphyrins.[22] In the excitation profile for metal free phthalocyanine, both the totally and the non totally symmetric bands were enhanced, which confirmed RR scattering by the Herzberg-Teller mechanism.[23]

VOPc:Raman and IR of Thin Solid Films, SERS and Symmetry Assignment

As pointed out in Chapter one Pcs have remarkable physical and chemical properties. Thin solid films and or Langmuir-Blodgett films are two practical methods that can be used to fabricate phthalocyanine into application devices. Debe noted that organic thin films, and especially ordered organic thin films, are becoming important in novel technologies, and will provide specialized surfaces, membranes and optical

Figure 4.1 Infrared of VOPc in KBr pellet (A)

Infrared of a 200 nm thin solid film of VOPc evaporated onto a KBr crystal(B)

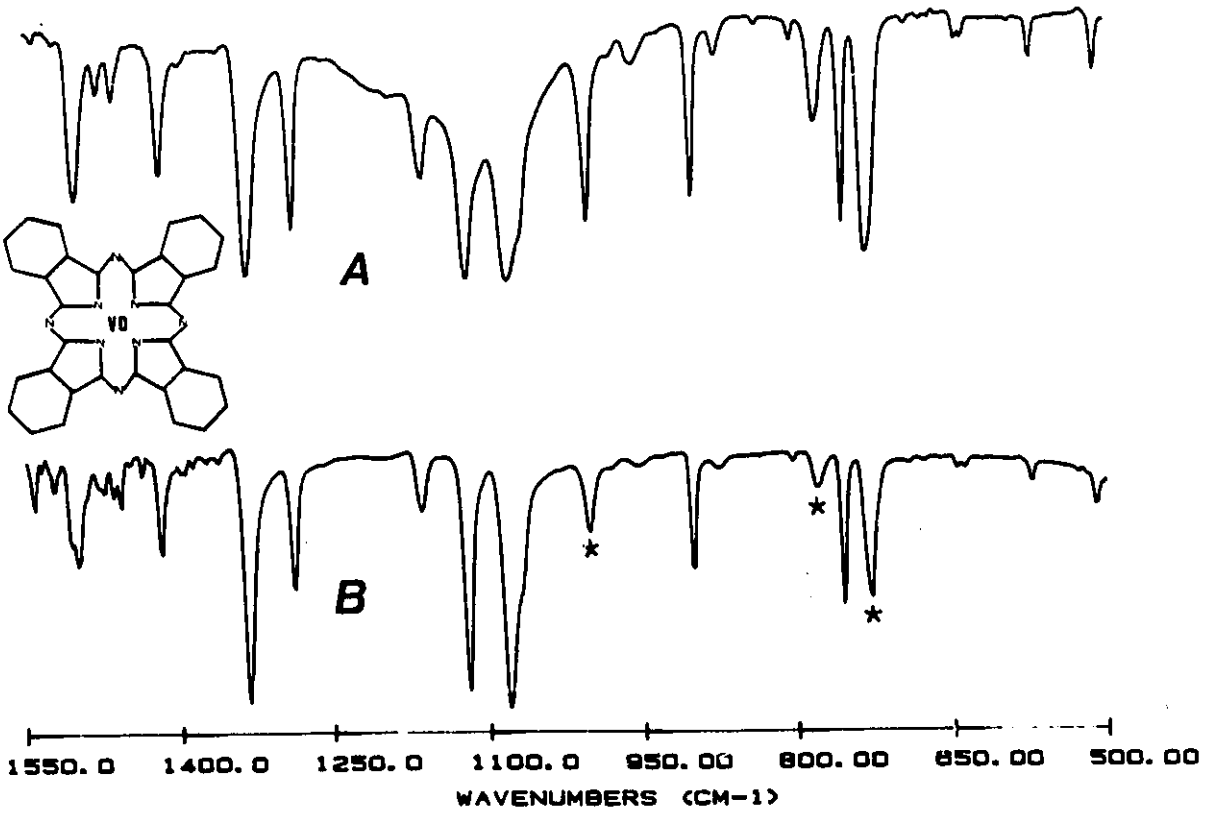
A
VO
B
1550.0
1400.0
1250.0
1100.0
950.00
800.00
850.00
500.00
WAVENUMBERS (CM-1)

Figure 4.1

response functions that cannot be provided by inorganic analogues.[24] In the development of the film device, it will be necessary to characterize and optimize the structure and the chemistry of the film. The molecular organization(whether it is amorphous, polycrystalline, or crystalline) can be non-destructively probed by infrared(IR) absorption and polarized Raman scattering. The results of a thin film of vanadyl phthalocyanine(VOPc) prepared at room temperature are presented.

Thin solid films of 200 nm VOPc were grown onto Corning 7059 glass slides and onto KBr crystals. The Raman and IR spectra can be interpreted as point dipoles interacting with an external electromagnetic field. The absorption of radiation is proportional to the square of the scalar product of transition moment and electric field. For infrared spectroscopy this means that the electric field and the change in the dipole moment must have a component in the same direction. For VOPc (assuming C_{4v} molecular point group) $23A_1 + 42E$ IR modes are expected. The change in the dipole moment for the A_1 and E modes are along the Z and the (X,Y) molecular axis respectively.

The infrared spectra of VOPc mixed with KBr to form a pellet, and of a 200 nm film are presented in Figure 4.1. The change in relative intensities between the two spectra was a good indication of partial molecular organization. In the KBr pellet there exists a random orientation of the VOPc molecules and the relative intensities of the A_1 and E modes would reflect the extent of the change in the dipole moment associated with the particular vibration. The decrease in relative intensity of the bands marked(*) in the thin film sample could be rationalized in terms of face-on

Figure 4.2 RS spectra(SS and SP components) of a 200 nm VOPc film on KBr excited with the 514.5 nm laser line

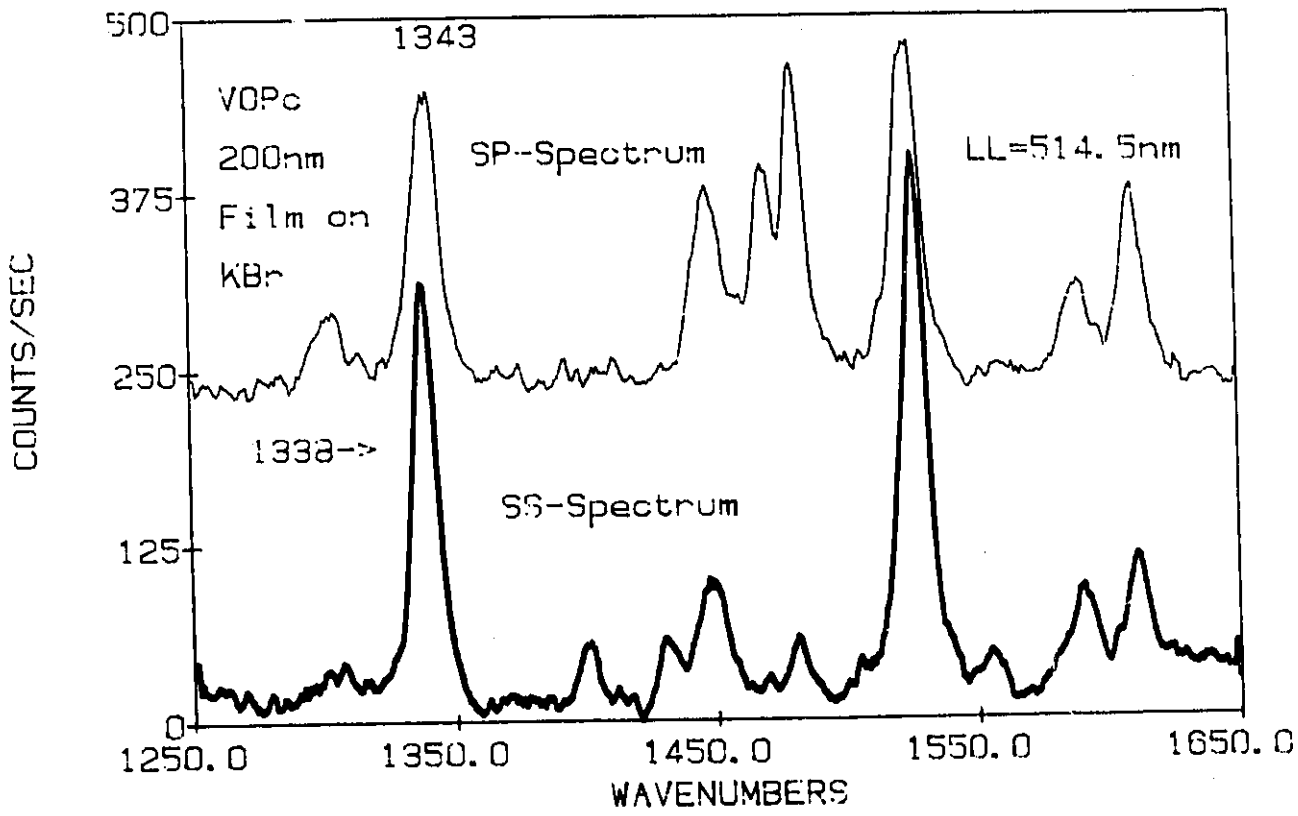
500
375
250
125
0
COUNTS/SEC
1343
VOPc
200nm
Film on
KBr
SP-Spectrum
LL=514.5nm
1338->
SS-Spectrum
1250.0
1350.0
1450.0
1550.0
1650.0
WAVENUMBERS

Figure 4.2

or edge-on molecular orientation. In the face-on description the molecular plane(the XY plane) is parallel to the substrate and strong E modes are expected in the IR spectrum since the electric field is parallel to the in plane transition moments. The edge-on organization for VOPc would have the molecules standing up with the XY molecular plane perpendicular to the substrate. In this case the totally symmetric bands would be observed with strong relative intensity and the E bands would be absent or weak.

In the IR spectrum of the 200 nm thin film the totally symmetric bands at 728, 779 and 1002 cm^{-1} decreased in relative intensity; however, the E bands were unaffected. The results clearly showed that there existed a certain degree of face-on molecular orientation for the 200 nm film of VOPc prepared at room temperature. The SS and SP polarized Raman spectra for the VOPc film are shown in Figure 4.2. The SS spectrum was dominated by totally symmetric modes. The SP spectrum however contained mostly B_2 and E modes. The differences in the SS and SP spectra were due to the partial molecular organization. Another important observation was the separation of the Raman bands at {1338(SS-spectra), 1343(SP-spectra) cm^{-1}} and {1517(SP-spectra), 1525(SS-spectra) cm^{-1}}. The doublet resulted from Davydov splitting, which is a solid state effect commonly observed in crystals.[25] Each Davydov component has distinct polarization properties that can be probed by polarized Raman spectroscopy. For example in thin solid films of chloroaluminum phthalocyanine the A_g(at 1339 cm^{-1}) and B_g(at 1344 cm^{-1}) doublet was assigned to Davydov splitting and the bands were well observed in the SS(or PP) and SP(or PS) spectra, respectively.[14]

For a molecular crystal with **m** molecules per unit cell, factor group symmetry **u**, and site group **v**, the number of Davydov components(**N(u,v)**) is given by:

$$N(u,v)=(m/h)\Sigma\chi_u(R)\chi_v(R) \qquad (4.1)$$

where h is the order of the factor group and $\chi_u(R)$ and $\chi_v(R)$ are the characters of the u and the v irreducible representation for the factor and site groups respectively.[14] The possible site groups for each space group can be found in correlation tables. Crystals of VOPc were reported to be triclinic with factor group C_1 and two molecules per unit cell.[26] The observed doublet in the spectra resulted from two molecules per unit cell, C_1 factor group, and C_1 site group. The assignment of the symmetry species of the Davydov components is addressed in the next section(Raman studies of VOPc on highly reflecting surfaces).

The SERS of 1 nm VOPc evaporated onto a 10nm Ag island film and on Ag-Sn spheres are shown in Figure 4.3. The SERRS of 1 nm VOPc evaporated onto Ag and Au islands is shown in Figure 4.4. The vibrational frequencies in the SERS and SERRS spectra for all three substrates were observed unshifted with respect to those recorded for the VOPc film on glass or on the KBr crytal. The results suggest that there were no strong metal-molecule interactions that could perturb the vibrational energies of VOPc. The molecules were therefore *physisorbed* onto the SERS substrates and the Raman enhancement was attributed to the electromagnetic mechanism. The components of the Davydov doublet were observed as one strong

Figure 4.3 Top: SERS(multiplied by 5) for 2 nm VOPc on Ag islands.

Bottom: SERS of 1 nm VOPc on Ag-Sn spheres

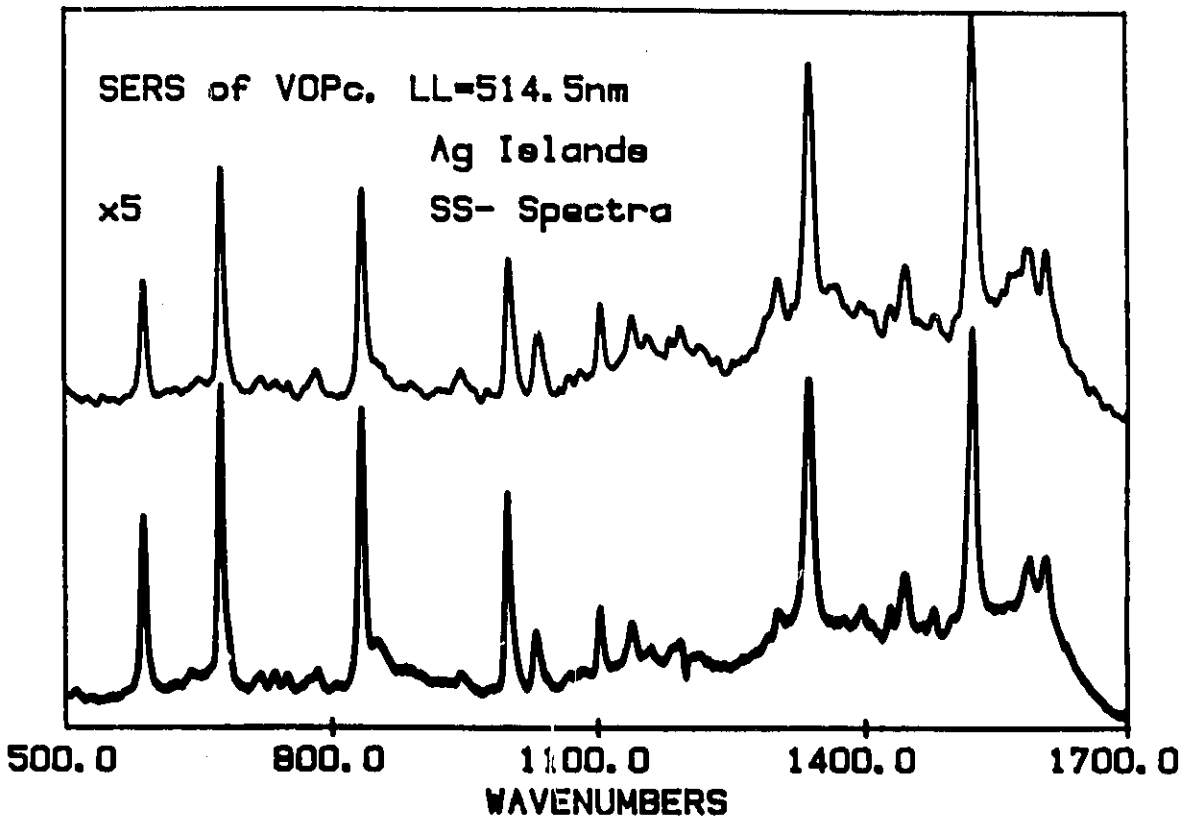
SERS of VOPc. LL=514.5nm
Ag Islands
x5
SS- Spectra
500.0
800.0
1100.0
1400.0
1700.0
WAVENUMBERS

Figure 4.3

band in all four polarized SERS and SERRS spectra. The observations confirm that the doublet was a solid state effect which was not present at the low surface coverage of 1 nm. The doublets were, however, observed for a 65 nm film of VOPc deposited on silver coated tin spheres. Another important observation in the SERS and SERRS spectra was the similarity of all Raman components in the SS, and SP spectra. The spectra were all depolarized and further discussion is given in the next section(Raman studies of VOPc on highly reflecting surfaces).

The SERS, SERRS and the infrared data of a 200 nm thin solid film were used to assign the symmetry of the bands in VOPc. Assuming a C_{4v} molecular point group, the infrared spectra would contain only A_1 and E species, whereas the A_1, B_1, B_2 and E bands were expected in the Raman or surfaced enhanced Raman spectra. Bands that were observed exclusively in the Raman spectra could be assigned to B_1, and B_2 representations. A strong band in the Raman with a weak counterpart in the IR was most likely an A_1 vibration. A band observed with strong intensity in the infrared and weak intensity in the Raman was assigned to an E representation. The symmetry assignment for VOPc is given in Table 4.2.

Figure 4.4 SERRS spectra of 2 nm of VOPc on Ag and Au islands films. Both spectra are SS polarization.

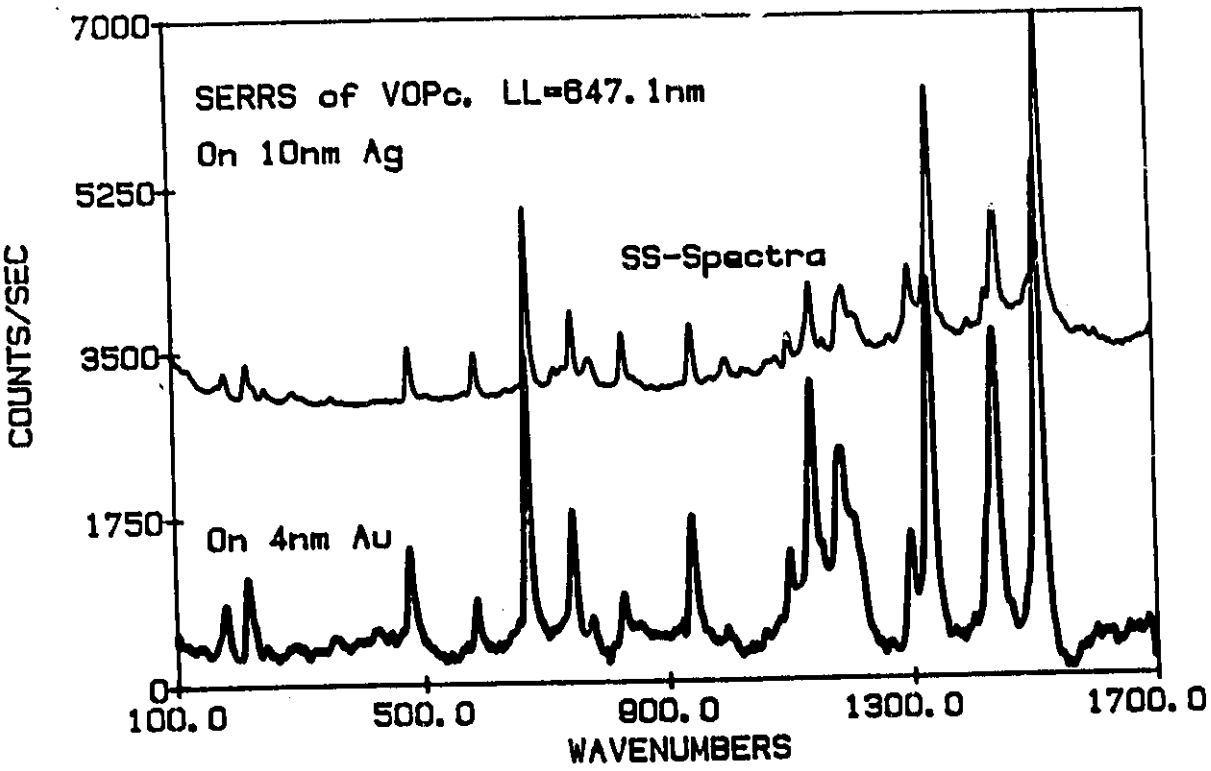
7000
5250
3500
1750
0
SERRS of VOPc. LL=647.1nm
On 10nm Ag
SS-Spectra
On 4nm Au
COUNTS/SEC
100.0
500.0
900.0
1300.0
1700.0
WAVENUMBERS

Figure 4.4

TABLE 4:2 Molecular Frequencies of VOPc

infrared (200-nm film)	SERS	SERRS	symmetry
	187 w	187 w	
	222 m	222 m	
	234 m	234 w	
	254 w	252 w	
	297 w	296 w	
419 w			E
457 w			E
	484 w	484 w	
508 w			E
572 w			E
	590 vs	590 w	A_1
637 w			E
644 w			E
676 vw	678 vs	678 vs	A_1
692 vw			E
728 s	721 w		A_1
	738 w		
753 s	753 w	750 w	E
779 w	777 w		A_1
	786 w		
802 w			E
	836 vs	833 w	A_1
	855 w		
875 w			
900 s			E

TABLE 4:2 Cont'd Molecular Frequencies of VOPc

infrared (200-nm film)	SERS	SERRS	symmetry
	947 w	946 w	
954 w			
1002 m	1001 vs	1001 w	A_1
	1033 w		
1080 vs			E
	1106 w	1105 w	A_1
1119 vs			E
	1141 m	1140 m	A_1
1163 m			E
1288 s			E
	1304 w	1304 m	
1333 vs			E
	1338 vs	1338 vs	A_1
	1398 w		
1418 s			E
1428 w	1430 w	1428w	E
1448 w	1443 m	1443 w	
1457 w			E
1463 w	1467 w		E
1477 w	1479 w		E
1500 s			E
1505 sh			
1521 w	1525 vs	1523 vs	A_1
	1589 m	1589 w	A_1
	1610 m	1610 w	

Raman Studies of VOPC on Reflecting Surfaces

Ultrathin films of VOPc were evaporated on smooth metal surfaces of Ag, Cu, and Au. Metal films(200 nm thick) were formed by evaporating metal at a rate of 0.5 nm/s to glass substrates maintained at room temperature. An overcoat of 10 nm of VOPc was then evaporated onto the metal coated substrate which was maintained at 200 °C. Long delay times of 7 s/cm^{-1} were required to obtain polarized Raman spectra of these samples. All spectra were recorded at an angle of incidence of 60°.

The SS, SP, PP, and PS spectra for 10 nm VOPc on smooth silver are shown in Figure 4.5 and Figure 4.6. It can be seen that there were essentially two different types of spectra since the SS=PP spectrum and the SP=PS spectrum. This was a clear indication that the relative intensity of different irreducible representations was sensitive to the molecular orientation of the molecules on the surface. The spectra could not be entirely considered in the context of surface selection rules for adsorbates on a reflecting surface.[27] At 514.5 nm and for Ag, Cu, Au surfaces, Raman modes transforming as a_{zz}(z normal to the surface) should give strong Raman signals followed by a_{xz} and a_{yz}, while a_{xx}, a_{yy} and a_{xy} should be weak. The main signals in the SS(or PP) spectra were assigned to the A_1 irreducible representation. The SP(or PS) however contained mostly E and B_2 species.

Similar polarized spectra were also recorded for VOPc evaporated onto glass coated with a 200 nm film of Au and Cu. The SS and SP spectra for VOPc on smooth Au is shown in Figure 4.7. Polarization effects in RRS(excitation at 647.1 nm) were not as pronounced as they were in the RS recorded with the 514.5 nm laser

Figure 4.5 SS and SP Raman Spectra of 10 nm thin film of VOPc deposited on 200 nm Ag film.

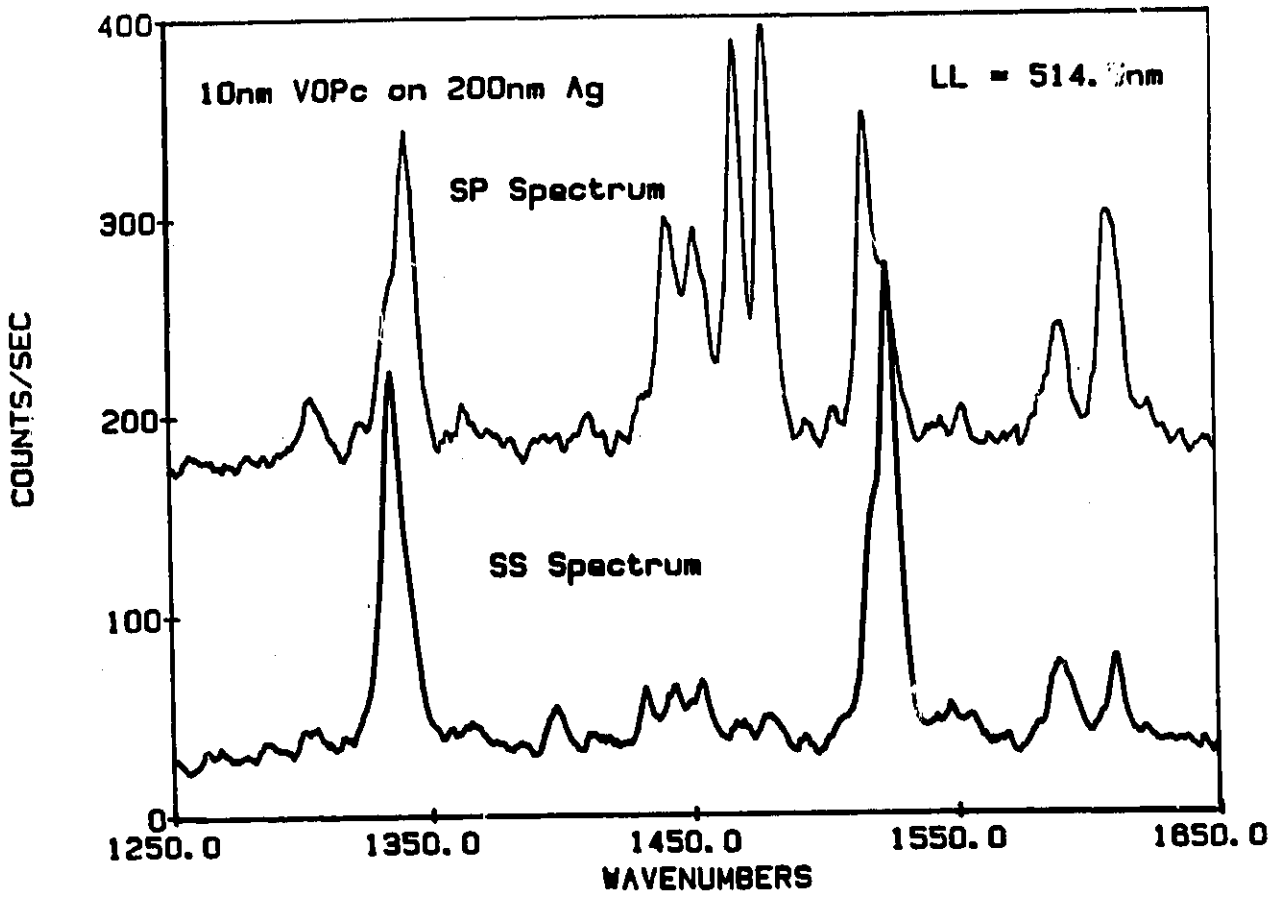
400
300
200
100
0
10nm VOPc on 200nm Ag
LL = 514.5nm
SP Spectrum
SS Spectrum
COUNTS/SEC
1250.0
1350.0
1450.0
1550.0
1650.0
WAVENUMBERS

Figure 4.5

Figure 4.6 PP and PS spectra for 10 nm VOPc on 200 nm Ag film

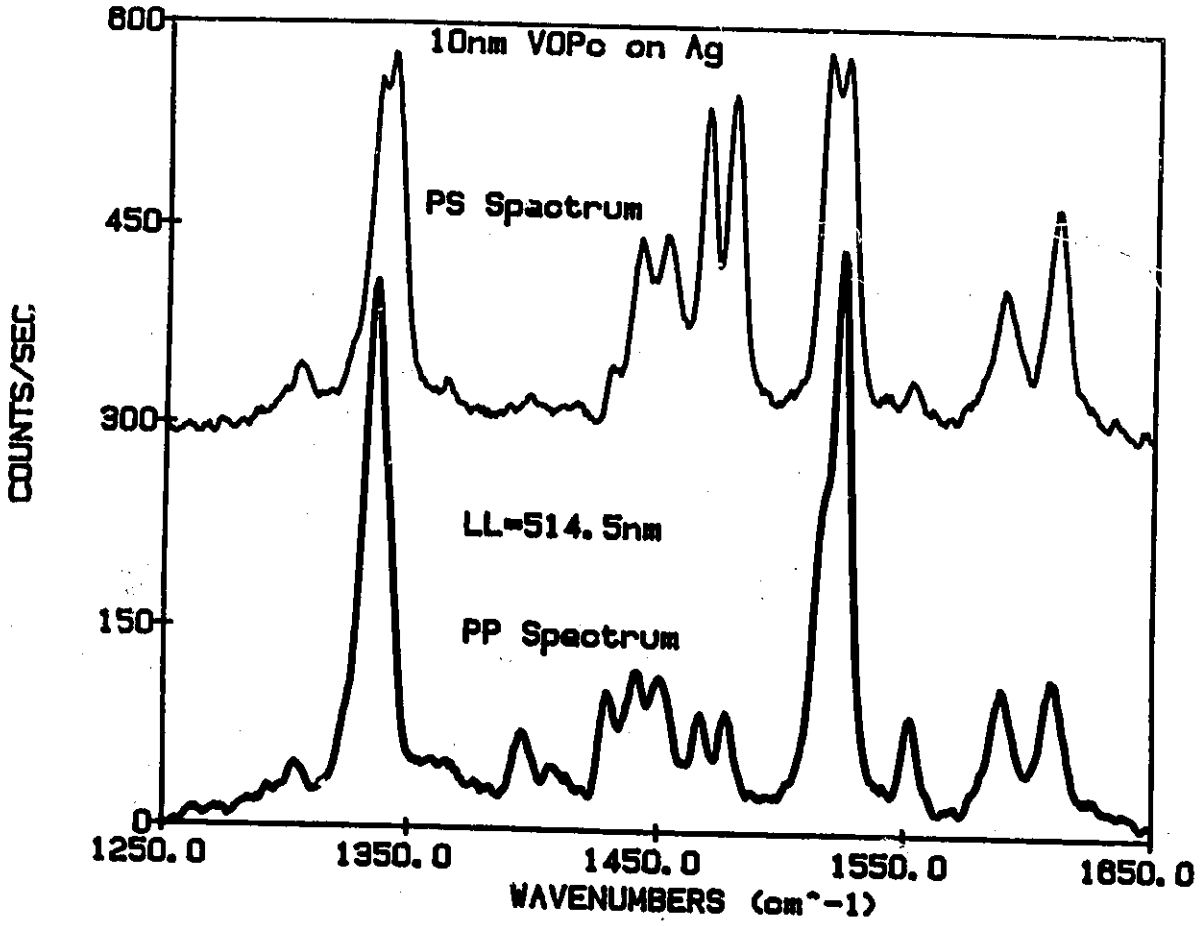
10nm VOPo on Ag
PS Spectrum
LL=514.5nm
PP Spectrum
COUNTS/SEC
800
450
300
150
0
1250.0
1350.0
1450.0
1550.0
1650.0
WAVENUMBERS (cm^-1)

Figure 4.6

line.

Enhanced Raman intensity(minor enhancement due to reflection) was indeed observed for totally symmetric bands with P-polarized incident light at an angle of incidence of 60°. The intensity of the A_1 species in the PP spectrum was about 2.5 times stronger than in the SS spectrum. The results were in agreement with the favourable excitation of P-polarized light based on the Fresnel coefficients and the enhanced normal fields. In Raman spectroscopy one would have normally expected to observe the totally symmetric bands with more intensity in the SS spectra than the PP spectra. For a 200 nm VOPc film on glass, the overall intensity of the A_1 modes in the SS spectrum was indeed stronger than that of the PP spectrum for a 60° incidence For adsorbed molecules on mirror surfaces, the total S-polarized field on the molecule was diminished by the out-phase component of the S-polarized reflected light.

Davydov doublets were distinctly observed in the 1340 cm^{-1} and 1520 cm^{-1} regions with components of different irreducible representations. The 1338 and 1525 cm^{-1} bands were assigned to an A_1 type in the SERS of VOPc. The second components at 1343 and 1517 cm^{-1} were only observed in the SP and PS spectra and were not observed in the infrared. These bands hence were not E species. The only possible assignment for both frequencies was to the B_2 irreducible representation. The symmetry assignment of VOPc in the isoindole spectral region is found in Table 4.3.

The samples[10 nm VOPc/(200 nm metal)] were then overlaid with a rough surface of silver by evaporating 10 nm silver onto the samples maintained at 200 °C. The absorption spectrum for the silver island film on glass showed a plasmon

Figure 4.7 Ramar. spectra of 10 nm thin film of VOPc on 200 nm Au

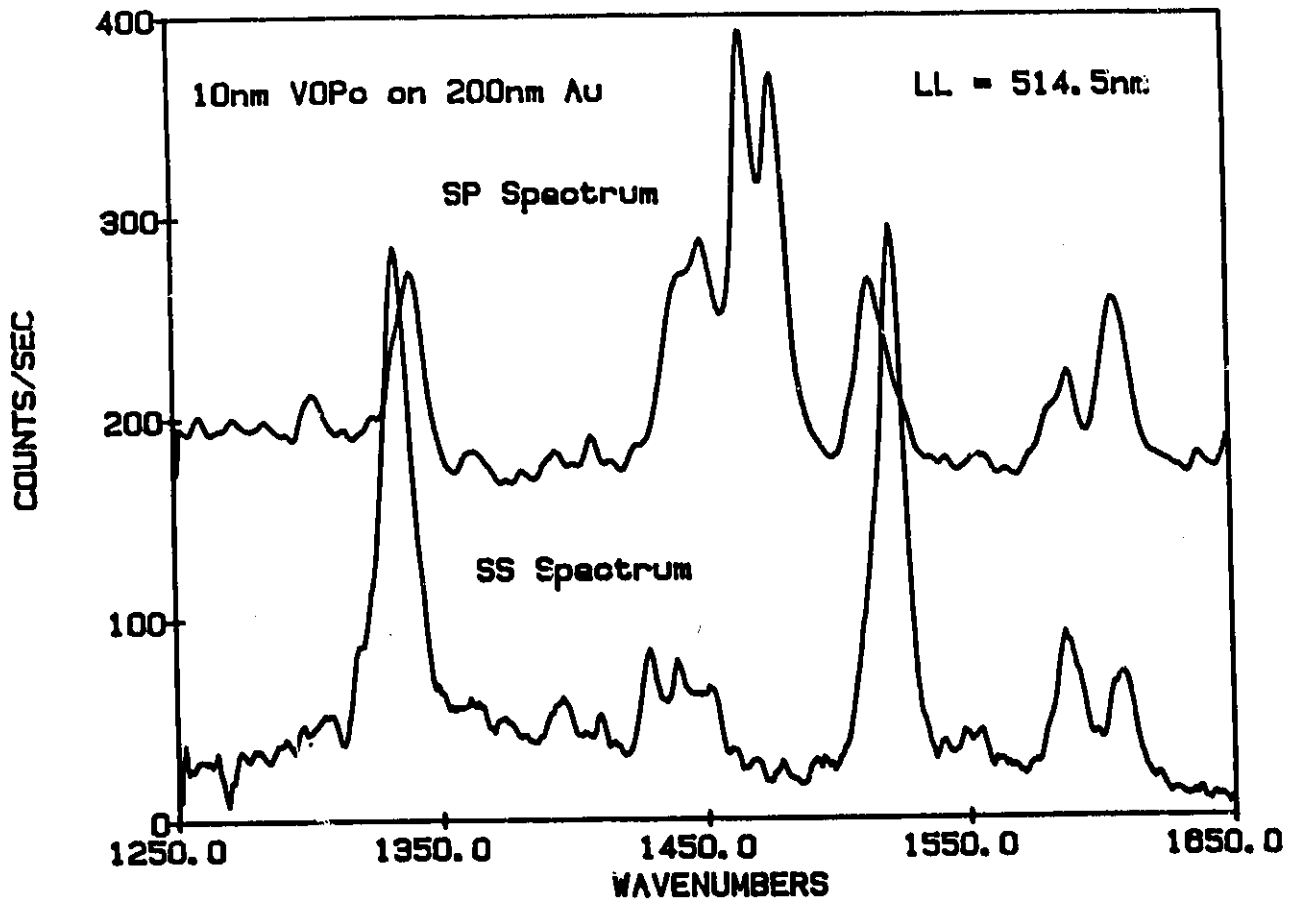
10nm VOPo on 200nm Au
LL = 514.5nm
SP Spectrum
SS Spectrum
COUNTS/SEC
400
300
200
100
0
1250.0
1350.0
1450.0
1550.0
1650.0
WAVENUMBERS

Figure 4.7

TABLE 4.3 Symmetry Assignments in the Region of the Isoindole Stretching Vibrations for VOPc

IR	SP	SS	SERS	Symmetry
1288 s				E
	1304 w	1304 vw		B_2
1333 s				E
	1337 sh	1337 sh	1338 s	A_1
	1343 vs			B_2
1398 vw		1398 w	1398 w	A
1419 m				E
		1430 w	1430 w	
	1442 m	1442 w	1443 w	B_2
	1453 m	1453 w	1453 w	B_2
1463 m	1467 vs	1467 w	1467 w	E
1479 m	1479 vs	1479 w	1479 w	E
1500 s				E
	1517 vs	1517 vs		B_2
1521 w	1525 sh	1525 vs	1525 vs	A_1
1541 w	1541 w			E
	1589 m	1589 w	1589 w	A_1
1610 w	1610 s	1610 w	1610 w	E

Figure 4.8 SERS of 10 nm overlayer of Ag evaporated onto the (10 nm VOPc/200 nm Ag) sample. SS and SP polarized spectra

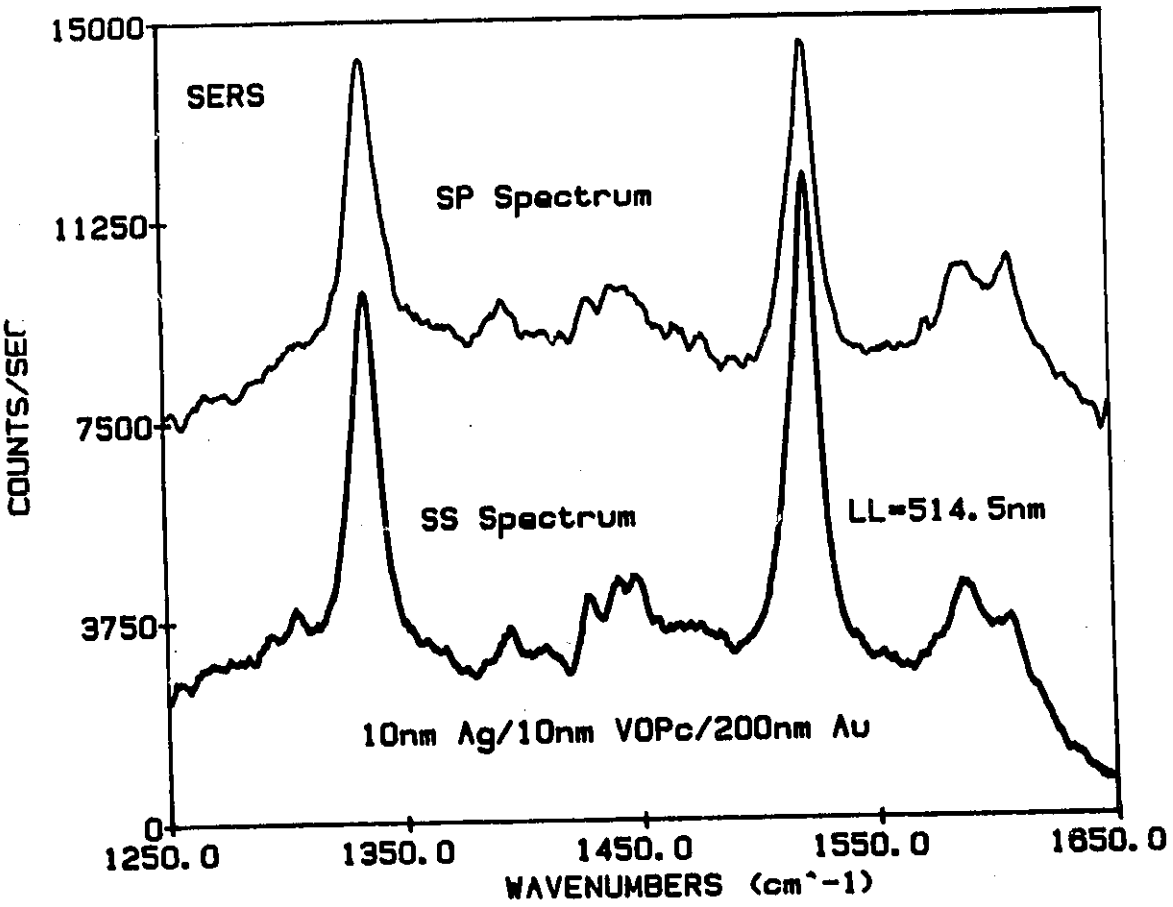
15000
11250
7500
3750
0
COUNTS/SEC
SERS
SP Spectrum
SS Spectrum
LL=514.5nm
10nm Ag/10nm VOPc/200nm Au
1250.0
1350.0
1450.0
1550.0
1650.0
WAVENUMBERS (cm^-1)

Figure 4.8

absorption centred at 500 nm. Molecular vibrations in SERS and SERRS were observed unshifted with respect to the values recorded in the thin solid film and indicated that the molecules were *physisorbed* onto the metal surface. Under similar conditions it was found that the overall intensity in the SERS spectra was less than that in the SERRS spectra. The greater scattering efficiency in SERRS was attributed to the superposition of two enhancements via 1) a large scattering cross section due to excitation in resonance with the molecular electronic absorption of VOPc, and 2) electromagnetic enhancement due to resonance with the localized surface plasmons on the silver island film. Another important observation was that the polarized spectra that were recorded for VOPc on smooth metal were replaced by depolarized spectra when the samples were overlaid with the island film of silver. SERS spectra were depolarized, in the sense that all four polarization combinations(i.e., SS, SP, PP, PS) gave rise to the same general spectrum. For a practising Raman spectroscopist this means that polarization techniques like those used to probe individual symmetry species in crystalline samples cannot effectively be used in a SERS investigation. The depolarization effect in SERS can be seen by comparing Figures 4.4 and 4.8. The spectra in Figure 4.8 also showed that the Davydov doublets were reduced to a single band in the 1340 and 1520 cm^{-1} region. Evaporating the overlayer of silver had the effect of interfering with the solid state effect that gave rise to Davydov splitting.

IR and SERS of LB Monolayers of VOPcTTB and ZnPcTTB

The vibrational characterization of vanadyl tetra-*tert*-butylphthalocyanine (VOPcTTb) and zinc tetra-*tert*-butylphthalocyanine(ZnPcTTb) was attempted by considering the IR , RS and SERRS data. Both molecules have a four-fold principal axis and the *tert*-butyl groups could produce four isomers.[28] The first step was to separate the frequencies of the parent molecule(i.e., VOPc[11] and ZnPc[12]) from those of the *tert*-butyl groups. A direct comparison of the IR and RS spectra of the parent molecule with the *tert*-butyl substituted molecules allowed a clear separation of the Pc and *tert*-butyl frequencies. The IR spectra illustrated in Figure 4.9 showed that a number of new bands were present in the spectra of VOPcTTB. These bands were assigned to the *tert*-butyl moieties and marked(t) in the spectrum. The VOPc vibrations affected by the substitution were the wagging vibrations of the peripheral C-H groups at 728 cm^{-1} and the C-H bending at 1119 cm^{-1}. The C-H stretching vibrations of the *tert*-butyl groups were observed with strong relative intensity in the IR. Similar observations were made for ZnPcTTb. The RS and RRS spectra were dominated by the vibrational frequencies of the parent Pc molecule. This was in agreement with the fact that the Raman cross section of molecular vibrations associated with conjugated systems are much larger than those of saturated groups.

SERRS of Langmuir-Blodgett layers of VOPcTTb and ZnPcTTb were also studied. The first step was to obtain the isotherm which would give the stable pressure range at which the Langmuir layer could be transferred to the SERS substrate. The phthalocyanines were dissolved in toluene([Pc]=2.5 $x10^{-4}$ M) and

Figure 4.9 Infrared absorption spectra of VOPc and VOPcTTb in KBr pellets.

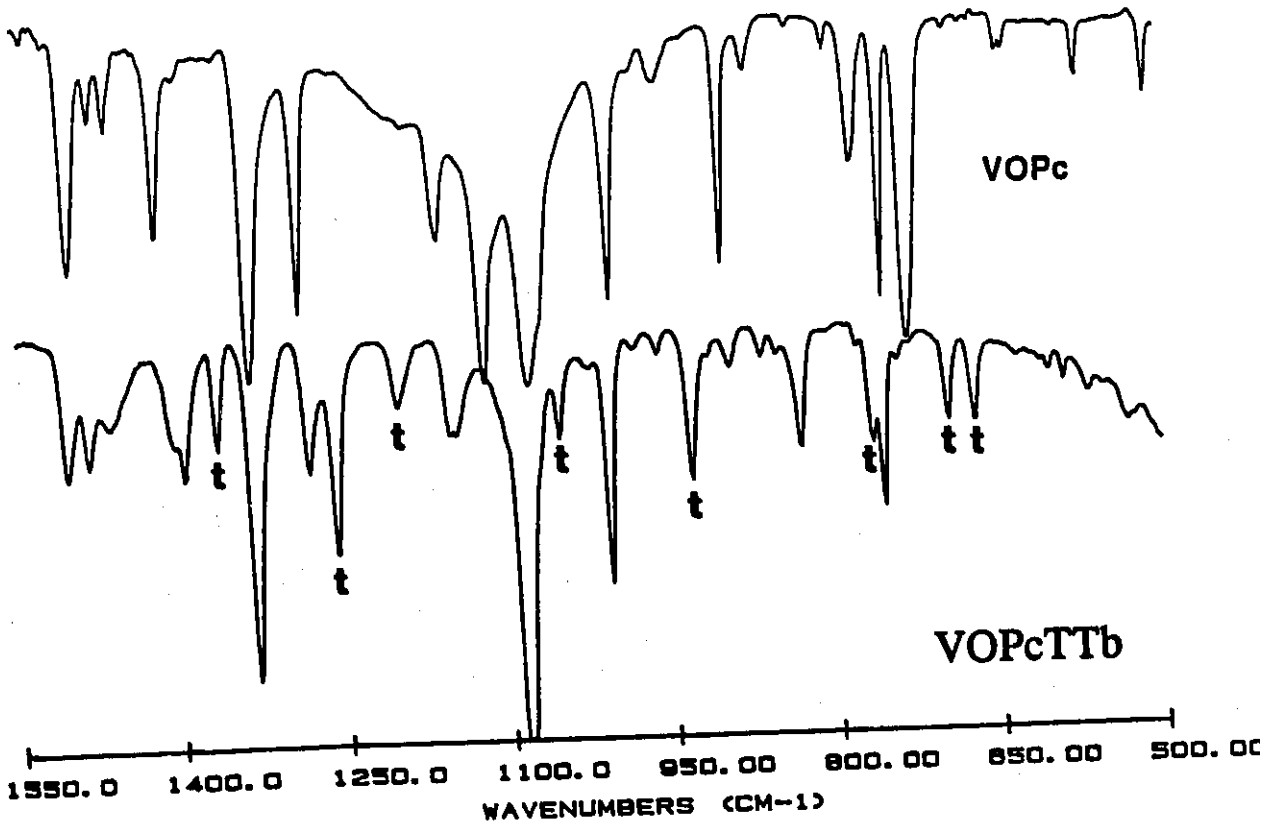
VOPc
t
t
t
t
t
t
t
t
VOPcTTb
1550.0
1400.0
1250.0
1100.0
950.00
800.00
650.00
500.00
WAVENUMBERS (CM-1)

Figure 4.9

Figure 4.10 Surface pressure versus area isotherms for VOPcTTb and ZnPcTTb.

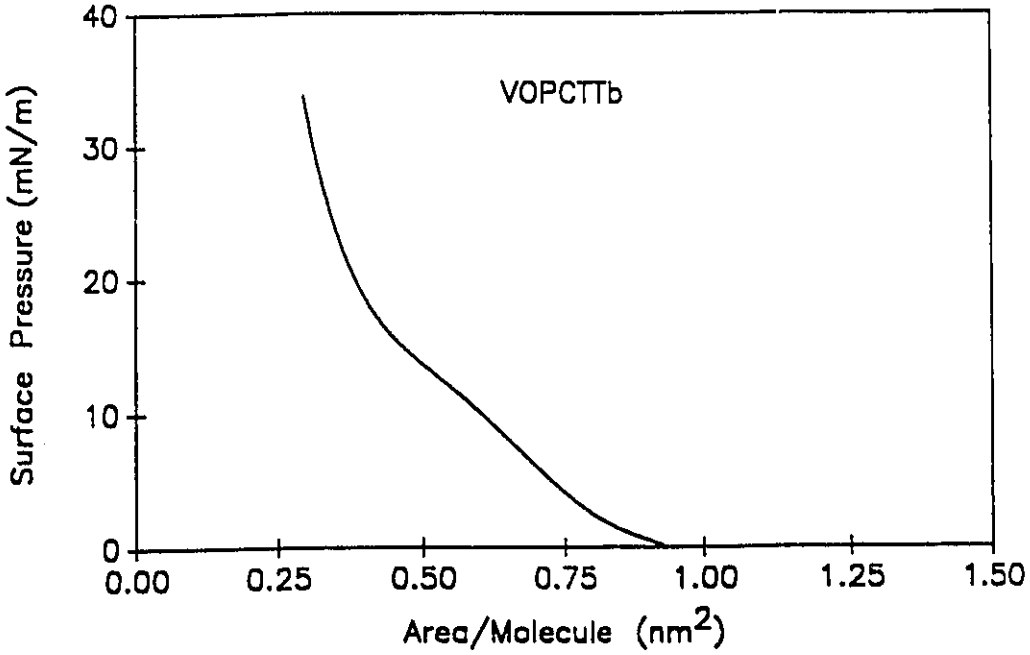
VOPCTTb
Surface Pressure (mN/m)
40
30
20
10
0
0.00
0.25
0.50
0.75
1.00
1.25
1.50
Area/Molecule (nm2)

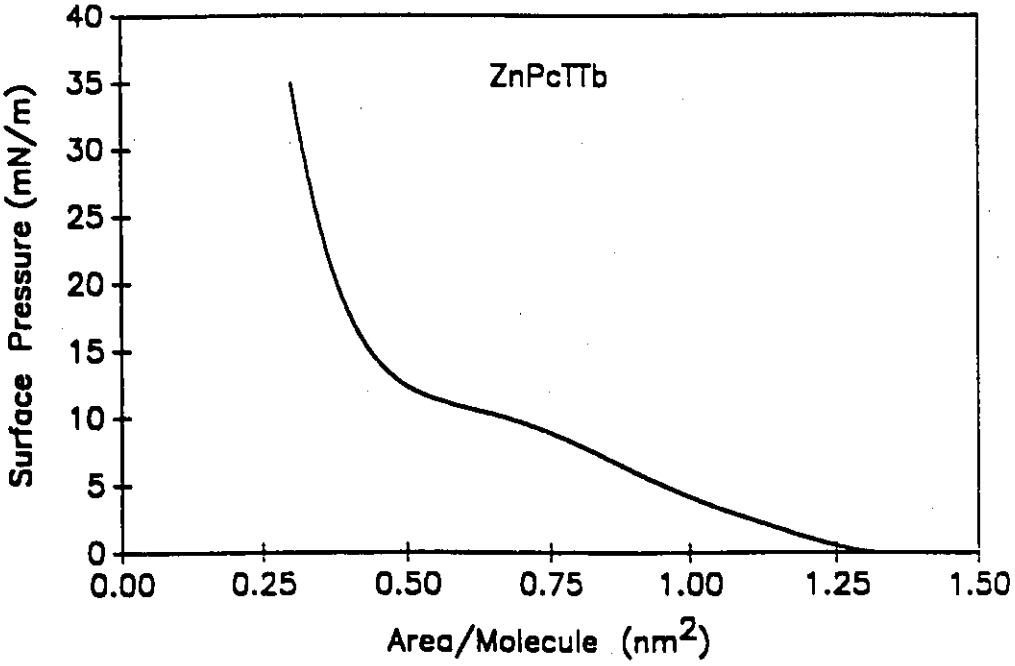
ZnPcTTb
Surface Pressure (mN/m)
40
35
30
25
20
15
10
5
0
0.00
0.25
0.50
0.75
1.00
1.25
1.50
Area/Molecule (nm2)

Figure 4.10

spread by a syringe onto the subphase which was thermostated at 20 ℃. For both molecules, the compression rate during the acquisition of the isotherm was 0.001 nm^2/molecule/s. The isotherms were reproducible for both phthalocyanines and are presented in Figure 4.10. The isotherm showed that surface pressures less than ca. 35 mN/m could be used for LB transfer. The surface pressure was measurable at ca. 1 nm^2/molecule. At the molecular area ca. 0.5-0.3 nm^2 the surface pressure increased steadily as expected for the monolayer in a tightly packed crystalline state. The limiting area was found by extrapolating the most linear part(where the surface pressure increased steadily with molecular area) to zero surface pressure. The limiting area for both molecules was about 0.5 nm^2/molecule. The isotherm of ZnPcTTb was reported in 1985 by Hann et al.[29] who used xylene as the spreading solvent. Their isotherm also showed that the surface pressure was measurable at ca. 1.4 nm^2 but their limiting area of 1.20 nm^2/molecule was much larger than that in our study. Roberts et al.[30] noted that the isotherm is dependent on the spreading solvent, yet three[29-31] groups who all used xylene as the spreading solvent report 0.87nm^2, 0.96nm^2, and 0.60nm^2 for the limiting area for CuPcTTb. The inconsistent data from the these groups suggest that serious research in the isotherm of phthalocyanine derivatives is still required. Molecular association as described by Snow et al.[32] cannot completely account for the range in the limiting areas reported for CuPcTTb where the bulky *tert*-butyl groups are expected to reduce or prevent aggregation. Our group, in collaboration with Dr. DeSaja at the Universidad de Valladolid(in Spain) is currently comparing isotherm data collected under similar experimental conditions but

on different film balances.

Langmuir-Blodgett monolayers of ZnPcTTb and VOPcTTb were transferred to clean glass slides, Ag-Sn spheres, and 10 nm Ag island films at a constant surface pressure of 10 mN/m. The substrate was immersed in the subphase prior to spreading the phthalocyanine solution. Compression was done under constant surface pressure mode. The monolayer was maintained at 10 mN/m, for a period of time(ca 30 min.) that it took the moving barrier to completely stabilize and remain at a constant position. The stable Langmuir layer was then transferred to the substrate at a rate of 4.8 mm/min. The entire process was completely repeated in multilayer LB assemblies. The transfer ratio(defined[33] as the ratio of the area removed from the water surface to the area on the substrate coated with the monolayer) was near unity on the glass substrates, 1.7 on Ag-Sn spheres, and 1.2 for Ag island films. Transfer ratios in excess of unity were attributed to the increase in surface area due to the surface roughness in the SERS substrates.

A linear dependence of absorbance was noted for 1,2 and 3 LB layers of ZnPcTTb and VOPcTTb on glass and suggested uniform deposition of Pc during each transfer cycle. The SERRS spectra(SS, SP, PP, PS) for one LB of ZnPcTTb or one LB VOPcTTb were all identical to the RRS (SS polarization) for 3 LB on glass. Consequently, the SERRS spectra were all depolarized(i.e., the relative intensities of bands in the SS-component were equal to those in the SP, PP or PS spectrum). Similarly all SERS spectra excited with the 514.5 nm line were all depolarized. Since all the fundamental frequencies were observed unshifted from their values in LB films

on glass or in thin solid films, the molecules were *physisorbed* onto the SERS surfaces. The SERRS of VOPcTTb and ZnPcTTb are presented in Figures 4.11 and 4.12. For both molecules the SERRS spectra was dominated by frequencies of the macrocycle, and the relative intensity of the peripheral groups was almost negligible. A partial characterization of the vibrational spectra of VoPcTTb and ZnPcTTb is presented in Tables 4.4 and 4.5.

Figure 4.11 SERRS spectra of 1 LB of VOPcTTb on Ag-Sn spheres. S and P incident polarization and total collection.

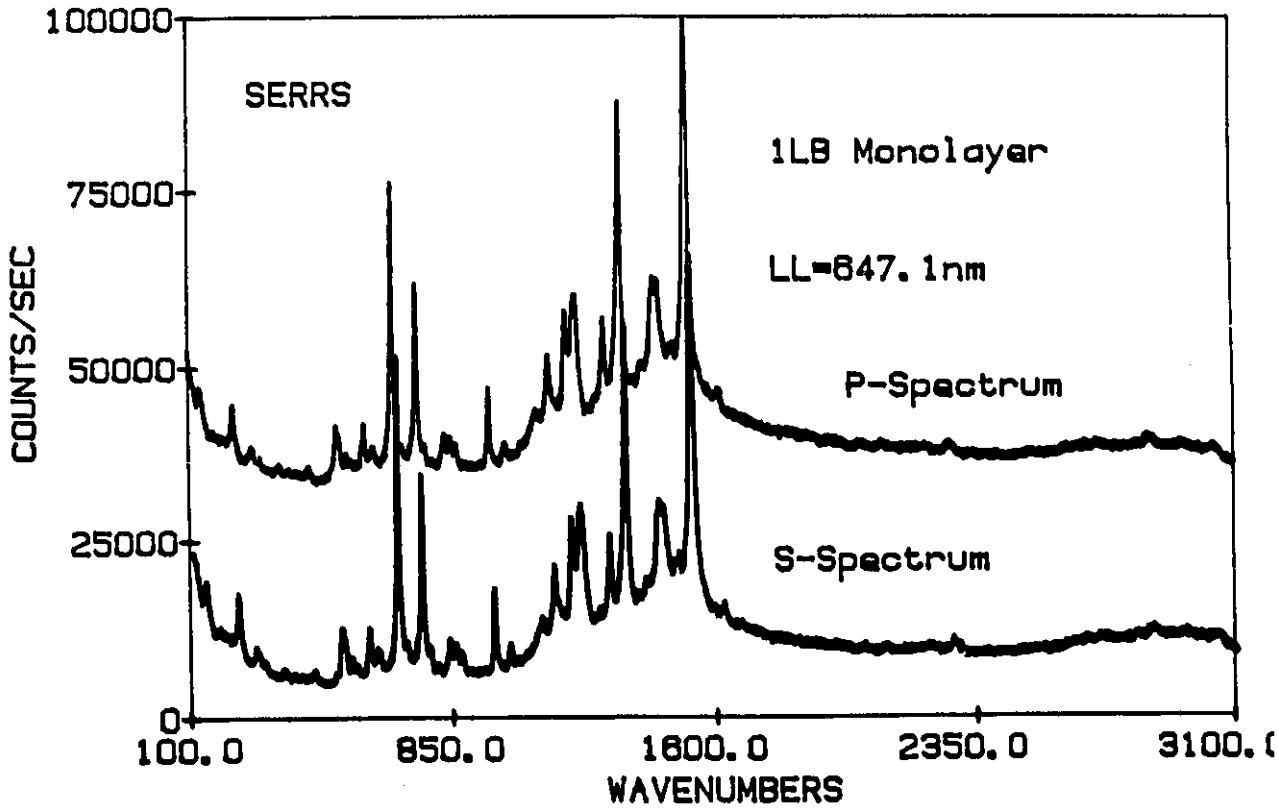
100000
75000
50000
25000
0
COUNTS/SEC
SERRS
1LB Monolayer
LL=647.1nm
P-Spectrum
S-Spectrum
100.0
850.0
1600.0
2350.0
3100.0
WAVENUMBERS

Figure 4.11

Figure 4.12 SERS of one LB of ZnPcTTb on Ag-Sn spheres.

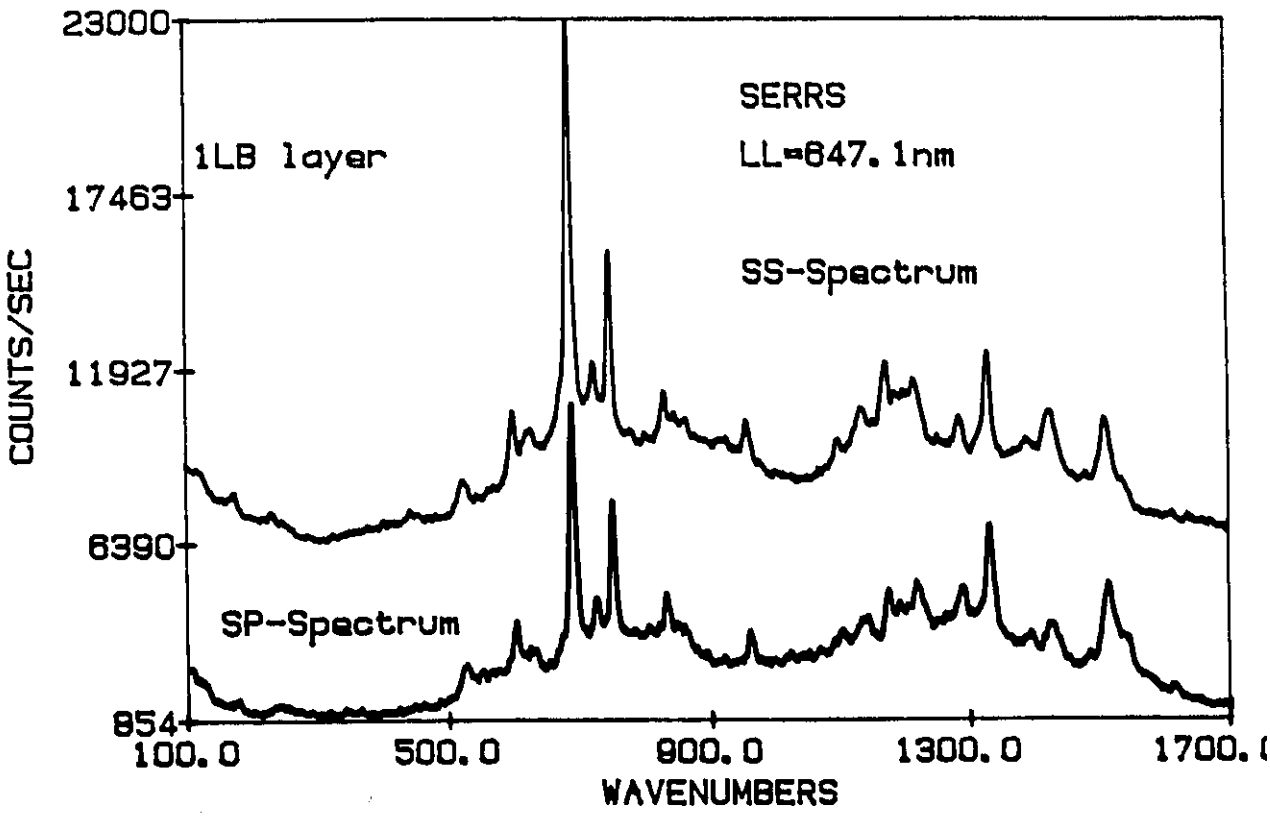
23000
17463
11927
6390
854
COUNTS/SEC
1LB layer
SERRS
LL=647.1nm
SS-Spectrum
SP-Spectrum
100.0
500.0
900.0
1300.0
1700.0
WAVENUMBERS

Figure 4.12

Table 4.4 Observed Vibrational Frequencies of VOPcTTb

Infrared	RS(solid)	SERRS	Assignment
	132 m	132 w	Pc deformation
		226 w	Isoindole def.
	278 m	278 w	Pc deformation
530 m		525 m	t-butyl def.
546 w		550 vw	t-butyl def.
601 w	603 m	603 m	Benzene def.
	631 m	631 w	t-butyl wag
	685 vs	685 vs	Pc breathing
695 m			t-butyl wag
	708 w	708 w	Pc
755 m	754 m	754 s	Pc
765 m			t-butyl wag
778 w		777 w	Pc
830 m	831 m	831 w	Pc ring st.
851 w	850 m	850 w	Pc
865 w	865 m	865 w	C-H bend (tb)
930 s			C-H bend (tb)
960 w	956 w	958	Benz. ring
	1003 s	1003 w	C-H bend (Pc)
1050 m			C-C st. (tb)
1086 vs		1089 vw	C-H bend (pc)
	1127 w	1127 m	C-H bend (Pc)
	1175 w	1175 m	C-H bend (Pc)
1200 m	1200 vw	1202 m	C-H bend (Pc)
1219 w			C-H bend (tb)
1257 s			C-H bend (tb)
1281 m	1282 w	1282 m	C-H bend (Pc)
1330 vs	1330 vs	1330 s	Pyrrole st.
1364 s			C-H- bend (tb)
1393 s	1387 m		Isoindole st.
1483 m	1478 w	1480 w	Isoindole st.
1503 m			Isoindole st.
	1523 vs	1523 vs	Pyrrole st.
	1584 m	1587 vw	Benzene st.
1613 m	1610 s	1610 vw	Benzene st.
2864 m			C-H st. (tb)
2902 m			C-H st. (tb)
2956 s			C-H st. (tb)
3072 w			C-H st. (Pc)

Table 4.5 Vibrational Frequencies of ZnPcTTb

Infrared	RRS (Film)	SERRS	Interpretation
		174 w	Pc deformation
	230 w	230 vw	Zn-N st.
526 m	526 m	526 w	t-butyl def.
567 m			t-butyl def.
588 m			t-butyl def.
603 m	601 m	601 m	Benzene, def.
670 s			t-butyl wag
	687 vs	687 vs	Pc breathing
735 sh		723 m	t-butyl wag
745 vs	748 s	748 s	Pc
763 s			t-butyl wag
779 w	782 w	779 vw	Pc
828 s	828 w	830 m	Pc ring st.
848 w	847 w	847 vw	Pc
862 w	861 w	863 vw	C-H bend (tb)
893 m			C-H bend (tb)
923 s		925 vw	C-H bend (tb)
958 m	958 m	958 m	Benz. ring
1006 w			C-H-bend (Pc)
1023 w			C-H bend (tb)
1048 s			C-C st. (tb)
1090 vs		1097 w	C-H bend (Pc)
1146 s			C-H bend (tb)
1151 s			C-H bend (tb)
	1172 m	1172 m	C-H bend (Pc)
1200 m	1200 sh	1200 vw	C-H bend (Pc)
	1216 m		C-H bend (tb)
1257 s		1254 w	C-H bend (tb)
1280 s	1285 m	1285 w	C-H bend (Pc)
1332 s	1330 s	1330 s	Pyrrole st.
1363 s			C-H bend (tb)
1393 s	1388 w	1392 vw	Isoindole st.
	1425 m	1424 m	Isoindole st.
1489 vs			Isoindole st.
	1510 vs	1510 s	Pyrrole st.
1540 w			Aza stretch
1559 w			
1614 s	1611	1614 w	Benzene st.
2866 s			C-H st. (tb)
2902 s			C-H st. (tb)
2955 vs			C-H st. (tb)
3075 m			C-H st. (Pc)

Energy Transfer in LB Monolayers and Selective Spectroscopic Tuning

It was recently shown that neat LB layers of N-octyl,N-isobutyl-3,4:9,10-perylene-bis-dicarboximide(PBDC) produced surface enhanced fluorescence with a broad emission at 648-nm which was attributable to excimer formation.[34] The broad emission was also observed for other perylene derivatives.[35] In a series of LB reports[34,36] it was shown that there were at least two processes that could be used to describe fluorescence from molecules adsorbed on rough metal surfaces. There is fluorescence enhancement that results from the electromagnetic field enhancement on the SERS surface and fluorescence quenching due to the nonradiative transfer of the electronic excitation energy to the surface plasmons.[34-38] In some cases luminescence may be completely removed for molecules in close proximity to a metal surface since the lifetime of the molecular excited state may be considerably shortened in the presence of the metal.[38] Further studies of energy transfer with LB on rough metal surfaces were considered in our laboratory. In particular our objective was to investigate energy transfer from a sensitizer(or energy donor) LB layer to an activator(or energy acceptor) LB layer on a rough metal surface. The energy transfer between dyes in LB assemblies on glass substrates is well documented in the classical studies by Kuhn and coworkers.[39-41]

The excimer emission of PBDC centered at 648 nm served as the energy donor and the broad absorption band of ZnPcTTb at 680 nm served as the energy acceptor. Three unique configurations of PBDC and ZnPcTTb were investigated on Ag-Sn spheres. The first sample was made by putting the donor layer adjacent the rough

metal surface[i.e., (1LB ZnPcTTb/1Lb PBDC/Ag-Sn)]. In the second assembly the configuration of donor and acceptor layers was reversed [i.e., (1LB PBDC/1LB ZnPcTTb/Ag-Sn)]. The third sample consisted of a mixed layer of ZnPcTb and PBDC in the mole ratio 1:1. In all LB preparations, the monolayer was compressed to a constant surface pressure of 10 mN/m and the substrate was withdrawn at a rate of 4.8 mm/min. The 514.5 nm laser line was used to study the energy transfer process. This laser line was in full resonance with molecular absorption band in PBDC and outside the visible absorption band of ZnPcTTb.

Surface enhanced resonance Raman scattering for sample one is shown in the lower trace of Figure 4.13. The intense broad band corresponds to the excimer emission of PBDC and there was no qualitative evidence of energy transfer between donor and acceptor layers. In our experiment, the absence of excimer emission would be indicative of good energy transfer. The upper spectrum where PBDC was separated from the surface by a layer of arachidic acid, was typically observed for enhanced fluorescence and long range electromagnetic Raman enhancement. As expected the fluorescence enhancement increased when the chromophore was separated by a spacer layer of arachidic acid from the rough surface.[36] The weak Raman intensity of PBDC bands in the upper spectrum can be attributed to the decay in the electromagnetic enhancement as the Raman scatterer was separated from the SERS surface.[42,43]

The spectra shown in Figure 4.14 were taken from a sample that was prepared by first overcoating one half of the SERS substrate with one monolayer of ZnPcTTb

Figure 4.13 Surface enhanced Raman and fluorescence of PBCD in a two layer structure. One LB of PBDC separated from the surface by one LB of arachidic acid(upper trace). The spectrum of the {1LB ZnPcTTb/1LB PBDC/Ag-Sn spheres} assembly is shown in the lower trace.

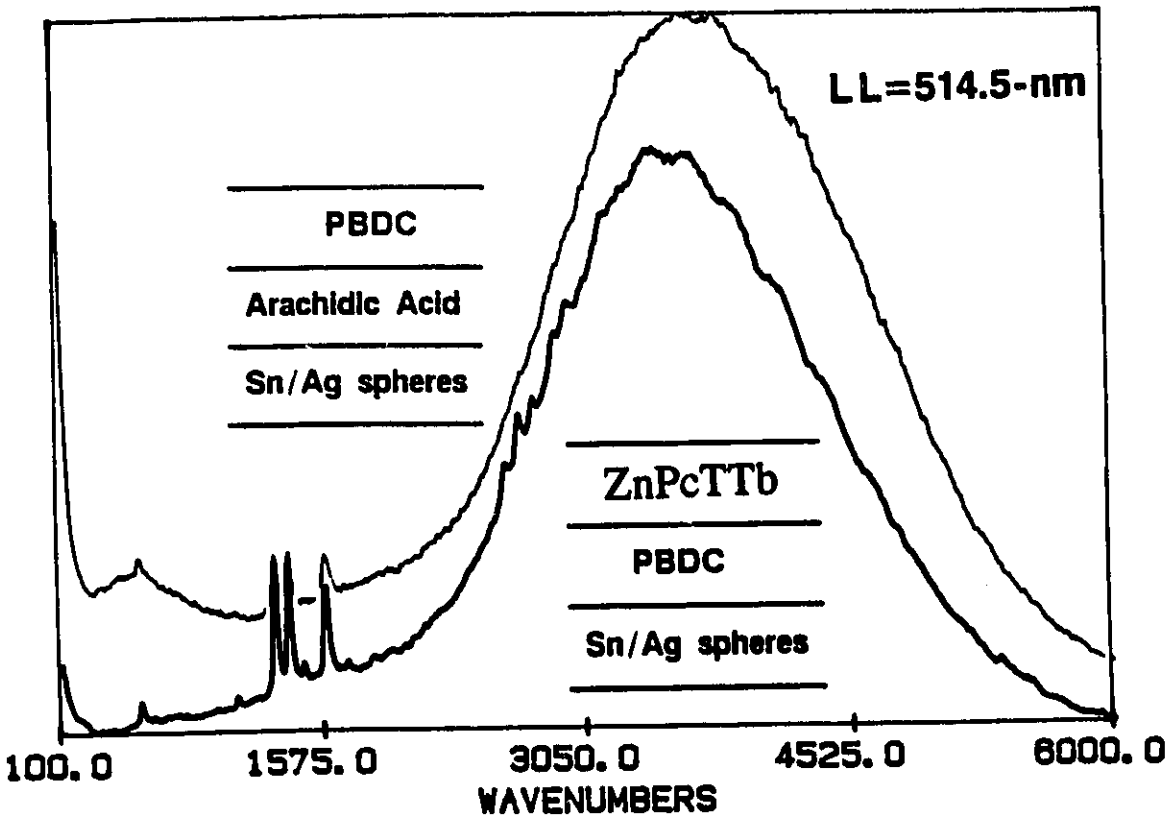
LL=514.5-nm
PBDC
Arachidic Acid
Sn/Ag spheres
ZnPcTTb
PBDC
Sn/Ag spheres
100.0
1575.0
3050.0
4525.0
6000.0
WAVENUMBERS

Figure 4.13

and then adding a second LB of PBDC to the entire substrate. The upper trace contained the typical SERRS and excimer emission of PBDC. The lower spectrum was recorded with the energy acceptor layer directly adjacent to the rough surface. In this case the excimer emission of perylene was completely quenched by the acceptor layer. The spectral evidence in Figures 4.13 and 4.14 clearly shows that the absorption efficiency of the acceptor(i.e., ZnPcTTb) layer was enhanced by the metal surface allowing complete energy transfer from the donor to the acceptor layer. The results are in agreement with enhanced absorption and luminescence of adsorbed molecules on rough metal surfaces.[38,44]

In the third sample a mixed monolayer of PBDC and ZnPcTTb in a 1:1 mole ratio was transferred to Ag-Sn spheres. The results indicated that there was very little energy transfer in the mixed LB layer since the excimer emission of PBDC was strongly observed.

The accumulative results indicate that the most efficient LB structure for energy transfer was the two layer assembly with the acceptor layer adsorbed directly onto the metal surface. It was also important to note that there was no interference from ZnPcTTb in the spectra recorded with 514.5 nm laser line. Spectra recorded with 647.1 nm(in resonance with red absorption band of ZnPcTTb) excitation gave typical spectra of ZnPcTTb without any interference from PBDC. The choice of laser lines in resonance with one or the other molecular species demonstrated selective spectroscopic tuning in a two component system. Excitation at 514.5 nm produced SERRS of PBDC without any spectral interference of ZnPcTTb. Excitation at 647.1

Figure 4.14 Surface enhanced Raman scattering and fluorescence of 1 LB of PBDC directly on Ag-Sn spheres(upper trace) and of the assembly {1LB PBDC/1LB ZnPcTTb/Ag-Sn spheres} (lower trace)

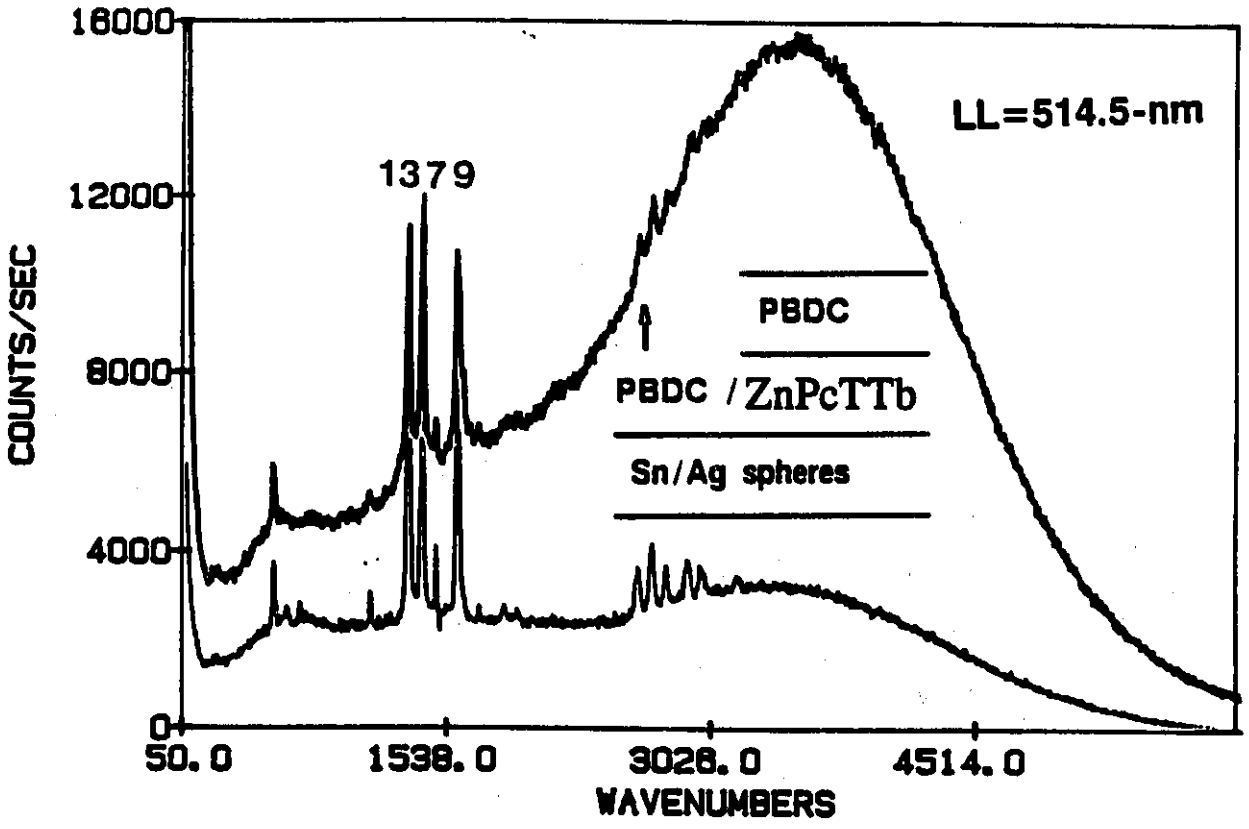
16000
12000
8000
4000
0
COUNTS/SEC
1379
LL=514.5-nm
PBDC
PBDC /ZnPcTTb
Sn/Ag spheres
50.0
1538.0
3026.0
4514.0
WAVENUMBERS

Figure 4.14

Figure 4.15 SERRS of ZnPcTTb for the assembly {1LB PBDC/1LB ZnPcTTb/Ag-Sn spheres}. Only the SERRS of ZnPcTTb is revealed with 647.1nm excitation.

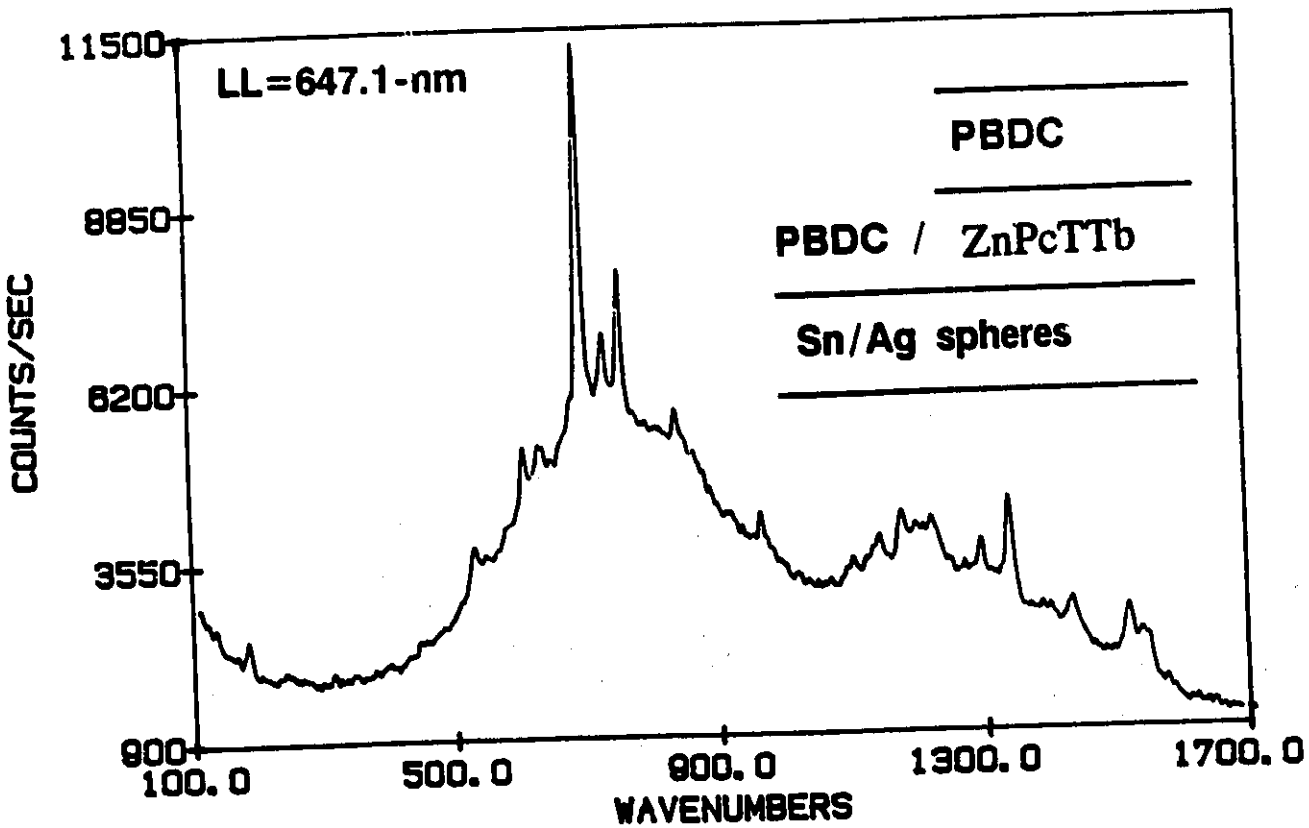
11500
8850
6200
3550
900
COUNTS/SEC
LL=647.1-nm
PBDC
PBDC / ZnPcTTb
Sn/Ag spheres
100.0
500.0
900.0
1300.0
1700.0
WAVENUMBERS

Figure 4.15

nm however was exclusively sensitive to the ZnPcTTb species and no Raman lines of PBDC were observed. The SERRS of ZnPcTTb was observed without any interference from PBDC as shown in Figure 4.15.

CHAPTER 5: SERRS of Langmuir-Blodgett Monolayers:Coverage Dependence

Early coverage dependence studies of SERS were conducted in ultra high vacuum. The experiments were designed to investigate the intensity relationship of the SERS signal as the surface coverage of the adsorbate increased from 0 monolayers(ML) to a few ML. The most difficult aspect in the early experiment were the uncertainties to which surface coverage was measured. Rowe et al. measured surface coverage by measuring the carbon densities derived from Auger electron spectroscopy.[1] A quartz crystal oscillator was used to monitor pyridine coverage in the work published by Seki et al.[2] Sands et al. used UV-photoemission spectroscopy to calibrate the surface coverage of pyridine.[3] Radioactive tracing was used to measure coverage in ^{14}CN on Ag island films.[4,5] Surface coverage was determined spectrophotometrically for cobalt phthalocyanine on Ag films.[6] In 1988, Dr. Cotton's laboratory and our group independently submitted reports that used the Langmuir-Blodgett technique(for the first time) to investigate the SERRS intensity versus coverage dependence.[7,8] Both groups used mixed monolayers composed of dye and fatty acid to control precisely the surface coverage.

The surface coverage was controlled using mixed monolayers of vanadyl tetra-*tert*-butylphthalocyanine(VOPcTTb) and arachidic acid in various mole ratios of VOPcTTb:arachidic acid. All monolayers were spread from toluene solutions. Stock solutions of VOPcTTb(2.67×10^{-4} M) and arachidic acid(1.07×10^{-3} M) were used to prepare mixed solutions containing both species. In all cases the appropriate volume of the arachidic acid solution was added to 2 ml of the stock VOPcTTb solution to give the corresponding mole ratio of VOPcTTb:arachidic acid. Mixed monolayers were transferred to Ag-Sn spheres

and 4 nm Au island films. An internal standard(VOPcTTb:arachidic acid=10:1) was used to account for differences that may have existed among the SERS substrates. In particular, one LB of the internal standard was transferred to one half of the SERS substrate. The sample of variable composition was then transferred to the remaining portion of the SERS slide. The substrate was immersed into the subphase prior to monolayer compression. The Langmuir layer was compressed to 10 mN/m for ca. 25 min before being transferred at a rate of 4.8 mm/min. In another type of experiment, more than one mixed LB was transferred to the SERS substrate. These experiments were used to investigate the coverage dependence for mixed multilayer assemblies.

All coverage dependence studies for a given batch of SERS slides were run within the same day in attempt to keep the optical path, the power of the laser and other optical parameters constant. The samples were spun in a rotating cell, with the laser probing a circle of radius ca. 0.25 cm on the sample. This spinning sample effectively allowed scattering from an area average and not from a single location. The absorption spectra of 3 LB of VOPcTTb on glass and 4 nm Au island film showed a well defined broad band centred at 706 nm and 650 nm respectively. SERRS with excitation at 647.1 nm was therefore in resonance with both the molecular electronic absorption of VOPcTTb and the localized surface plasmons of Au. SERRS was also measured for VOPcTTb on Ag-Sn spheres.

SERRS was observed to peak at submonolayer coverage for cobalt phthalocyanine vacuum evaporated onto Ag islands.[6] The decrease in SERRS intensity was attributed to damping[6] of the surface plasmon resonance by the adsorbed layer. Zeman et al. used two theoretical models to show that overall Raman intensity factor was heavily dependent on

Figure 5.1 Submonolayer SERRS coverage dependence on Ag-Sn spheres and Au island films. The curve is for the 685 cm^{-1} band of VOPcTTb normalized to the internal standard(VOPcTTb:arachidic acid=10:1)

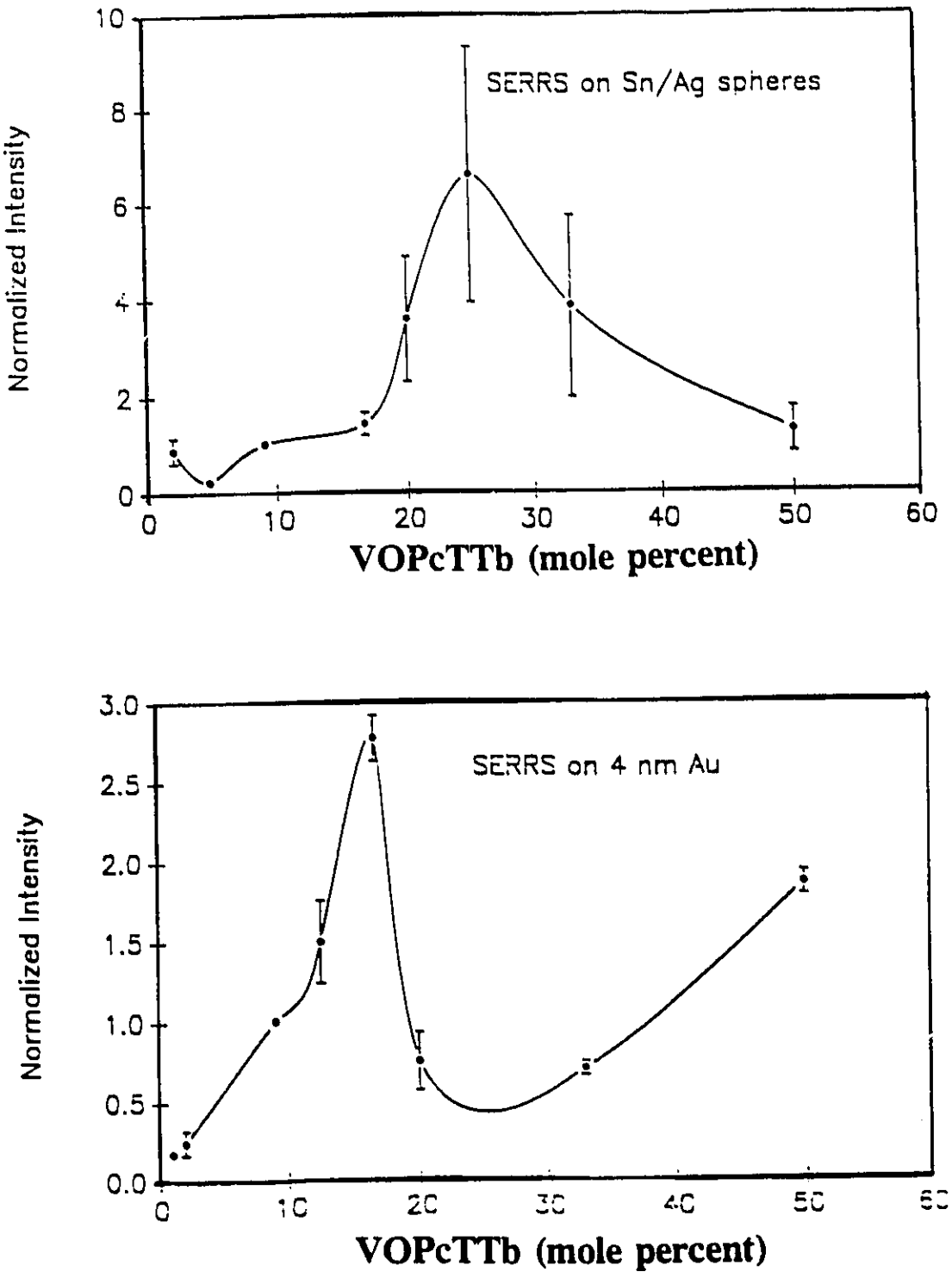
SERRS on Sn/Ag spheres
Normalized Intensity
VOPcTTb (mole percent)
SERRS on 4 nm Au
Normalized Intensity
VOPcTTb (mole percent)

Figure 5.1

surface coverage.[6] Dipole-dipole[10] interactions between molecules have been also predicted to affect surface coverage dependence. In our case minimal changes were observed between the absorption spectrum of 4 nm Au island film and the absorption spectrum of the composite(VOPcTTb + Au island). The amplitude did, however, vary slightly. In SERRS, overcoating the surface with an absorbing layer, could in the extreme case, eliminate the plasmon resonance and remove the electromagnetic enhancement.[11] Garoff et al. have calculated the effect of dye concentration on the absorption spectrum of silver spheroids. Their work showed that the dye initially broadens and damps the silver resonance and eventually causes splitting for thicker dye coatings.[12]

The distribution of the arachidic acid molecules within the VOPcTTb matrix cannot be directly addressed. Fluorescence studies, however, have shown that a good distribution of the fluorescent probe was observed among the host molecules.[9] In this work we assumed that a homogeneous mixed monolayer was formed. All SERRS showed that the fundamental vibrations of VOPcTTb were not altered by the rough metal surface or the arachidic acid molecules. The SERRS submonolayer coverage dependence for the totally symmetric, macrocycle band at 685 cm^{-1} of VOPcTTb is presented in Figure 5.1. The bars in Figure 5.1 indicate the range of the observed experimental values. The data points were obtained by measuring the relative intensity of the sample(of variable coverage) to the internal standard on the same slide. The SERRS intensity versus coverage on Au island and Ag-Sn spheres showed a maximum at submonolayer coverage. Maximum intensity was observed at 17 and 25 mole percent VOPcTTb on Au island films and Ag-Sn spheres respectively. Zeman et al.[6] and Kim[7] et al. also observed a maximum of about 0.1 ML in their SERRS study. The

coverage variation(.1-.25 ML) between the three groups could be rationalized in terms of the shape of the metal particles which was theoretically shown to affect the field enhancement.[6] At least for our data, the aspect ratio difference between Ag-Sn spheroids(spheres) and Au(oblate) island was a possibility, but without any detailed theoretical and further experimental work the prediction was not totally conclusive. Self absorption could not account for SERRS decrease with increasing phthalocyanine coverage. In a recent article[13] it was shown that the resonance Raman scattering from 2 LB of ytterbium bisphthalocyanine on glass was almost twice that for 1 LB, which confirms that self absorption could not be a major contributor in reducing resonance Raman scattering.

Another important feature in our coverage dependence study was that the relative intensities of the vibrational fundamentals for different surface coverage were consistently seen with the same general pattern. The fundamental frequencies and the relative intensities in SERRS were also identical to 3 LB transferred on glass. As shown in Figure 5.2, the relative intensities for VOPcTTb at 20 mole percent and 10 mole percent were identical. The relative intensities in the SERRS spectra recorded by Zeman et al. for 0.1 ML and 36 ML were, however, remarkably different especially in the isoindole region.[6] We have only observed changes in the relative intensity in the Pc vibrational spectra when the excitation source was tuned in-resonance and off-resonance to the electronic transition.[14] Kim et al. also observed that the relative intensities were independent of surface coverage.[7]

Coverage dependence studies of SERRS were also investigated by adding more than 1 LB to the SERS substrate. In this work multilayers of 10 mole percent VOPcTTb were

Figure 5.2 SERRS of 20 mole percent and 10 mole percent of VOPcTTb on Ag-Sn spheres and Au on island film respectively. Spectra were taken with ST polarization and 50 mW of the 647.1 nm laser line.

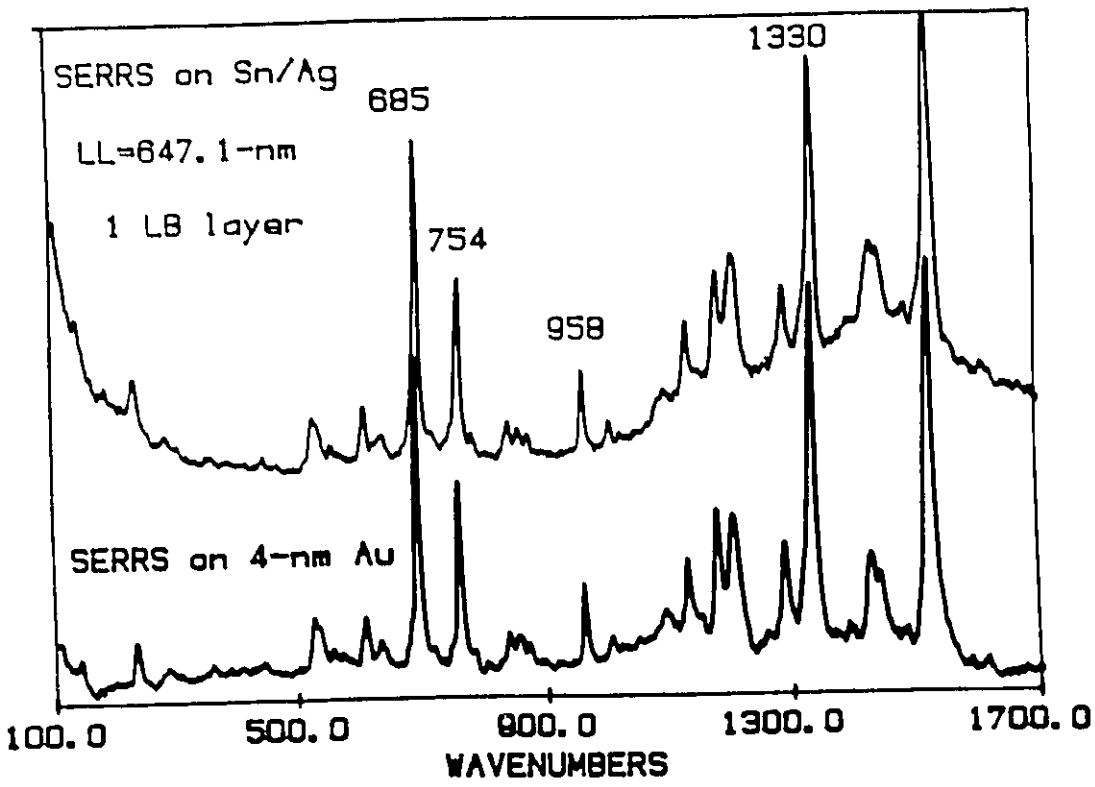
SERRS on Sn/Ag
LL=647.1-nm
1 LB layer
685
754
958
1330
SERRS on 4-nm Au
100.0
500.0
900.0
1300.0
1700.0
WAVENUMBERS

Figure 5.2

transferred to sections of the Ag-Sn spheres slide to give 1,2,3 and 4 LB layers. The integrated SERRS for the 685 and 1523 cm^{-1} bands of VOPcTTb were measured. The integrated SERRS intensities(I) for both bands showed a continuous increase in going from 1LB→2LB→3LB→4LB(i.e., $I_{1LB} < I_{2LB} < I_{3LB} < I_{4LB}$) as shown in Figure 5.3. The largest marginal increase was observed in going from 2LB to 3LB samples. The increase in intensity with the number of layers could be rationalized in terms of the long range electromagnetic enhancement.[15,16] In this respect the second, third, and fourth layers contributed to increase the total SERRS intensity.

SERRS coverage dependence of VOPcTTb evaporated onto Ag-Sn spheres showed the negative dependence with increasing coverage as shown in Figure 5.4. In this work, VOPcTTb was evaporated onto the same substrate in order to keep the enhancing properties of the substrate constant. In Figure 5.4 the decreasing effect of the SERRS signal with increasing coverage was clearly determined, despite the experimental uncertainties in measuring the film thickness of VOPcTTb. The results showed that the emission of the radiative surface plasmons was diminished or quenched with increasing film thickness.

Figure 5.3 SERRS coverage dependence for the 685 and 1524 cm^{-1} bands of VOPcTTb as function of the number of mixed layers(10 mole percent of VOPcTTb).

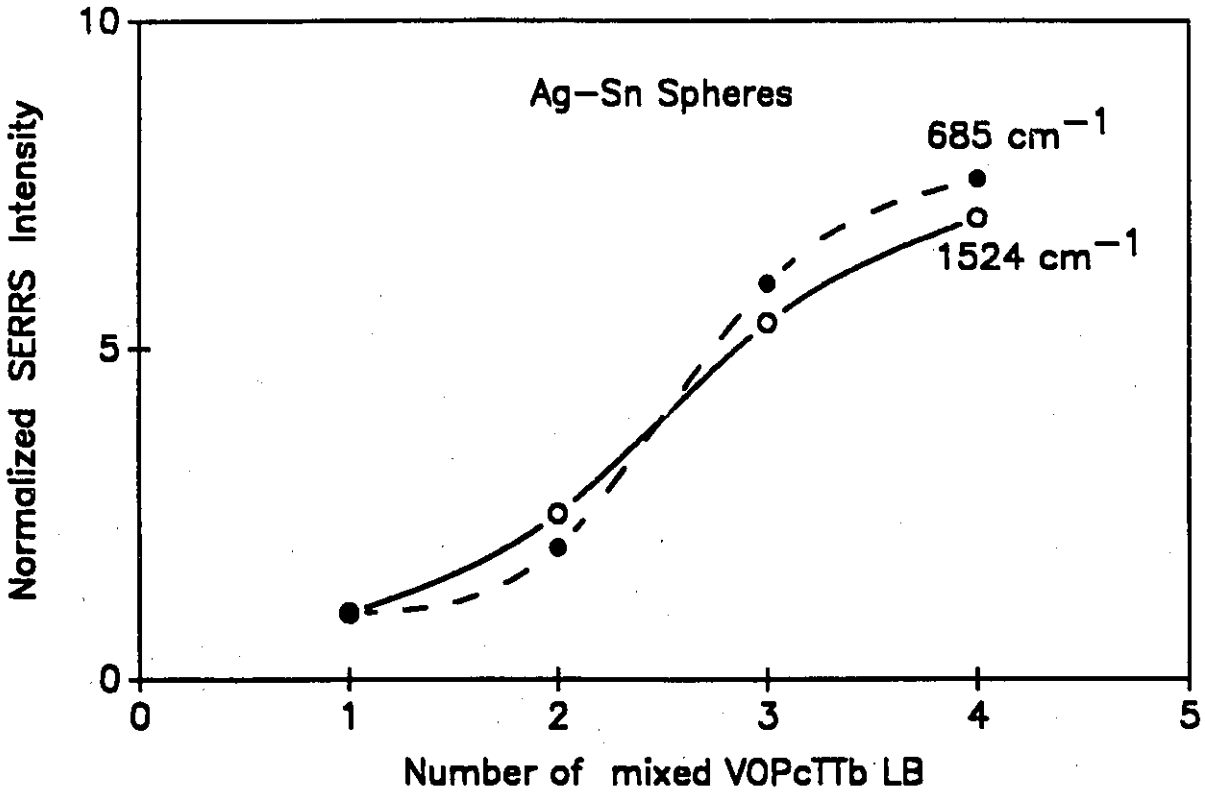
Ag–Sn Spheres
685 cm^{-1}
1524 cm^{-1}
Normalized SERRS Intensity
Number of mixed VOPcTTb LB
0
5
10
0
1
2
3
4
5

Figure 5.3

Figure 5.4 SERRS coverage dependence on the 685 cm^{-1} band of VOPcTTb for vacuum evaporated films on Ag-S.. spheres. Data are normalized to the 10 nm sample. Data was taken from SS and PP polarized spectra.

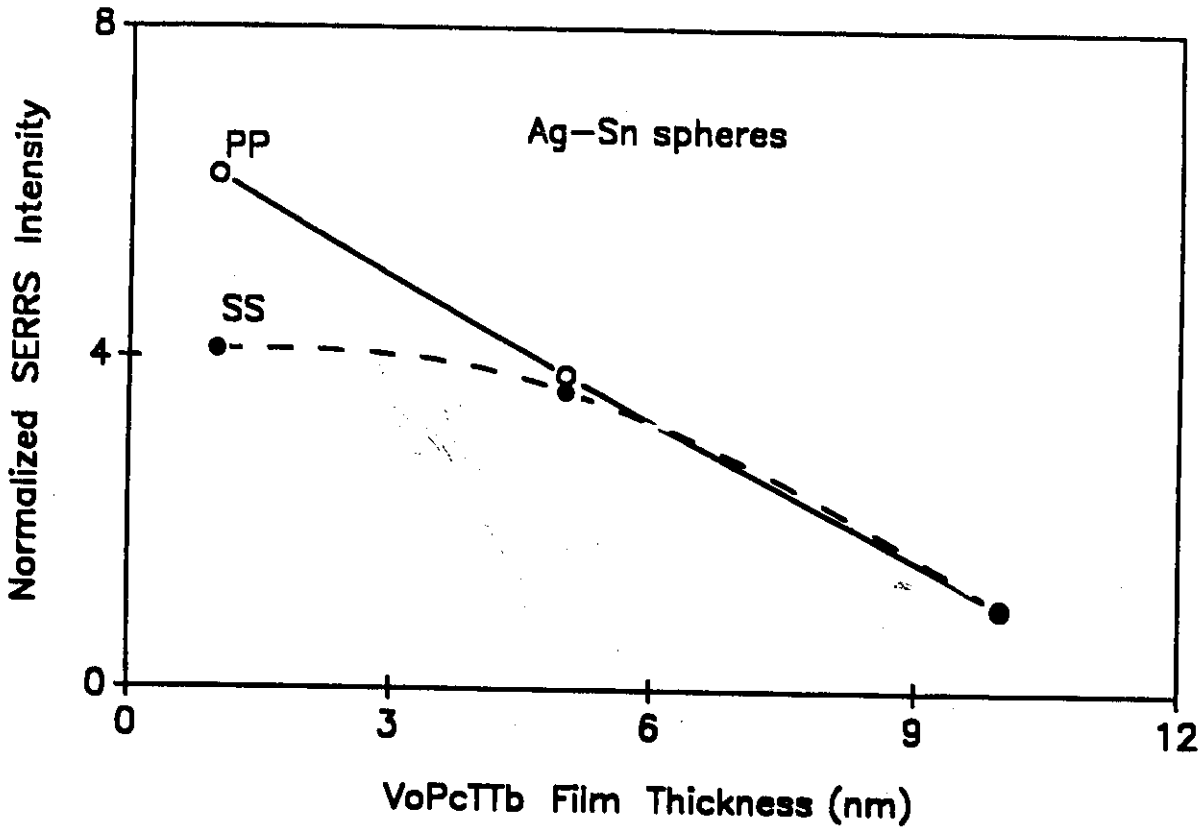
8
4
0
Normalized SERRS Intensity
PP
SS
Ag—Sn spheres
0
3
6
9
12
VoPcTTb Film Thickness (nm)

Figure 5.4

CHAPTER 6: Blue and Green Forms of Rare Earth Bisphthalocyanines

Introduction

Two phthalocyanine rings joined by a central lanthanide(Ln) element form a series of complexes known as the rare earth bisphthalocyanines($LnPc_2$). The general molecular structure is shown in Figure 6.1. X-ray diffraction analysis for the neodymium bisphthalocyanine($NdPc_2$) complex showed that the Nd atom occupied a central position in between two staggered(ca.45°) Pc ligands.[1] The metal was eightfold coordinated to the pyrrole nitrogens atoms and Nd-N bonds lengths varied from 2.39-2.49 Å. One ring in the $NdPc_2$ complex was saucer shaped towards the Nd atom and the other macrocycle was planar. The first report by Kirin et al. pointed out that two forms of $NdPc_2$ were produced in the reaction of rare earth acetates and o-phthalonitrile.[2] During product isolation by chromatography, a blue and a green zone was formed on the aluminium oxide column. The blue and green solutions were characterized by intense absorption bands at 634 nm and 672 nm respectively. The optical spectrum of the green material of the Nd complex was similar to the monophthalocyanine complexes and it was concluded by Kirin[2] et al. that the green compound was composed of a single Pc ligand. The visible absorption band of the blue Nd complex was however similar to spectra of tin bisphthalocyanine and the blue form of the Nd complex was assigned to contain two Pc rings. The elemental analysis of the blue form of the Nd complex was consistent with the bisphthalocyanine structure.[3] No elemental analysis was however reported for the green complex which decomposed in dimethylformamide to give metal free phthalocyanine.

Figure 6.1 Molecular structure of lanthanide(Ln) bisphthalocyanine

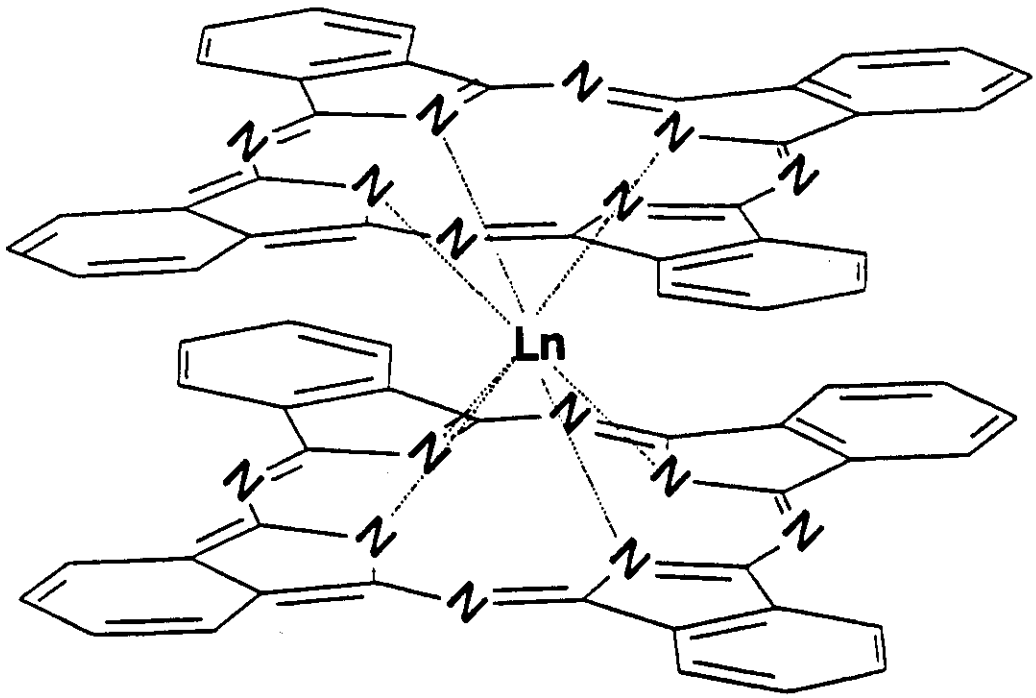

Figure 6.1

MacKay et al. however isolated stable green and blue forms of gadolinium phthalocyanines.[4] They reported that both compounds were bisphthlocyanine complexes. The latter group also noted that the colour of lanthanide bisphthalocyanine complexes was attributed to changes in the π-electron distribution during the formation of anions, cations, or neutral species rather than the formation of monophthalocyanine and bisphthalocyanine. Kasuga[5] et al. isolated three products in the reaction of neodymium acetate and o-phthalonitrile. They characterized $NdPc_2H$(λmax 345 and 636nm), $NdPc_2$ (λmax 324, 470, and 676 nm) and $PcNdCH_3COO$(λmax 336, and 675nm). Elemental analysis was used to confirm the structure of the neodymium bisphthalocyanine complexes.

The band at 470nm is always observed in bisphthalocyanine complexes which are green in colour. This absorption band is also characteristic of the phthalocyanine free radical($Pc^{\cdot}$) [6] ligand as observed in Pc radicals[7] of $H(Pc^{\cdot})$ and $Li(Pc^{\cdot})$. The green form of $NdPc_2$ would therefore contain a Q absorption band at 676 nm, a free radical band at 470, a Soret band at 324 nm. The structural formula $Pc^{2-}Nd(III)Pc^{\cdot-}$ is used to describe the green form and it takes into account the free radical nature of one Pc ligand. The free radical Pc ligand in lutetium phthalocyanine($LuPc_2$) complexes has been confirmed by ESR where a g-value ca 2 was measured.[8-10] The free radical bands in $LuPc_2$ disappeared by chemical reduction with hydrazine[11] or by electrochemical[8] reduction. In the literature, the structure of blue form of lanthanide bisphthalocyanine complexes has been cited as $LnHPc_2$ [i.e., $GdHPc_2$[4], $NdPc_2H$[5], $LuHPc_2$[12] The extra hydrogen in the blue form of lutetium bisphthalocyanine(or

$LnHPc_2$) was never confirmed in the X-ray crystal structure.[12]

The electrochromic properties of rare earth bisphthalocyanines have also been studied.[13-19] The electrochromic effect is used to describe the faradaic electrochemical reaction that results in a colour change of a material deposited on the surface of an electrode.[13] The electrochromism of $LnPc_2$ is attributable to the generation of different π species(i.e., neutral, cations and anions) depending on the applied potential. LB films of $LuPc_2$ transferred to an indium tin oxide electrode exhibited reversible colour change from purple(-2 V vs. SCE)↔blue(-1.7 V)↔green(0 V)↔brown-red(1.2 V).[14]

Our interest in lanthanide bisphthalocyanine complexes was in the potential use of these molecules as ultra thin films and Langmuir-Blodgett monolayers. The additional aim was to use surface enhanced Raman scattering, infrared, and uv-vis spectroscopy to collectively characterize the green($LnPc_2$) and blue($LnHPc_2$) forms of underivatized lanthanide bisphthalocyanine complexes and octa-*tert*-butylbisphthalocyaines of lanthanide elements($LnPc^t_2$).

The assignment of IR and Raman bands to internal coordinates for the green and blue forms of $LnPc^t_2$ has not been addressed in the literature.

Stable green and blue forms of octa-*tert*-butylbisphthalocyanine of rare earth elements were obtained from Dr. L. Tomilova from the Organic Intermediates and Dyes Institute(Moscow) during her visit(in 1991) to the University of Windsor. The synthesis of these compounds has been described elsewhere.[20,21] The synthesis of all rare earth bisphthalocyanine complexes begins with the formation of the

monophthalocyanine which converts to the green bisphthalocyanine form. Prolonged heating gives the blue form of the rare earth bisphthalocyanine.

Thin films(ca.200 nm) of $LnPc_2$ were sublimed to Corning 7059 substrate and halide crystals. Langmuir layers of $LnPc'_2$ were spread from benzene solutions onto an aqueous subphase(pH=5.5, temp.=15 °C). Monolayers were transferred under constant surface pressure(15 mN/m) mode to the glass, and SERS substrates.

Electronic Absorption Spectra of $LnPc'_2$

In Figure 6.2 the visible electronic spectra of the green and blue form of an early and late lanthanide phthalocyanine complex are shown. The typical bands observed for all green forms of $LnPc'_2$ were: Soret band(320 nm with a shoulder near 340 nm), radical[6,11] anion(460-490 nm) and Q-band at 667-687 nm. The spectra presented in Figure 6.2(A,D) were similar to literature[5,17] spectra of $NdPc_2$ and $LuPc_2$. In some reports[4,14,18], the structural formula of the green form of $LnPc_2$ was incorrectly written as $HLnPc_2$ which does not account for the free radical and charge balance for the neutral molecule.

The blue complexes of $LnPc'_2$(or $LnHPc'_2$) have the characteristic signature as shown in Figure 6.2(B,D). Unlike the green analogues there was no absorption band in the 460-490 nm spectral window. These spectra were similar to the proposed blue form of $GdHPc_2$[4], $NdHPc_2H$[5] and the complexes of tetra(n-butyl)ammonium$LnPc_2$[22]. The absorption spectrum of the latter compound would suggest that the absorption spectrum of the blue form of lanthanide bisphthalocyanine could be due to $(Pc^{2-}$ $Ln(III)Pc^{2-})^{-}H^{+}$. Zirconium and hafnium bisphthalocyanine also form blue solutions

Figure 6.2 Electronic absorption spectra of the green(A) and blue (B) form of $NdPc^{t}_{2}$, and green(C) and blue(D) form of $LuPc^{t}_{2}$

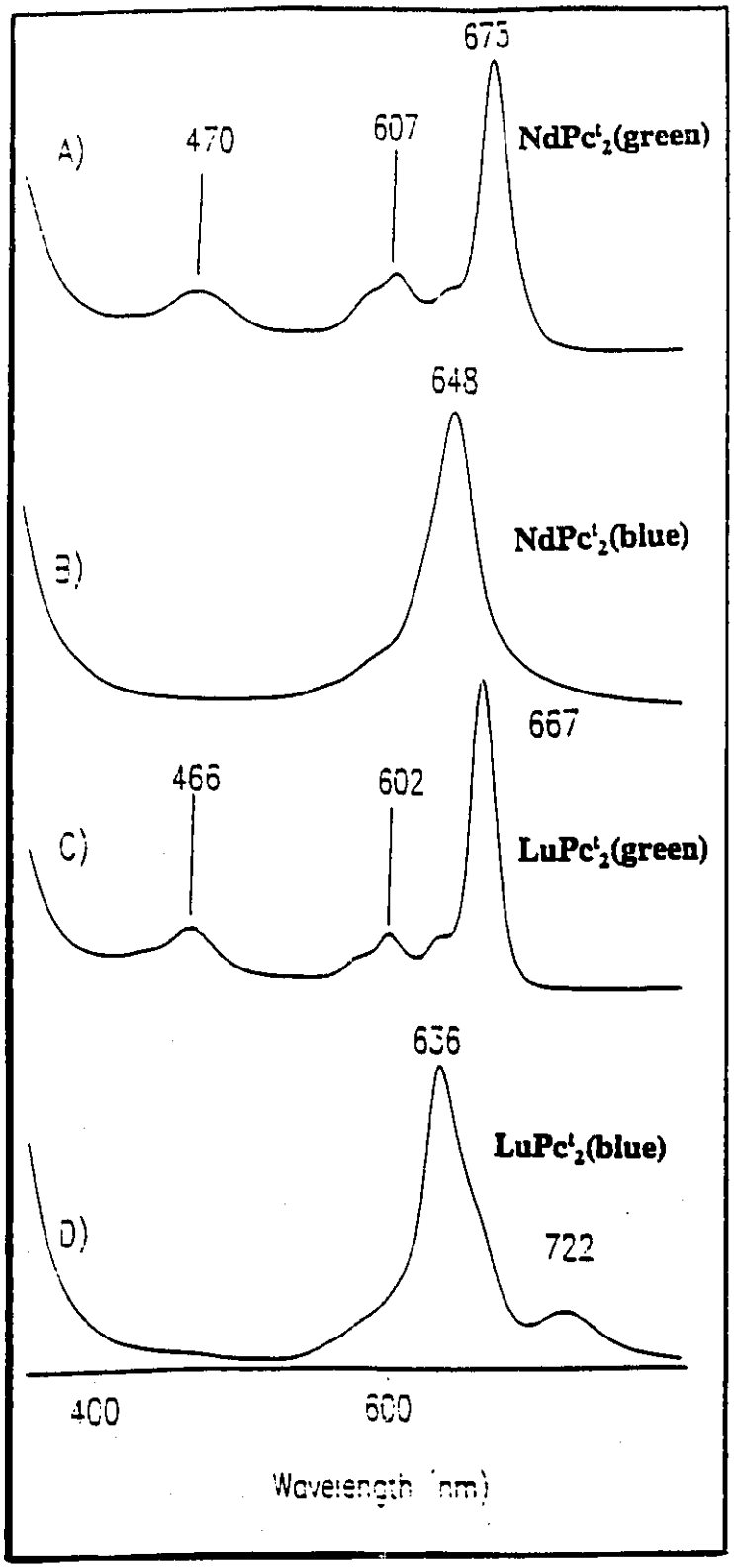
675
A)
470
607
NdPc$^{t}_{2}$(green)
648
B)
NdPc$^{t}_{2}$(blue)
667
466
602
C)
LuPc$^{t}_{2}$(green)
636
LuPc$^{t}_{2}$(blue)
D)
722
400
600
Wavelength (nm)

Figure 6.2

and their absorption spectra are similar tothe blue form of lanthanide bisphthalocyanine complexes.[23] Since the oxidation state of the metal in $ZrPc_2$ and $HfPc_2$ is IV, the blue colour could originate from two Pc^{2-} ligands.

At ca. 700 nm, a weak satellite of the Q band was observed in the spectra of $LnHPc^t_2$(Ln=Ho, Er, Tm, Yb, Lu). The band was absent in spectra of $LnHPc^t_2$(Ce, Pr, Nd, Sm, Eu, Gd, Tb, Dy,). The splitting of the Q band into another band(i.e., satellite or weak shoulder band) has been attributed to exciton interaction between the two Pc rings.[22]

Thin Films of $LnPc_2$

Using $LnPc_2$(green material) as the starting material, thin films were simultaneously evaporated onto NaCl disks and glass substrates. Green films were obtained for $LnPc_2$(Ln=Gd, Tb, Dy, Ho, Er, Tm, Yb, Lu). For these complexes the visible spectra of the thin film and the solution spectra of the thin film dissolved in benzene were identical to the solution spectra of the starting material. The absorption spectra for $LuPc_2$ are shown in Figure 6.3. Early rare earth elements in the $LnPc_2$(Ln= Pr, Nd, Sm, Eu) series however, produced blue coloured films. The absorption spectra for $NdPc_2$ are also shown in Figure 6.3. When the film was washed with benzene a blue-green solution was collected and an insoluble film remained on the glass slide. The absorption spectrum of the insoluble film was distinctly identified as H_2Pc by the strong bands at 665 and 700 nm and weaker bands at 602 and 640 nm. The IR spectrum of the thin film of $NdPc_2$ on NaCl also contained the N-H stretching vibration at 3290 cm^{-1} and another band at 1007 cm^{-1}

Figure 6.3 Visible spectra of an evaporated film(200 nm) of $NdPc_2$ and $LuPc_2$ (i), solution of film washed with benzene (ii), and starting material dissolved in benzene(iii)

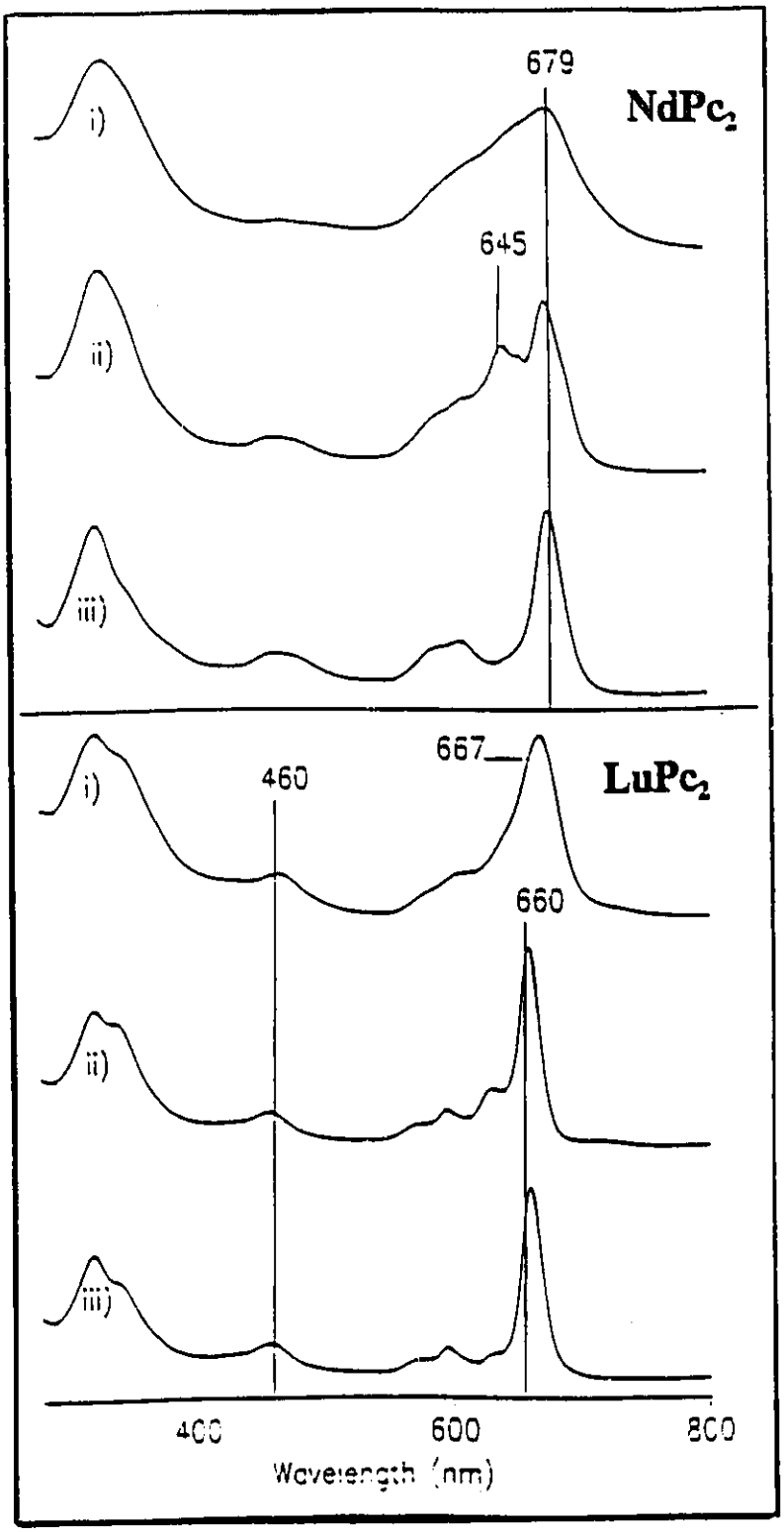
679
NdPc2
i)
645
ii)
iii)
667
460
LuPc2
i)
660
ii)
iii)
400
600
800
Wavelength (nm)

Figure 6.3

which are seen only in H_2Pc analogues.[14,24-26] The absorption spectrum of the blue-green solution contained two strong absorptions at 645 and 679 nm that were observed in the spectra of isolated green and blue forms of the $NdPc'_2$ analogues. The starting material, however, gave an absorption spectra typical of the green form of $NdPc_2$. Traces of H_2Pc were not found in the IR spectrum of the starting material. Metal free phthalocyanine was therefore produced during sublimation. The sublimation results obtained for $NdPc_2$ were also observed for $LnPc_2$(Ln= Pr, Sm, Eu).

Chemical Redox and Acid Effects on $LnPc'_2$

In the early studies of lanthanide bisphthalocyanine complexes, MacKay[4] et al. proposed an acid base equilibrium to account for the observed blue and green colours. M'Sadak[27] et al. showed that chemical reduction (with triethylamine) of the green form of the $LuPc_2$ produced the blue form. Addition of acetic acid to the chemically reduced $DyPc_2$(blue complex) produced the original green complex.[27] Our absorption spectra recorded in the reaction of the green form of $PrPc'_2$ and $LuPc'_2$ with different acids are presented in Figure 6.4.

The red shifted Q-band to ca. 705 nm was typically observed for the oxidized Pc ligand. The addition of CF_3COOH, HNO_3 or H_2SO_4 produced the red complex. The reaction of HCl and CH_3COOH with $LnPc'_2$ also produced the red complex, although the rate was slower than with HNO_3. $LnPc'_2$ (Ln= Ce, Pr, Nd) were not stable in CF_3COOH or HNO_3 and decomposed to give metal free phthalocyanine. The spectral evidence suggests that acids strongly interact with π system of the Pc

Figure 6.4 Visible spectra for the reaction products of $LuPc^{I}_{2}$(green material) with with CH_3COOH (i), HNO_3 (ii), hydrazine(iii), $PrPc^{I}_{2}$(green material) CF_3COOH (i), HNO_3(ii), one after HNO_3 addition(iii)

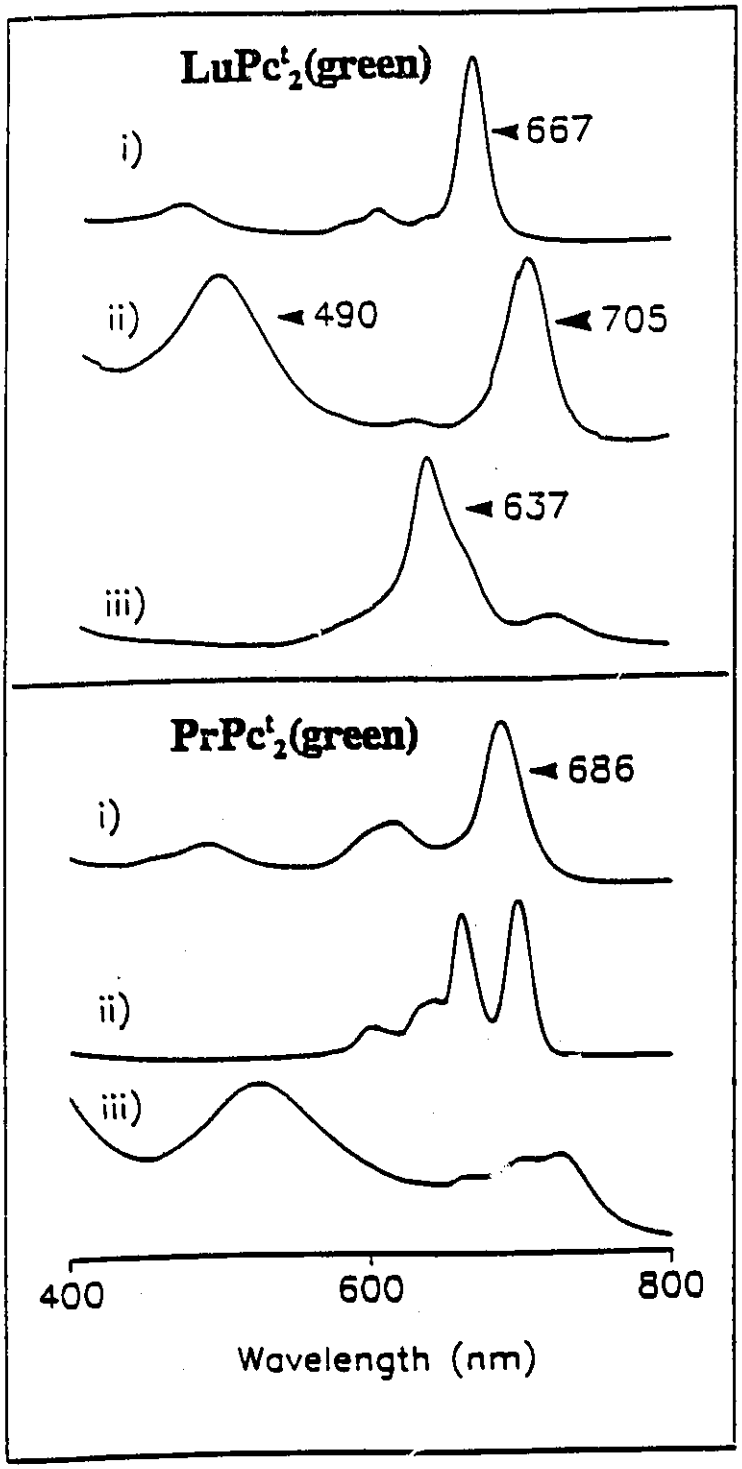
LuPc$^t_2$(green)
i)
667
ii)
490
705
iii)
637
PrPc$^t_2$(green)
i)
686
ii)
iii)
400
600
800
Wavelength (nm)

Figure 6.4

ligand to produce changes in the electronic distribution. These results suggest that under these mild conditions the oxidation state of the rare earth element was not affected in the green↔blue inter conversion.

Raman Spectra of Green and Blue Forms of $LnPc^{t}_{2}$

LB monolayers of the green and blue form of $LnPc^{t}_{2}$ were transferred to glass slides, 4 nm gold island(SERRS) and 4nm Ag(SERS) island films. As shown in Figure 6.5 for $HoPc^{t}_{2}$, the spectral features of the green and blue form were maintained in LB assemblies. The SERRS spectra of $HoPc^{t}_{2}$ are shown in Figure 6.6. The characteristic pattern of relative intensity in the SERRS spectra of $LnPc^{t}_{2}$(Ln= Nd, Sm, Er, Tm, Yb, Lu) was similar to those in Figure 6.6. The main difference between blue and green forms of $HoPc^{t}_{2}$ is shown in the inset of Figure 6.6. The spectral differences observed with the 647.1 nm laser line(full resonance with the blue form) persisted in the SERRS spectra obtained with the 676.4 nm laser line(full resonance with the green form) as shown in Figure 6.7. The band at 729 cm^{-1} was therefore not selectively enhanced by the resonance Raman effect. The strong band at 685 cm^{-1} was characteristic of the macrocycle breathing mode and is normally the most intense band in SERRS or RRS of Pc. In highly symmetric molecules(i.e., MgPc, CuPc, ZnPc, with D_{4h} point group symmetry) two bands at 685 cm^{-1} and 747 cm^{-1} are normally seen in the macrocycle region.[28] Complexes of lower symmetry(i.e., SnPc[29] with C_{4v} point group symmetry) however contain three bands at 681 cm^{-1}, 733 cm^{-1} and 747 cm^{-1}. For the blue form of $HoPc^{t}_{2}$ three bands were observed at 685 cm^{-1}, 729 cm^{-1} and 747 cm^{-1} which suggested lower symmetry for the

Figure 6.5 Visible absorption spectra for LB monolayers of the green and blue form of $HoPc^{I}_{2}$. There were four LB on each side of the glass substrate

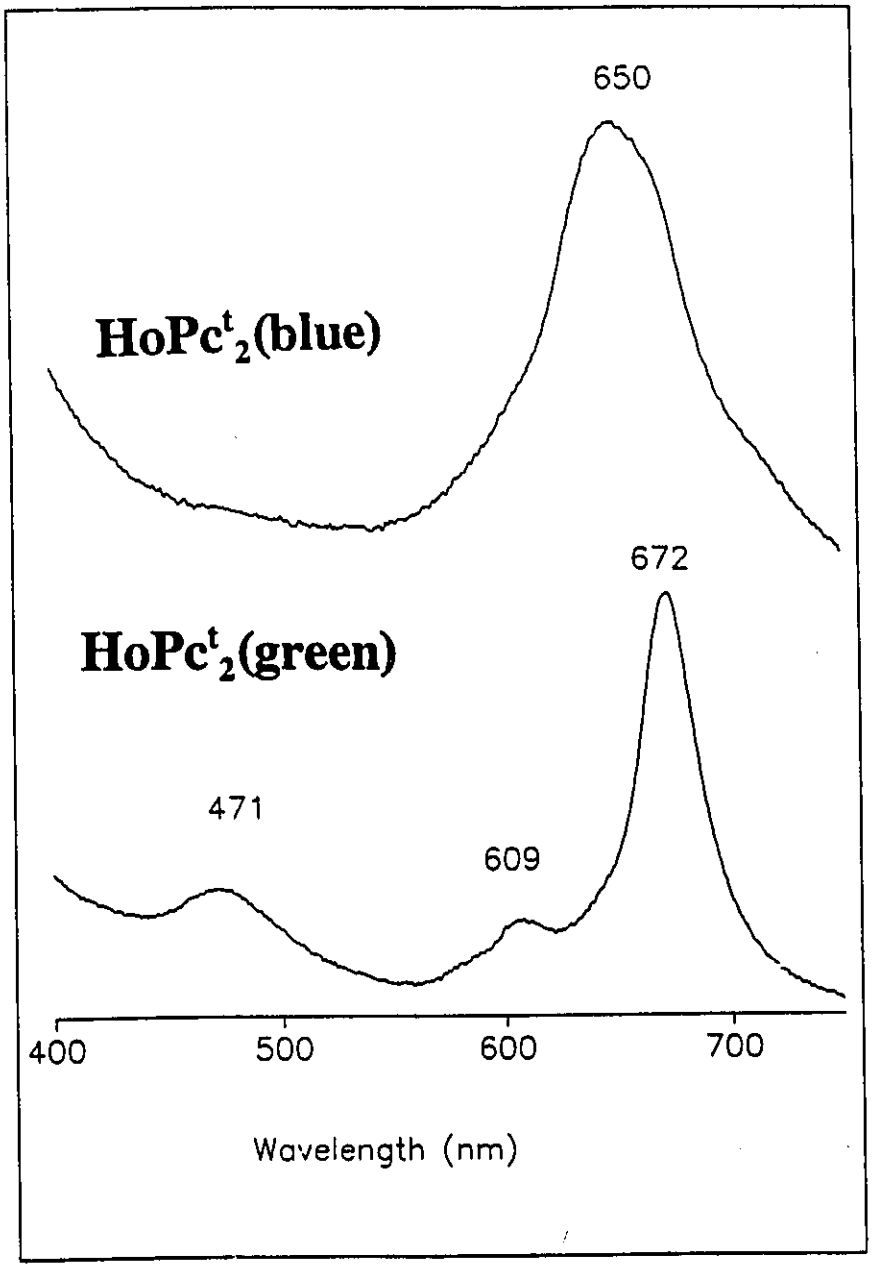
650
HoPc$^t_2$(blue)
672
HoPc$^t_2$(green)
471
609
400
500
600
700
Wavelength (nm)

Figure 6.5

Figure 6.6 SERRS with the 647.1 nm laser line of one LB of $HoPc^{t}_{2}$ blue and one LB monolayer of $HoPc^{t}_{2}$ green on Au island films. The expanded spectral region of the blue (A), and green (B) are shown in the inset. The ST spectra were recorded.

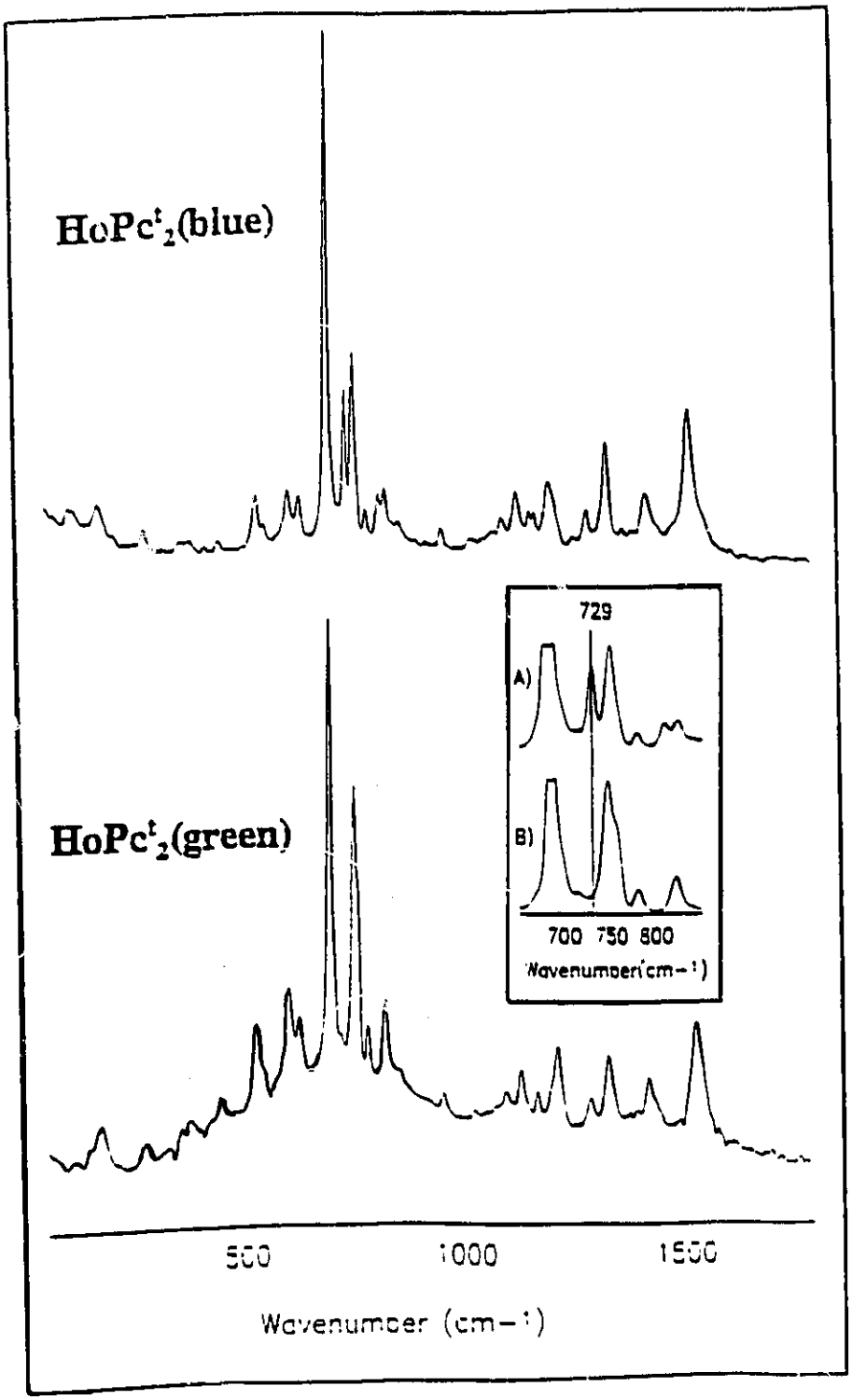
HoPc$^t_2$(blue)
HoPc$^t_2$(green)
729
A)
B)
700 750 800
Wavenumber(cm^{-1})
500
1000
1500
Wavenumber (cm^{-1})

Figure 6.6

Figure 6.7 SERRS with the 676.1 nm laser line of one LB of $HoPc^{t}_{2}$ blue and one LB monolayer of $HoPc^{t}_{2}$ green on Au island films. The expanded spectral region of the blue (A), and green (B) are shown in the inset. The ST spectra were recorded.

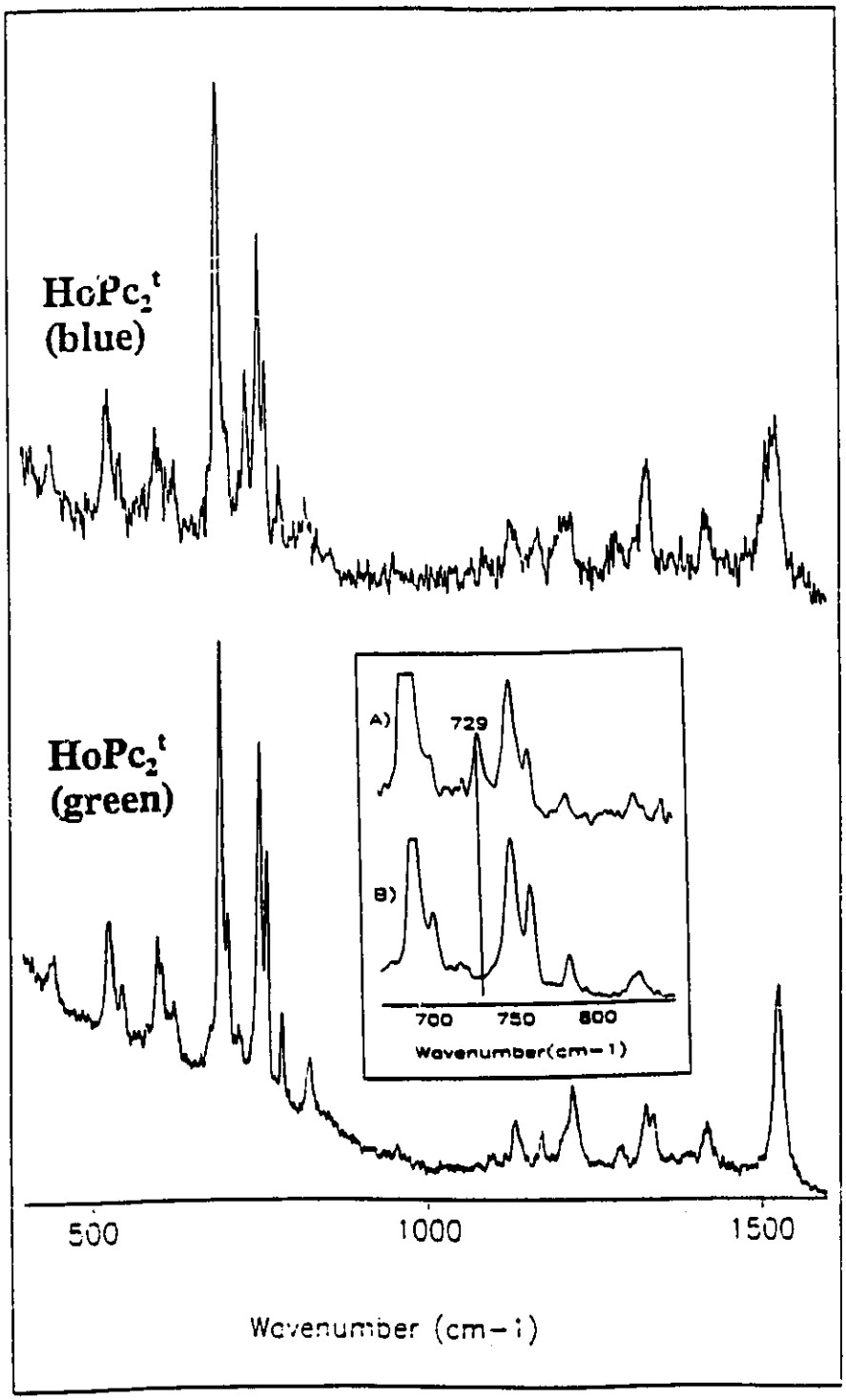
HoPc2t
(blue)
HoPc2t
(green)
A)
729
B)
700
750
800
Wavenumber(cm-1)
500
1000
1500
Wavenumber (cm-1)

Figure 6.7

blue form. The lower symmetry could result from two unequal Ln-Pc distances or the speculated hydrogen(i.e. $LnPc_2H$) as proposed by Moussavi[12] et al. and Kasuga[5] et al. A D_{4d} structure can be envisioned in the totally symmetric case with perfect staggered configuration and equivalent Ln-Pc distances. Differences in the Ln-Pc distance would reduce the symmetry to C_{4v} or even lower, and the strong band at 729 cm^{-1}, as observed in the blue form of $HoPc^t_2$, could derive its intensity from an allowed irreducible representation of a lower symmetry point group. The SERS of one LB of green and blue forms of $HoPc^t_2$ on 4 nm Ag, and excitation at 514.5 nm showed that the only difference was in the pattern of relative intensity. The observed SERRS frequencies for $HoPc^t_2$ are listed in Table 6.1.

Infrared spectra of Blue and Green Forms of $LnPc^t_2$

The pattern of relative intensities for the green and blue forms of $HoPc^t_2$ are shown in Figure 6.8. The same trend was also observed for the two forms of $LnPc^t_2$(Ln=Nd, Sm, Er, Tm, Yb, Lu). The intense bands at 728 cm^{-1} and 1115 cm^{-1}, which are normally observed in the IR spectra of unsubsituted bisphthalocyanines($LnPc_2$), were not seen in the spectra of the octa-*tert*-butyl bisphthalocyanine complexes of rare earth elements.[30] These bands have a large contribution from the C-H bending modes and are no longer observed in the $LnPc^t_2$ complexes because of the partial substitution by *tert*-butyl groups. The IR spectrum of the green form always contained a strong band at 1318 cm^{-1} which decreased in relative intensity in the spectrum of the blue form. A strong band at about 1079 cm^{-1} was always present in the blue form of $LnPc^t_2$ compounds. Walton[31] et al. posulated

TABLE 6.1

Observed Vibrational Frequencies of the Green and Blue Form of $HoPc^{t}_{2}$. Infrared of a KBr pellet, and surface-enhanced Raman spectra observed with 647.1 nm excitation of one LB on Au.

Green Form		Blue Form		Assignment
IR	SERRS	IR	SERRS	
	173 w		173 w	
	272 m		273 m	
	349 w		353 w	
	370 w		372 w	
	437 w		442 w	
	524 m		524 m	t-butyl def.
	542 sh.		544 w	t-butyl def.
	596 m		596 m	t-butyl def.
	620 m		621 m	
674 w		674 w		
687 w	685 vs	689 w	683 vs	Pc-breathing
700 w		697 w		
			728 s	
	747 s		750 s	Pc-ring
755 s	753 sh	755 vs		Pc-ring
782 w	781 m	782 w	780 m	Pc-ring
			809 m	
820 w	822 m		824 m	
833 m		830 s		t-butyl
855 w		855 w	855 w	
896 w		896 w		C-H bend (tb)
909 w		909 w		C-H bend (tb)
919 w		919 s	917 vw	C-H bend (tb)
953 w	951 w	953 w	951 m	Benzene ring
1022 vw	1022 w	1022 vw		C-C stretch (tb)
1047 w		1047 m		C-H bend (Pc)

Table 6.1 (continued)

		1079 vs		Pc-ring
1092 w	1095 w		1092 m	C-H bend (tb)
1100 w				
1128 vw	1127 m		1126	C-H bend (tb)
	1157 w		1158 w	
	1168 m		1169 w	
1201 w			1201 w	
1219 w	1214 m	1219 w		C-H bend (tb)
1256 m		1256 s		C-H bend (tb)
1282 m	1285 w	1282 m	1285 m	C-H bend (tb)
1318 vs		1322 s		C-H bend (Pc)
	1325 m		1328 m	Pyrrole-stretch
1363 m		1363 m	1367 w	C-H bend (tb)
1384 w				
1394 m			1394 m	
1412 m				
	1418 m		1420 m	Isoindole
stretch				
1463 m		1463 w		
1482 w		1486 m		
1510 w				
			1517 m	Pyrrole stretch
	1525 m			Pyrrole stretch
1612 m		1612 m		Benzene stretch
2863 w		2863 w		C-H stretch
(tb)				
2903 w		2902 w		C-H stretch
(tb)				
2957 m		2957 m		C-H stretch
(tb)				

Figure 6.8 Transmission infrared spectra in KBr matrix $HoPc^{I}_{2}$ green (A), and $HoPc^{I}_{2}$ blue (B). Spectral resolution was 1 cm^{-1}.

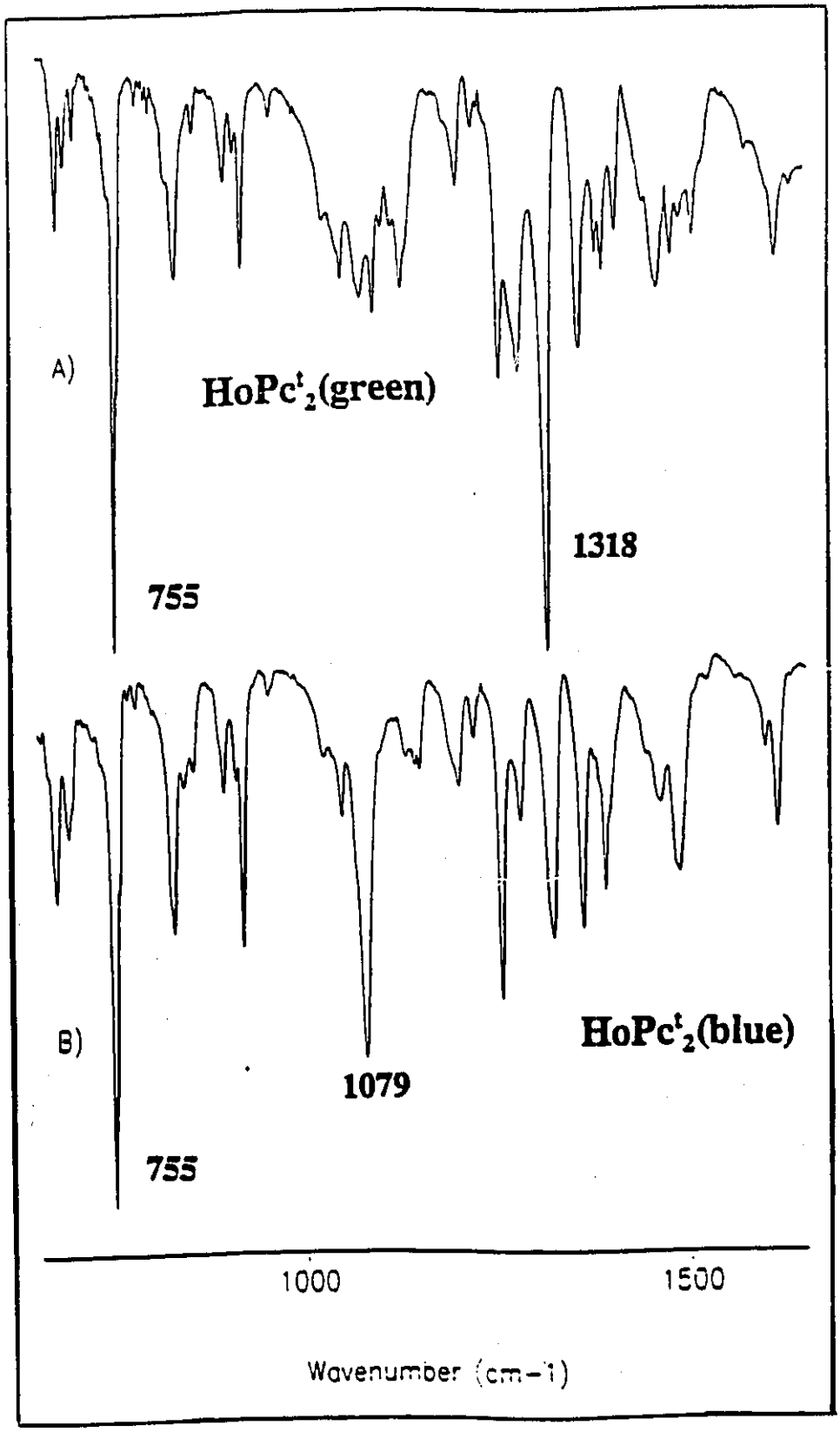
A)
HoPc$^{t}_{2}$(green)
1318
755
B)
HoPc$^{t}_{2}$(blue)
1079
755
1000
1500
Wavenumber (cm−1)

Figure 6.8

that the 1070-1080 cm^{-1} band may be characteristic of the blue form. We could not directly compare the diagnostic 1079 cm^{-1} band of our blue form of $LnPc'_2$ to the literature value of 1070 cm^{-1} reported for the blue form of gadolinium[4] bisphthalocyanine. The authors of the gadolinium complex published no IR spectra and their tabulated results did not include the pattern of relative intensity. The observed IR frequencies for $HoPc'_2$ are also presented in Table 6.1.

Thermal Inter Conversion of Green and Blue Forms

It was earlier shown that sublimation of the green form of $LnPc_2$(Ln=Pr, Nd, Sm, Eu) in the formation of thin films gave three products: H_2Pc and the green and blue forms of $LnPc_2$. The resonance Raman spectrum of the contaminated films contained the 730 cm^{-1} band(medium relative intensity) characteristic of the blue form. The 730 cm^{-1} band was, however, not observed in the SERRS spectrum of one LB monolayer of the green form of $LnPc_2$(Ln=Pr, Nd, Sm, Eu). The green→blue inter conversion could also be observed by IR spectroscopy. The 1079 cm^{-1} was only observed as a contaminant when the green form of $LnPc_2$(Ln=Pr, Nd, Sm, Eu) was sublimed during thin film fabrication. This band was not present in IR spectrum of the starting material mixed with KBr to form a pellet.

Pellets of KBr containing the green or blue form of $HoPc'_2$ were also tested for thermal interconversion. The pellet was heated to 200 °C for four hours in an oven. The IR spectrum that was recorded after heating the blue form was identical to the reference spectrum recorded prior to heating. An intense band 1079 cm^{-1} and reduced relative intensity were however observed for the green form of $HoPc'_2$ after

heat treatment.

Summary

The purpose of this investigation was to characterize the blue and green form of octa-*tert*-butylbisphthalocyanines and related compounds. The structure of the green form as $LnPc^{t}_{2}$(free radical) was supported by the visible band at 460-490 nm. The electronic spectra of the blue form of $LnPc^{t}_{2}$ does not contain the free radical band. Its absorption spectrum was similar to complexes of $ZrPc_2$ and $HfPc_2$ where two Pc^{2-} are attached to the central metal. The infrared and Raman data for the green and blue form of $HoPc^{t}_{2}$ were not similar and the difference was lower symmetry in the blue form. The presence of the extra hydrogen in the blue form could account for lower symmetry in the blue form. Chemical reduction of the green form with hydrazine produced the electronic spectrum of the blue form. Under these conditions the reduction was localized to occur on the Pc ligand. Addition of acid also altered the electronic spectrum or rare earth bisphthalocyanines. The green form of the early $LnPc_2$ (Ln=Pr, Nd, Sm, Eu) are not stable during evaporation and give a mixture of H_2Pc, blue and green form. Heating a KBr pellet mixed with the green form of $HoPc^{t}_{2}$ produced the characteristic IR band of the blue form.

CHAPTER 7: Chemical Reactivity of Phthalocyanine to NOX Gas

Introduction

The adsorption of small gases on phthalocyanine devices has been reviewed by Wright[1] and Snow et al.[2] Phthalocyanines are easily ionized and are good electron donors. The strongest interaction with oxidizing gases is predicted to occur at centres of high electron density(i.e., the nitrogen atoms of the macrocycle).[1] Thin films of certain phthalocyanines doped with electron accepting gases such as nitrogen oxide and nitrogen dioxide(NO_2) produced a significant increase(ca. six orders of magnitude) in the dark dc conductivity of the film.[2-4] In this thesis, the notation NOX is used to describe nitrogen dioxide gas in equilibrium with dinitrogen dioxide gas(i.e., $2NO_2 \leftrightarrow N_2O_4$). Electron donor gases like ammonia were, however, used to reverse the enhanced conductivity observed in films doped with NOX gas.[3,4] The interaction of NO_2 and phthalocyanine has received the most attention in the literature.

Conductivity studies on single crystals of MPc(M=Mn, Co, Ni, Cu, Zn, Pb, H_2) exposed to NOX showed a reduction in the activation energy.[5] Phthalocyanines are commonly classified as p-type semiconductors. The increase in Pc conductivity was attributed to the increase in the number of holes or charge carriers produced in the charge transfer reaction between NOX and Pc.[6] The toxicity of NOX has attracted the development of Pc chemical sensors for sensitive detection of NOX in the parts per million regime. Phthalocyanine as a general class of organic molecules satisfies the requirements of a good gas sensor.[7] Its conductivity varies with concentration and it can be operated at temperatures in excess of 100 °C to minimize

water condensation effects. Studies have shown that thin film morphology[8,9] and the temperature[10-12] of the sensor device affect the magnitude of the electrical signal generated by the interaction of NOX and Pc.

The most common Pc-gas conductivity device is the chemiresistor which consists of Pc evaporated onto an array of interdigital metal electrodes. The conductivity of the chemiresistor and changes in conductivity due to NOX adsorption are usually measured in vacuum. A surface acoustic wave(SAW) device was also reported to respond to changes in electrical conductivity and it was considered for Pc-NOX sensor application.[2]

The most recent Pc-NOX gas sensing device uses Langmuir Blodgett films of phthalocyanine. The LB technique would be advantageous since it offers reproducibility in film structure and faster response times than evaporated thin films.[13] Studies of copper mesoporphyrin IX diol exposed to 10 ppm of NOX showed that maximum sensitivity was reached with 5-10 LB.[14] The LB technique together with molecular engineering could be used to control the architecture of the film. Baker et al. introduced the first phthalocyanine LB chemiresistor.[15] Their device consisted of eight LB layers of an asymmetrically substituted copper phthalocyanine transferred to a glass substrate containing interdigital aluminium electrodes. This chemiresistor incorporating LB layers of the CuPc derivative was reported to respond linearly to 0→16 vapour parts per million of NOX. LB films of Pc have also been incorporated into an optical sensor device which uses surface plasmon(SP) resonances as a mode of detection.[16,17] In this work a few LB of Pc were transferred to a silver slide and the

Kretschmann configuration was used to couple P-polarized light to the SP of the silver film. The effect of NOX was to change the optical constants of the composite(Pc + Ag film) and shift the SP resonance curve.

Our interest in phthalocyanine and NOX was to investigate the interaction between the two species. The objective was to apply novel and sensitive techniques that could be used to monitor the adsorption process of NOX and phthalocyanine. To the best of our knowledge there was no thorough and comprehensive spectroscopic study that examined the reactivity of Pc to NOX. There were certainly no Pc + NOX Raman reports. The work by Schoch and Temofonte demonstrated that infrared transmission spectroscopy was not drastically sensitive to the interaction of NOX and Pc.[18] It should also be pointed out that the interaction between Pc and small molecules is central to the electrocatalytic[19] activity of Pc complexes and the use of Pc as catalysts[20].

Raman Scattering, SERS, and UV-Vis of Pc + NOX

Raman Scattering:Thin Solid Films and NOX

Thin solid films(200 nm thickness) on Corning 7059 of ytterbium bisphthalocyanine($YbPc_2$) and lutetium bisphthalocyanine($LuPc_2$) were prepared in the evaporator designated for organic materials. Reference Raman spectra were recorded prior to exposing the films to gas. A lecture bottle of NOX was purchased from Matheson or Aldrich. The Pc sample was placed into an in-house built cylindrical glass cell and evacuated to 300 Pa prior to NOX exposure. NOX was admitted until the pressure reached 600 Pa and the film was exposed to gas for one minute before

Figure 7.1 Raman spectra(ST polarization) of 200 nm $YbPc_2$ before and after NOX. The 514.5 nm laser line was the excitation source.

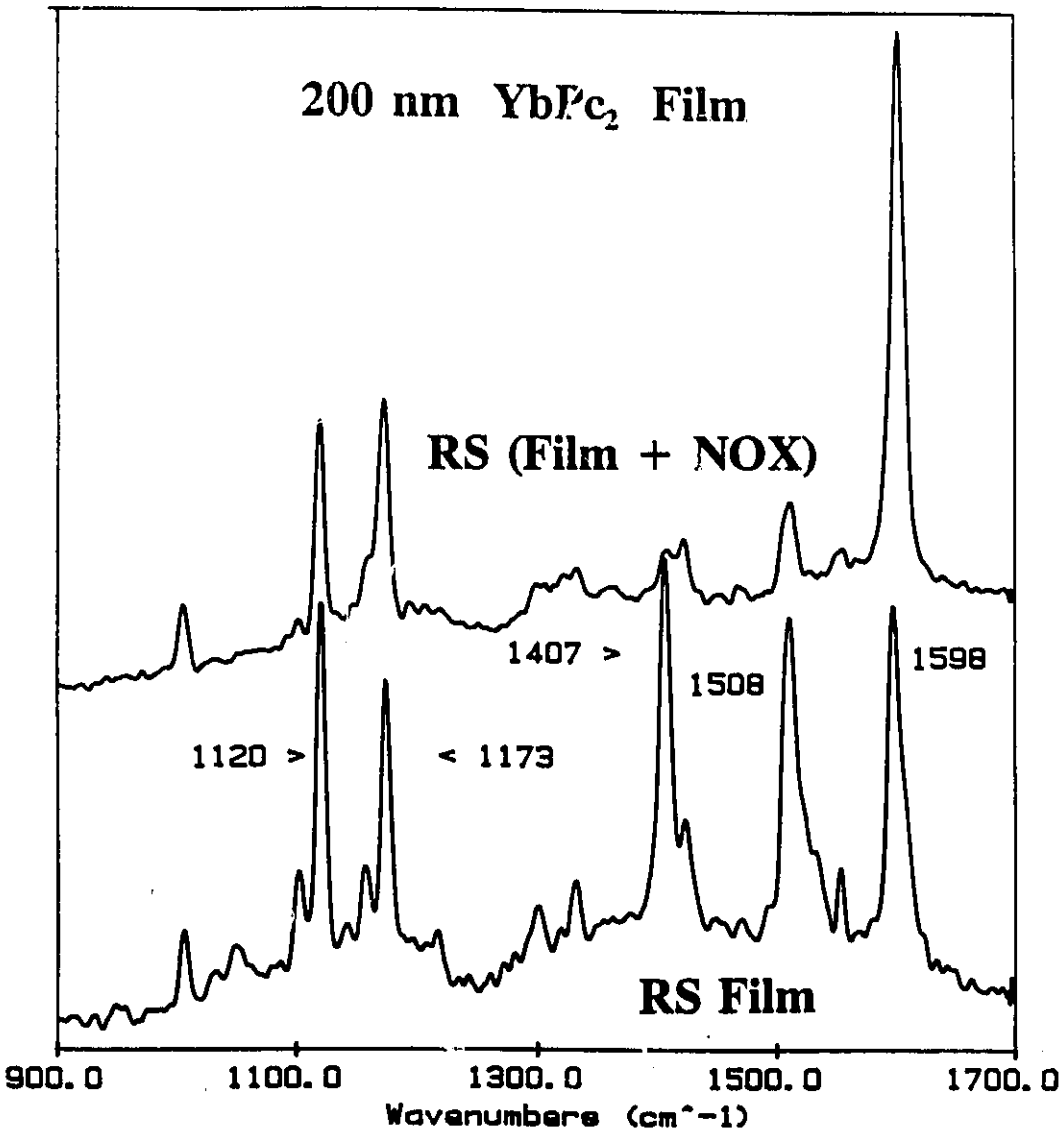
200 nm YbPc2 Film
RS (Film + NOX)
1407 >
1508
1598
1120 >
< 1173
RS Film
900.0
1100.0
1300.0
1500.0
1700.0
Wavenumbers (cm^-1)

Figure 7.1

removing the sample. Films of $YbPc_2$ and $LuPc_2$ readily decolorized from green→brown upon NOX exposure.

In Figure 7.1 the normal or off-resonance Raman spectrum of a 200 nm thin film of $YbPc_2$ before and after exposure to NOX is shown. Similar spectra were also observed for $LuPc_2$. The most drastic changes occurred in the pyrrole spectral region. The effect of NOX was to reduce the relative intensity of certain vibrational bands. The gas did not, however, change the frequency of the Raman bands. In particular, NOX strongly affected the macrocycle bands at 1407 cm^{-1} and 1508 cm^{-1}. The latter band has been assigned to the **C=C** pyrrole frequency in bisphthalocyanines complexes.[21] In Raman spectroscopy a decrease in scattering intensity could be associated with a loss of electron density in the nuclei involved in the vibration. The results were then interpreted in that NO_2 reacted with the bisphthalocyanine complex to remove electron density particularly from the **C=C** pyrrole. The remarkable sensitivity of Raman spectroscopy to the interaction between Pc and NOX led to the direct application of SERS, and SERRS. In particular, the objective was to study the adsorption and desorption processes on a single monolayer of phthalocyanine.

SERS:Phthalocyanine LB Layers and NOX

The work began with monolayer formation of $LuPc_2$ and $YbPc_2$. Both bispthalocyanine complexes were spread from chloroform onto a subphase maintained at 20 °C. The isotherms are shown in Figure 7.2. In the preparation of LB layers, the Langmuir layer was compressed to a constant surface pressure of 10 mN/m, and

Figure 7.2 Surface pressure-area isotherms of $LuPc_2$ and $YbPc_2$.

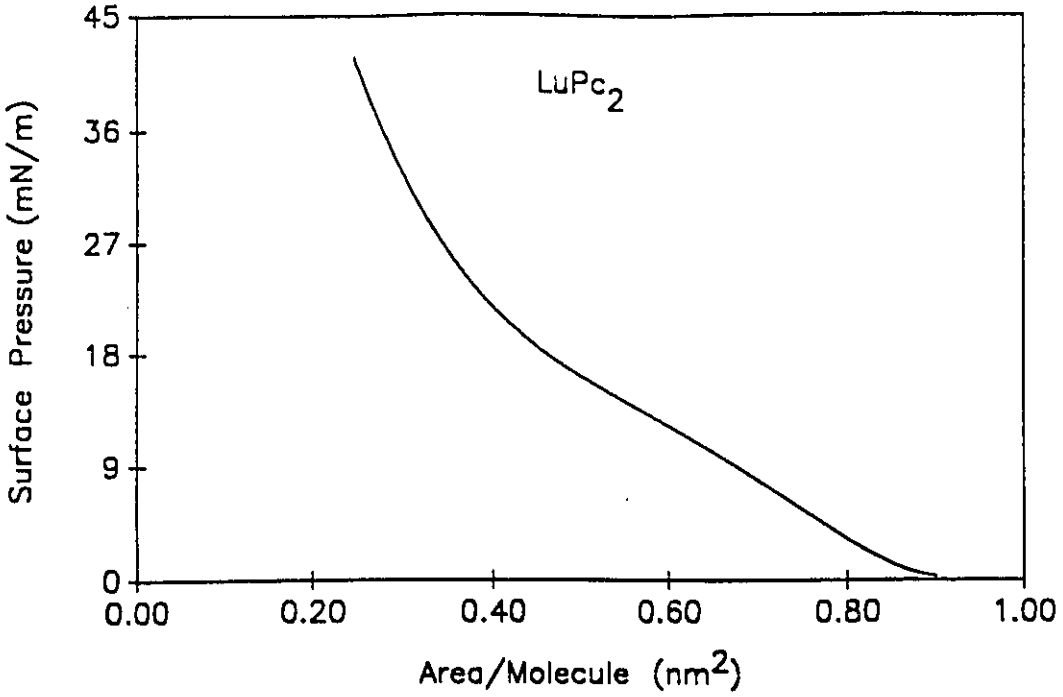
45
36
27
18
9
0
Surface Pressure (mN/m)
LuPc2
0.00
0.20
0.40
0.60
0.80
1.00
Area/Molecule (nm2)

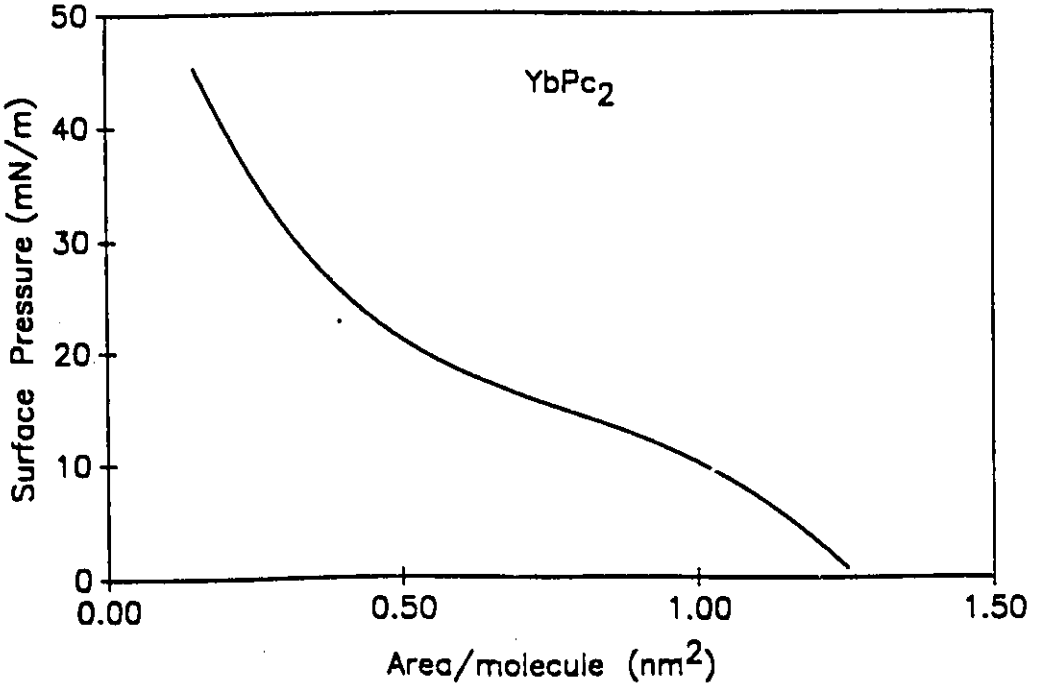
50
40
30
20
10
0
Surface Pressure (mN/m)
YbPc2
0.00
0.50
1.00
1.50
Area/molecule (nm2)

Figure 7.2

Figure 7.3 SERS(II=514.5 nm, ST polarization) spectra of one mixed LB of $YbPc_2$ before and after exposure to NOX gas

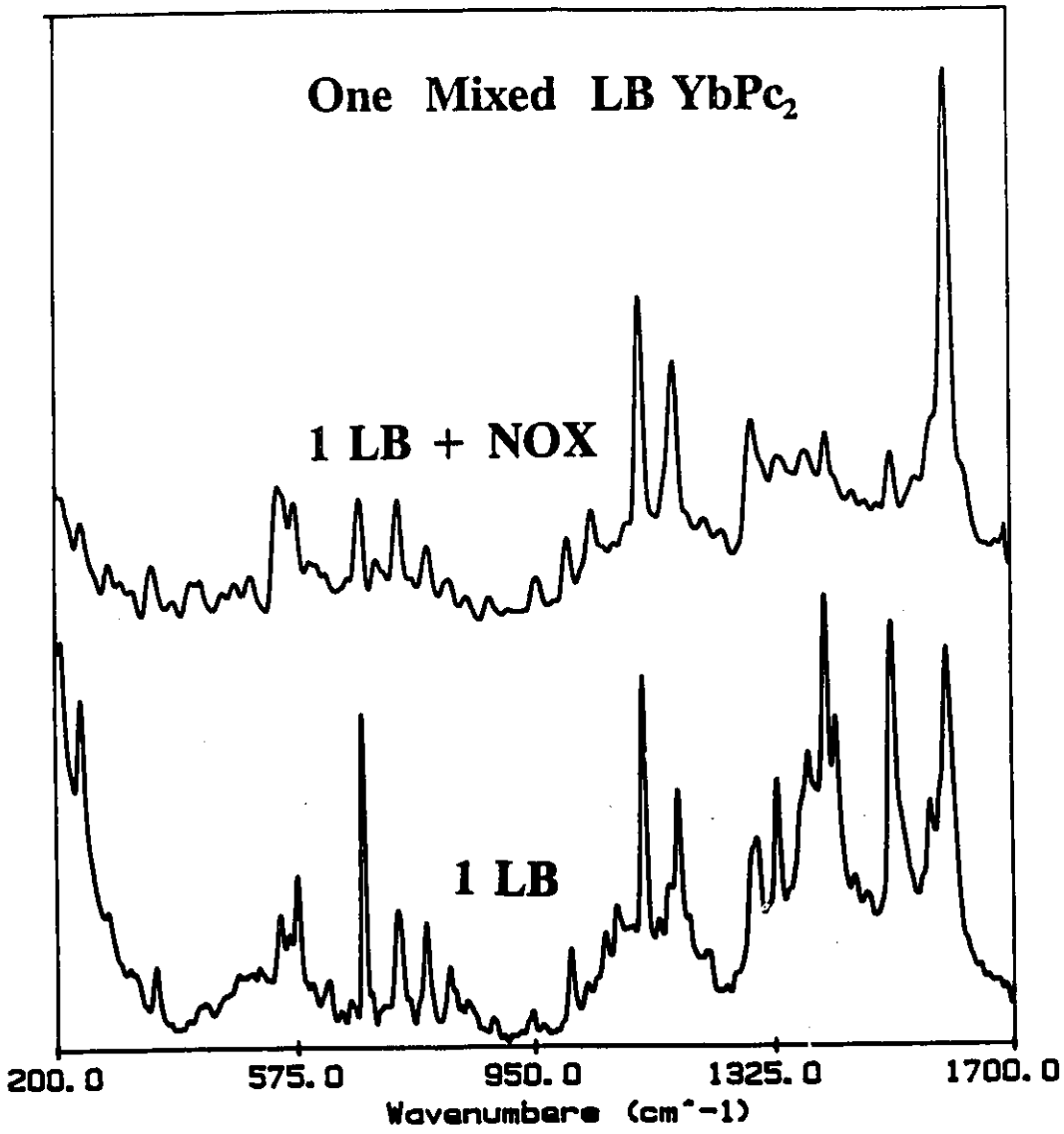
One Mixed LB YbPc2
1 LB + NOX
1 LB
200.0
575.0
950.0
1325.0
1700.0
Wavenumbers (cm^-1)

Figure 7.3

transferred at a rate of 4.8 mm/min to Ag-Sn spheres and hydrophillic glass slides. The transfer ratio for neat LB of $LuPc_2$ and $YbPc_2$ was on the average .9/layer. Petty et al. found that mixed monolayers of $YbPc_2$ were better suited for LB films.[22] We found that mixed monolayers in the mole ratio bisphthalocyanine:arachidic acid=3:1 were easy to work with and they gave near unity transfer ratio. The purpose of arachidic acid was to lubricate the otherwise rigid and fragile monolayer on the subphase.[23] The SERS of one mixed LB(3:1) of $YbPc_2$ on Ag-Sn spheres before and after the reaction with NOX is shown in Figure 7.3. The effect of NOX was similar to that observed for thin film(Figure 7.1). Unfortunately NOX also tarnished and reacted with the Ag in the SERS substrate. The reaction was so severe it caused a 4 nm Ag island film to turn transparent. It was shown by SERS that NOX attacked Ag powder to produce Ag_2O, $AgNO_2$ and $AgNO_3$.[24,25] The SERS of Ag-Sn spheres exposed to NOX is presented in Figure 7.4. The bands at 812(NO_2^-), 955(Ag_2O), and 1039(NO_3^-) cm^{-1} were attributed to the species formed in the reaction bewteen NOX and silver.[24,25] Though these bands were not present in the SERS spectra of one mixed LB of $LuPc_2$ or $YbPc_2$ exposed to NOX, an alternative SERS substrate was considered. Au island films of 4 nm thickness were extremely stable in the presence of NOX. They did not discolour and the uv-vis spectra before and after exposure were almost identical. The Au island film was suitable to monitor the desorption of NOX from Pc. The 647.1 nm laser line was used to excite the localized surface plasmons of the Au island film. Excitation at 647.1 nm for a Au island film covered with Pc produced SERRS.

Figure 7.4 SERS(λ=514.5 nm, ST polarization) spectra of Ag-Sn spheres exposed to NOX gas

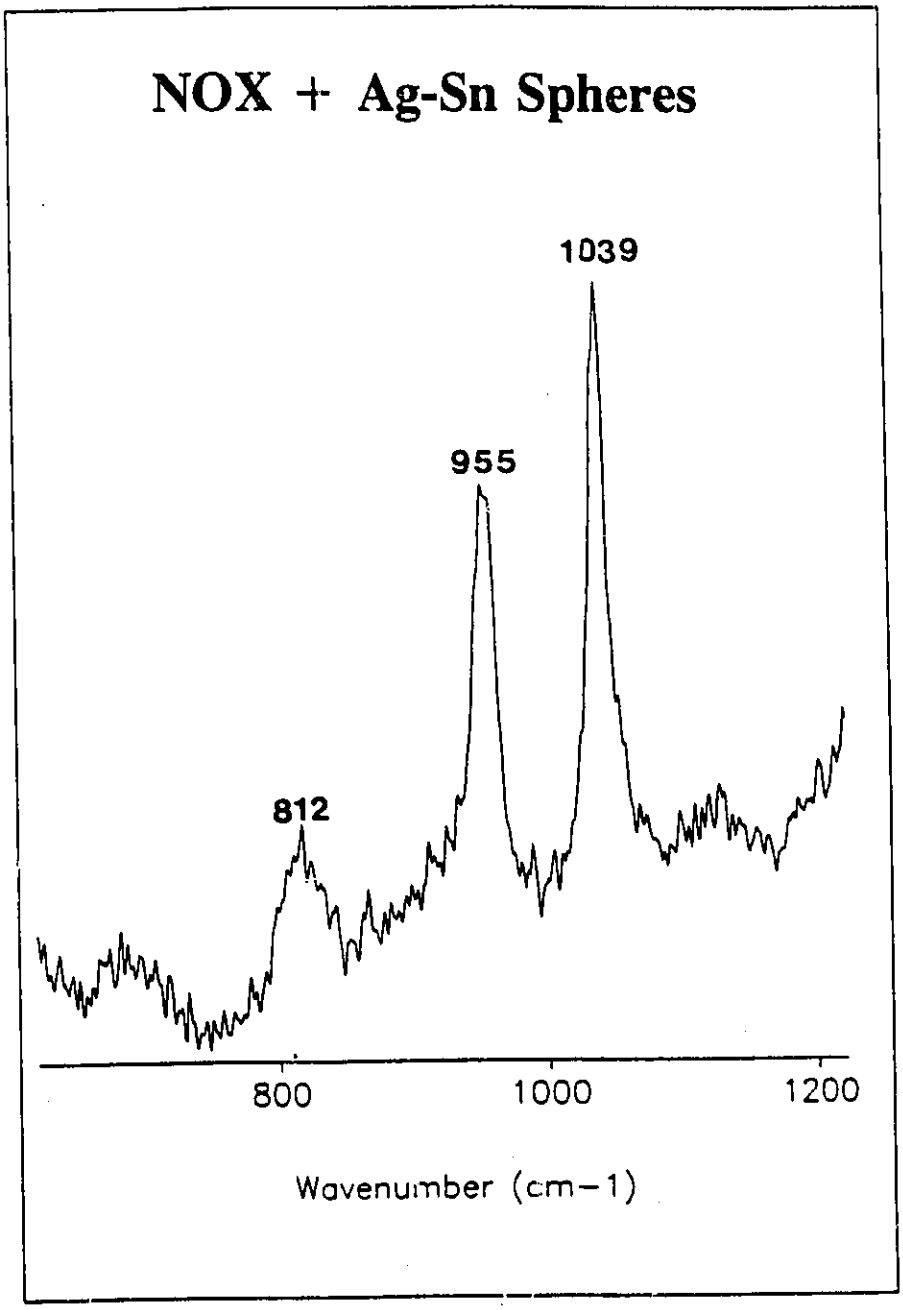

Figure 7.4

Figure 7.5 Surface pressure-area isotherms for CuPcTTb and H_2PcTTb

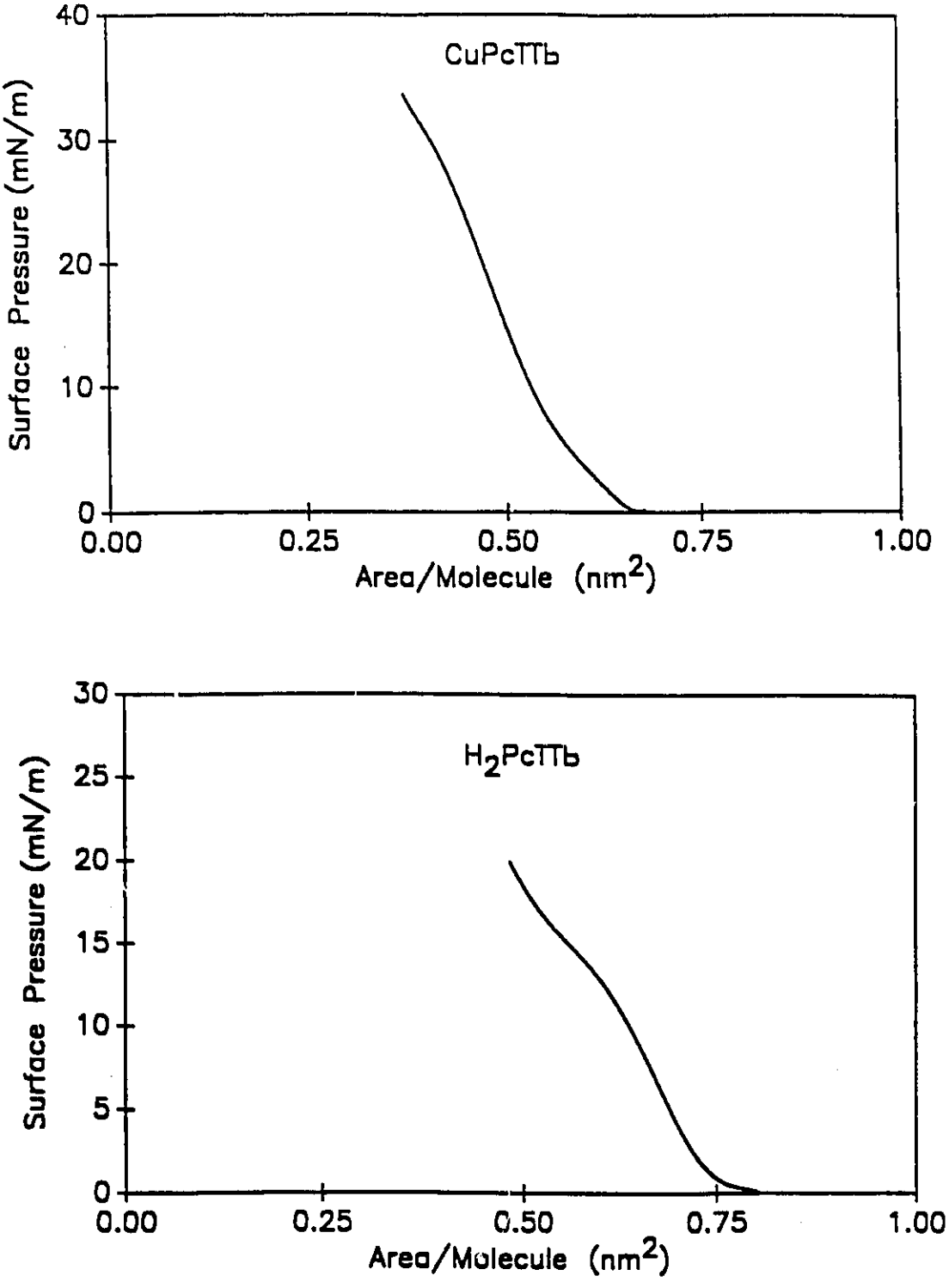
CuPcTTb
Surface Pressure (mN/m)
40
30
20
10
0
0.00
0.25
0.50
0.75
1.00
Area/Molecule (nm2)
H2PcTTb
Surface Pressure (mN/m)
30
25
20
15
10
5
0
0.00
0.25
0.50
0.75
1.00
Area/Molecule (nm2)

Figure 7.5

SERRS was used to monitor the chemical adsorption of NOX on one mixed(Pc:arachidic acid=3:1) monolayer of metal free tetra-*tert*-butylphthalocyanine(H_2PcTTb), copper tetra-*tert*-butylphthalocyanine(CuPcTTb), $LuPc_2$ and $YbPc_2$. The preparation of H_2PcTTb[23,26], and CuPcTTb[17,27,28] monolayers was previously reported by other groups. The pressure-area isotherms at 20 °C for neat CuPcTTb and neat H_2PcTTb spread from toluene solutions are presented in Figure 7.5. The isotherm of H_2PcTTb reported by Kovacs[23] et al. was similar to the one shown in Figure 7.5. The isotherm for CuPcTTb prepared in our laboratory was however very different than those reported in the literature.[17,27] Neat monolayers of H_2PcTTb, CuPcTTb, $YbPc_2$ and $LuPc_2$ were also transferred to glass slides. All monolayer work in this section was carried out at a constant surface pressure of 15 mN/m and 6 mm/min transfer rate.

Electronic absorption spectroscopy for LB films on glass was also used to monitor the adsorption and the desorption of NOX. The procedure used to treat LB films(on glass and on Au films) with NOX was identical to that described for thin solid films. Desorption studies consisted of evacuating the exposed film at 3 Pa for three hours.

In Figure 7.6 the SERRS for one mixed LB of H_2PcTTb before and after exposure to NOX is shown. Frequencies were observed with the same value in both spectra and the relative intensities showed only minor changes. The absorption spectrum for 8 LB on glass is shown in Figure 7.7. The upper spectrum in Figure 7.7 is typically observed in the solution[29] or the crystal[30] state of H_2Pc derivatives.

Figure 7.6 SERRS(ST polarization) spectra of one mixed LB of H_2PcTTb on a 4 nm Au island film (A) and after exposure to NOX gas (B)

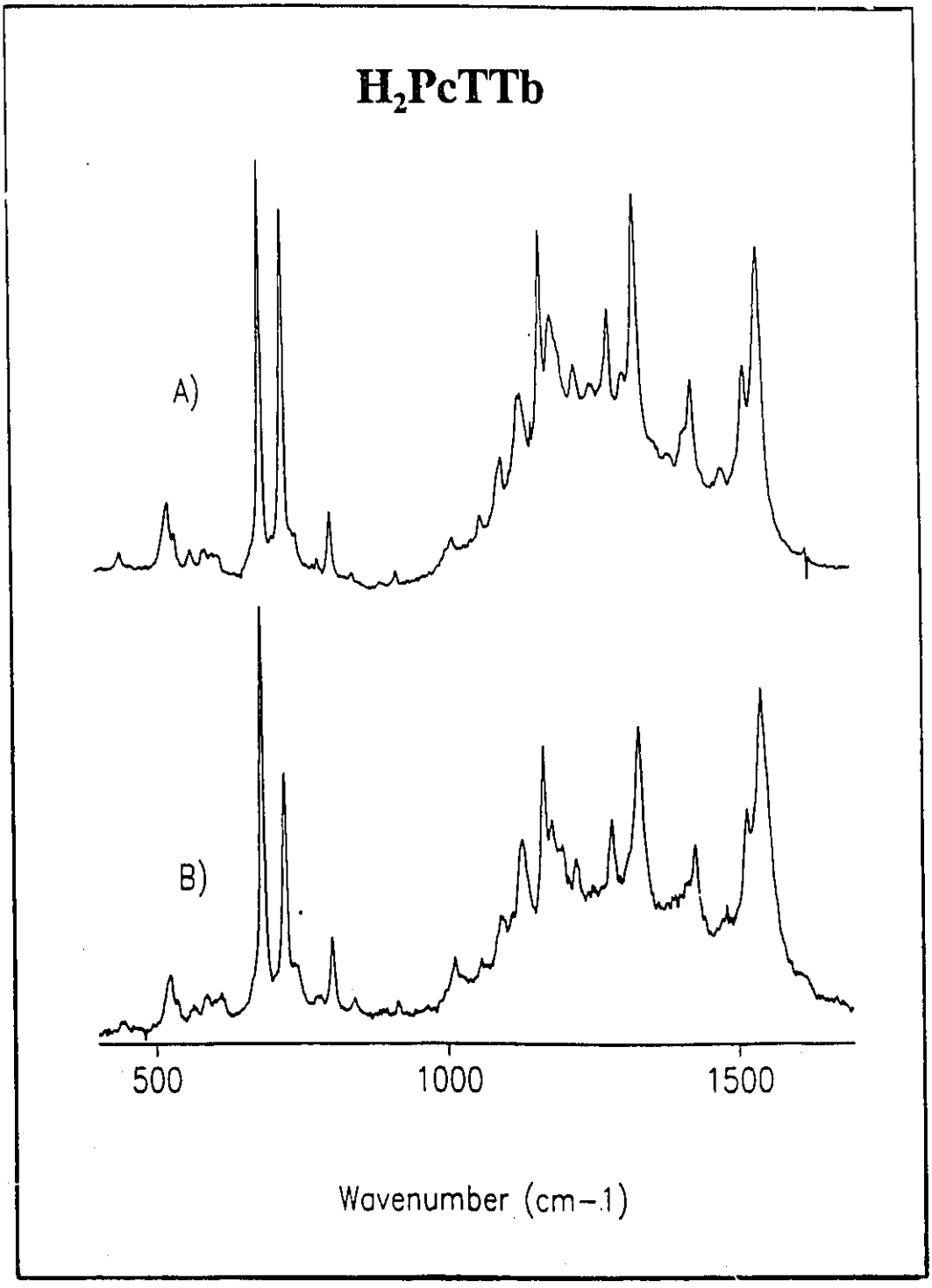

Figure 7.6

Figure 7.7 Electronic spectra of H_2PcTTb in solution (A), eight LB monolayers on glass (B), and eight LB exposed to NOX gas (C)

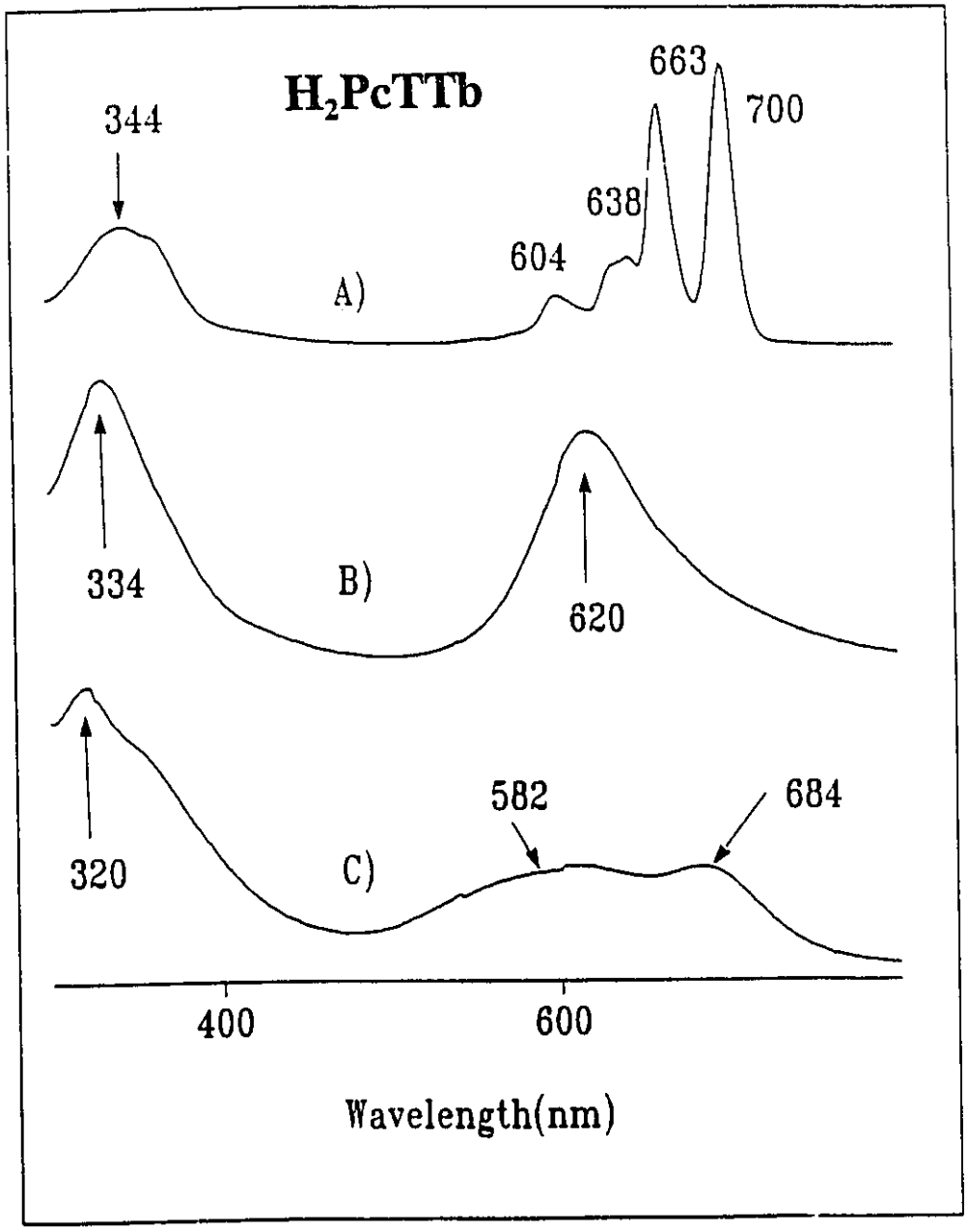
H2PcTTb
344
663
700
638
604
A)
334
B)
620
320
C)
582
684
400
600
Wavelength(nm)

Figure 7.7

The middle absorption spectrum contained a unique single peak for the Q-band. This band can be attributed to the π-π aromatic interactions in the LB film. The last absorption spectrum was recorded for the LB assembly exposed to NOX. The Q-band was split into two broad bands whose maximum corresponded to the band in the untreated LB sample(near 600 nm) and to the solution band(near 700). The splitting of the Q-band in the LB film suggested that NOX caused a disruption in the π-π aromatic interactions. NOX also self desorbed at room temperature and normal pressure and the middle spectrum in Figure 7.7 was recovered. The results of UV-vis and SERRS therefore strongly suggested that NOX was physisorbed to H_2PcTTb.

The reversible adsorption of NOX on one mixed LB of CuPcTTb is shown in Figure 7.8. SERRS spectra A) and B) were taken before and after exposure to gas respectively. The bottom spectrum was recorded after the sample was put in vacuum. The effect of NOX in spectrum B) was to reduce the relative intensity of the macrocycle breathing at 688 cm^{-1} and the pyrrole stretching band at 1530 cm^{-1}. Since Raman intensities originate from changes in the polarizability with the corresponding normal coordinate, an intensity decrease in a Raman band can be attributed to a loss of electronic density in the normal coordinate. The spectral evidence suggested that NOX polarized both the pyrrole and macrocycle groups. The interaction was, however, not strong enough to cause a shift in the vibrational frequencies. The electronic spectra for CuPcTTb and its interaction with NOX is presented in Figure 7.9. In the middle spectrum the Q-band was observed to split when gas was added. The result was similar to that observed in H_2PcTTb where NOX acted to only disturb

Figure 7.8 SERRS spectra(ST polarization) of one mixed LB of CuPcTTb on Au film (A), after exposure to NOX gas (B), and after desorption of NOX gas (C)

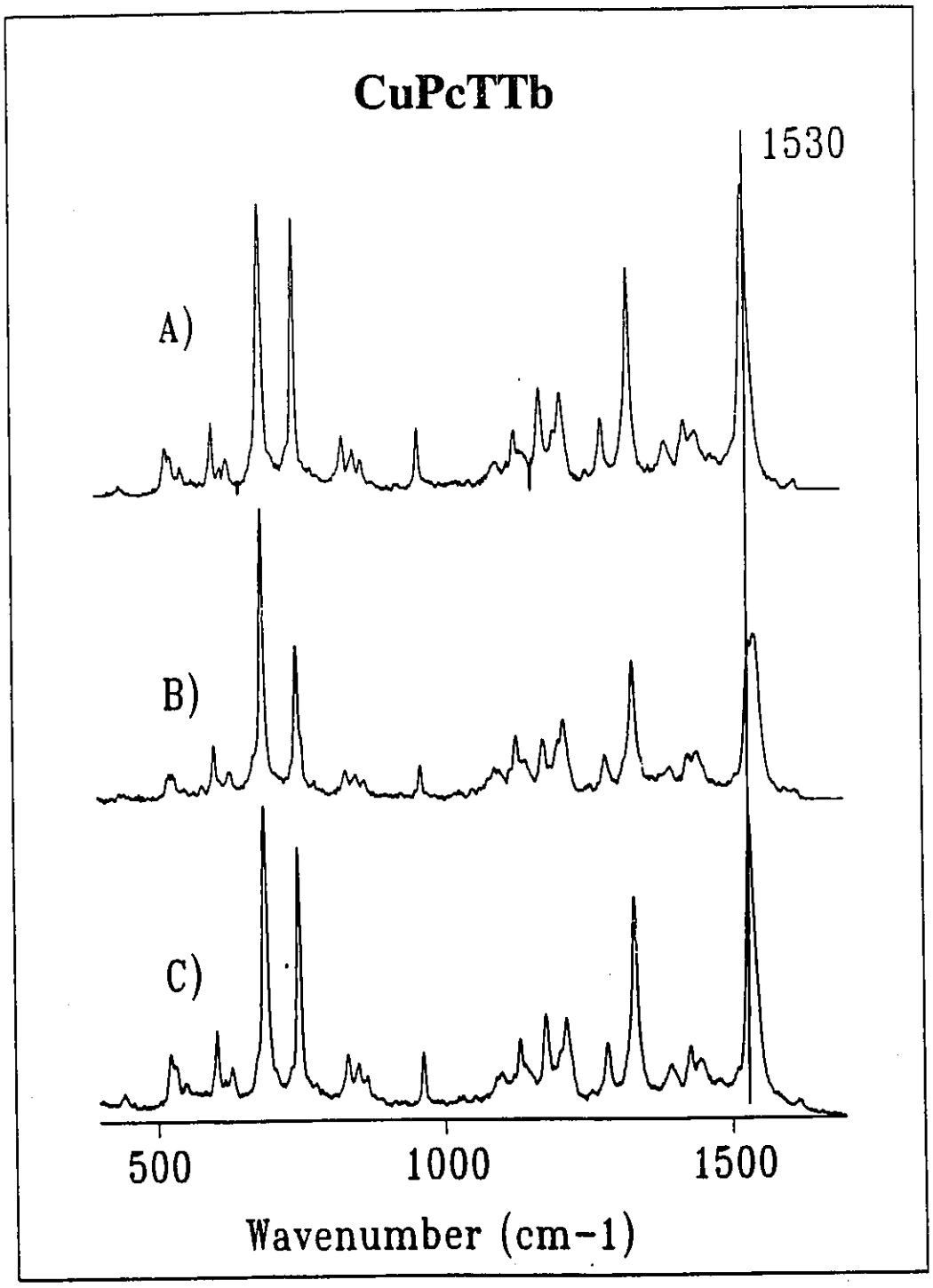

Figure 7.8

Figure 7.9 Absorption spectra of 5 LB monolayers of CuPcTTb (A), after NOX adsorption (B), and after gas desorption (C)

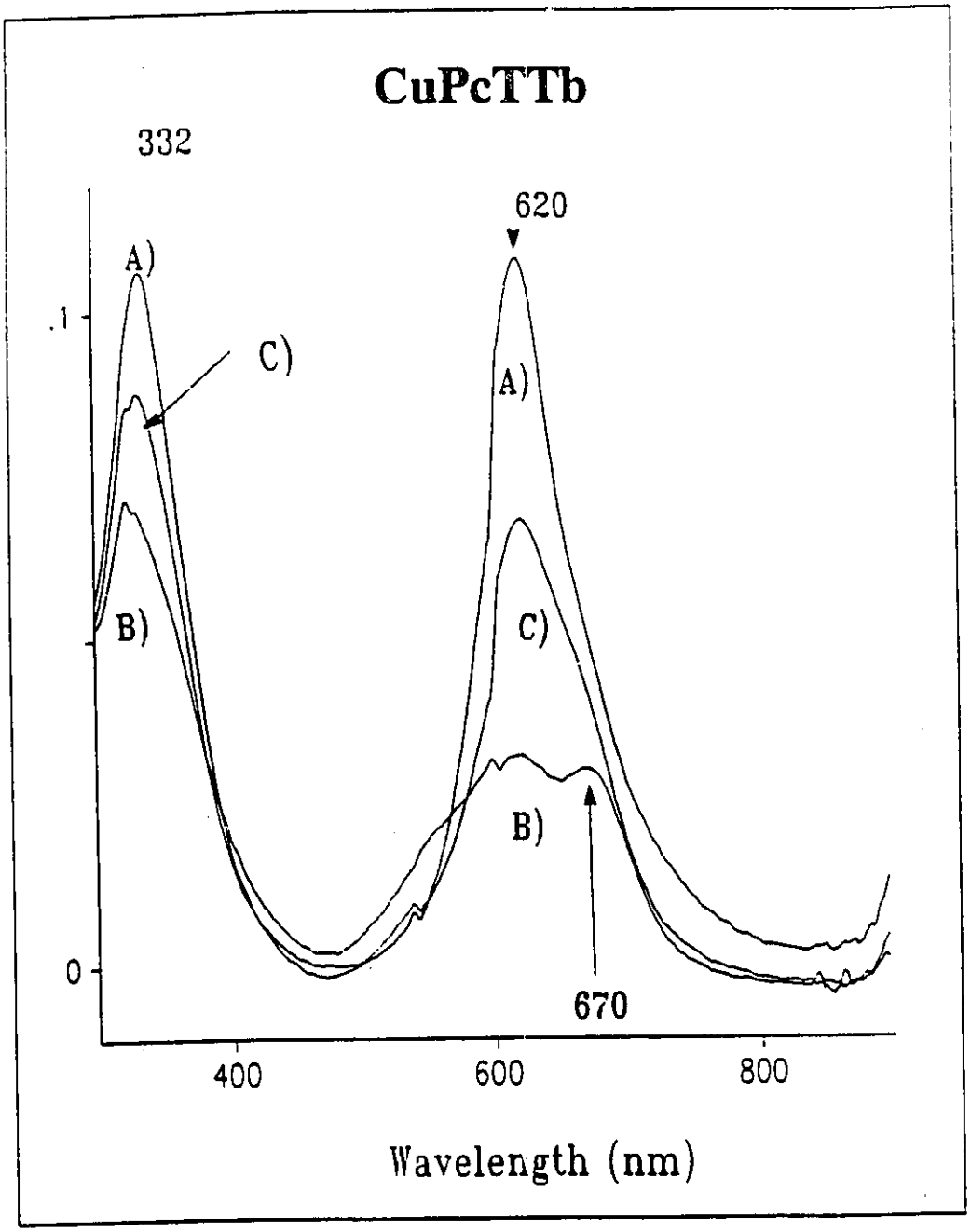

Figure 7.9

the π-π aromatic interactions. The bottom spectrum showed that NOX was desorbed from the multilayer assembly when placed in vacuum for three hours. The observed difference in the SERRS data for H_2PcTTb and CuPcTTb was therefore attributed to the metal. Indirect evidence for the proposed interaction was provided by Electron Paramagnetic Resonance(EPR) measurements in toluene solution. The EPR signal of CuPcTTb became silent after addition of NOX. The latter results suggested a direct NO_2-metal interaction. A diagram of the proposed molecular interaction between NO_2 and CuPcTTb is given in Figure 7.10.

The third type of phthalocyanine was a bisphthalocyanine where one atom was coordinated to two Pc macrocycles. The effect of NOX towards $LuPc_2$ or $YbPc_2$ was more drastic than in the previous two cases. The SERRS progress of one mixed LB of $YbPc_2$ exposed to NOX are presented in Figure 7.11. The SERRS spectrum before and after gas adsorption was more pronounced than in CuPcTTb or H_2PcTTb. The weak band at 1549 cm^{-1} became the most dominant band in NOX exposed sample. In the resonance Raman studies of lanthanide bisphthalocyanines[21] the band at 1524 cm^{-1} was assigned to C=N aza group. Based on the earlier discussion that NO_2 attacked the metal in CuPcTTb, the middle spectrum could be attributed to NO_2 coordinating to the lanthanide and decoupling the aza stretching vibration. The polarization effect of NO_2 was also sensed by the macrocycle band at 679 cm^{-1}. The NO_2-$YbPc_2$ adduct could thus be envisioned in terms of NO_2 attacking the metal and drawing electronic charge from the inner macrocyle ring. The SERRS in the bottom spectrum showed that the adsorption process was completely reversible. The electronic spectra of $YbPc_2$

Figure 7.10 Molecular diagram of CuPcTTb with one NO_2 molecule. The tert-butyl groups are represented by Tb

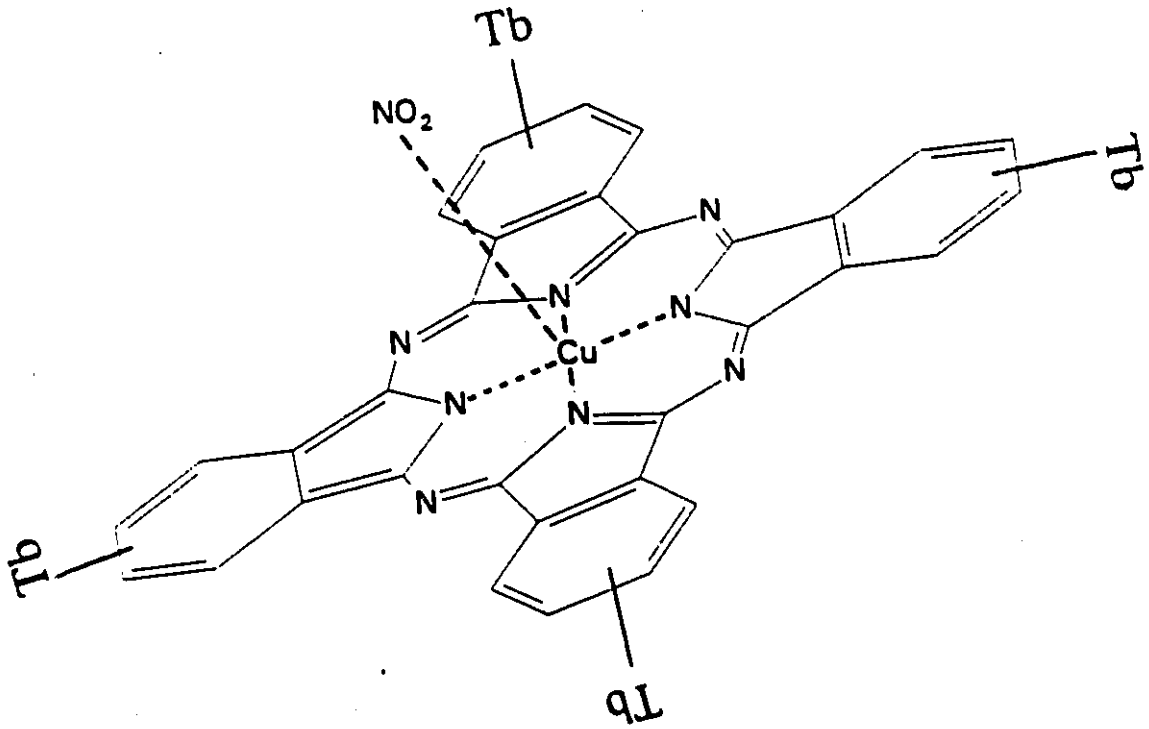

Figure 7.10

are shown in Figure 7.12. In the middle spectrum the effect of NOX was to shift the Q-band to higher wavelengths. The red shift was characteristic of the oxidized form of rare earth bisphthalocyanine.[22] For $YbPc_2$ or $LuPc_2$ the SERRS and UV-vis absorption spectra showed that desorption of gas was completely reversible.

In summary reversible adsorption of NOX on one mixed LB of CuPcTTb, $YbPc_2$, and $LuPc_2$ was clearly observed in the SERRS spectra. The oxidized macrocycle was identified in the absorption spectrum of rare earth bisphthalocyanine + NOX. Oxidation of the macrocyle resulted in a polarization of the macrocycle where the C=N aza groups were affected. The relative strength of the interaction between NOX and H_2PcTTb, CuPcTTb and rare earth bisphthalocyanine($LuPc_2$, $YbPc_2$) was weak, strong and very strong respectively. The drastic changes in the SERRS and absorption spectra observed for CuPcTTb and $YbPc_2$(or $LuPc_2$) support that the adsorption site was the metal centres.

The SERS data of one mixed LB of $YbPc_2$(Figure 7.3) and the Raman spectrum of the 200 nm film of $YbPc_2$(Figure 7.1) showed that the NOX also polarized the C=C in pyrrole. The accumulated data in RS, SERS and SERRS supported the notion that NOX strongly affected the macrocycle bands. In particular the C=C(pyrrole) and C=N(aza group) were mostly influenced by the oxidising gas. This Raman study thus demonstrated selective tuning in the reaction of NOX + Pc. The changes in C=C(pyrrole) were clearly observed with λ=514.5 nm(off-resonance excitation), while changes to C=N(aza group) were observed with λ=647.1 nm (resonance Raman scattering).

Figure 7.11 SERRS spectra(ST polarization) of one mixed LB of $YbPc_2$ on Au island (A), after NOX adsorption (B), and after desorption (C) The inset shows the expanded pyrrole frequency region.

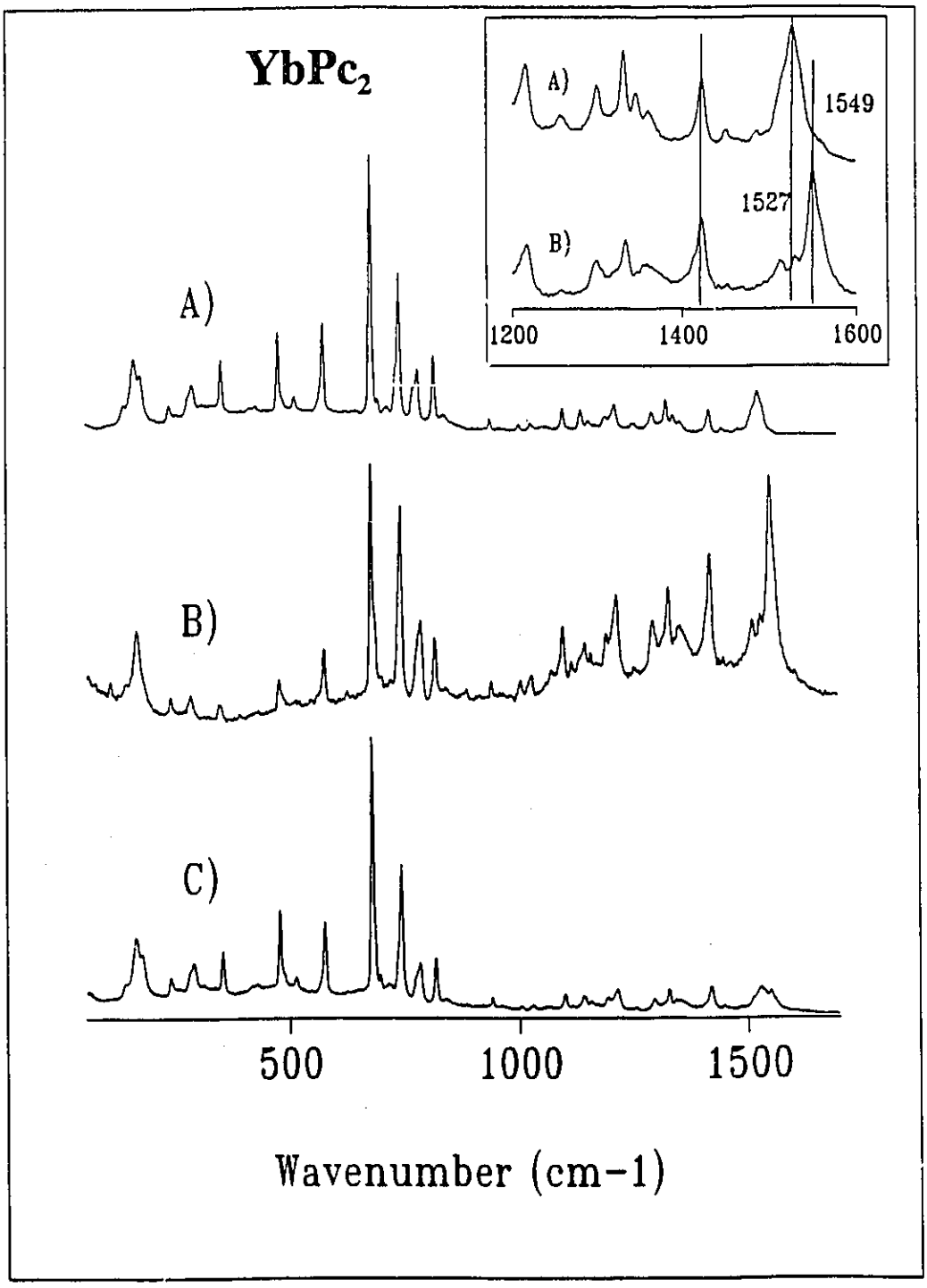
YbPc2
A)
B)
C)
500
1000
1500
Wavenumber (cm-1)
A)
1549
1527
B)
1200
1400
1600

Figure 7.11

Figure 7.12 Absorption spectra of three LB of $YbPc_2$ on glass (A), after NOX adsorption (B), and gas desorption (C)

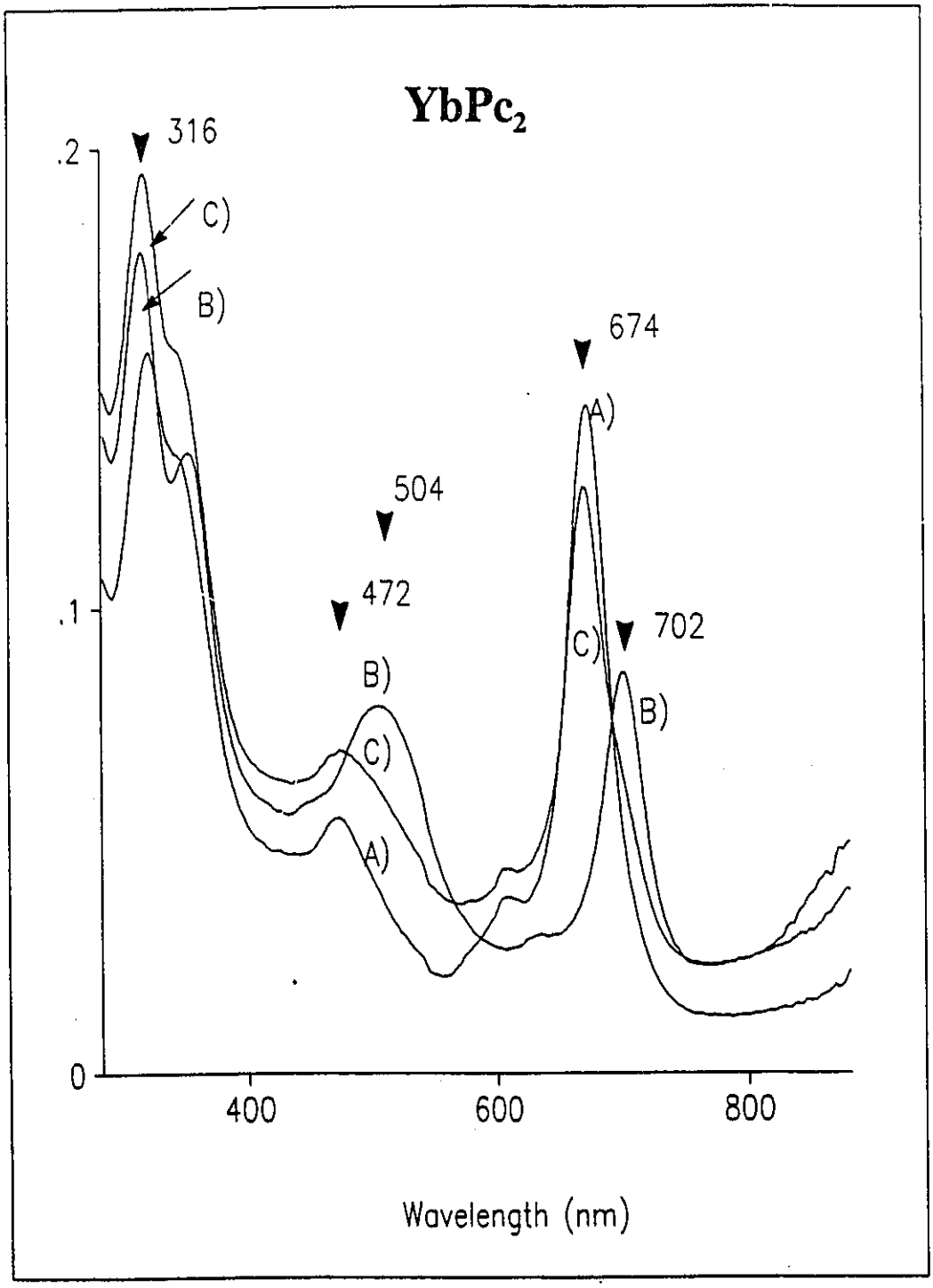
YbPc2
316
C)
B)
674
A)
504
472
C)
B)
702
B)
C)
A)
.2
.1
0
400
600
800
Wavelength (nm)

Figure 7.12

Oxidation and Reduction of Bisphthalocyanine

During the Raman work of Pc + NOX it became obvious that the redox properties of Pc were intrinsically important. We selected to investigate qualitatively the redox properties of a rare earth bisphthalocyanine since they showed the most changes to NOX. The chemical oxidation(with NOX) and reduction(with hydrazine) for a solution of $LuPc_2$ in chloroform is shown in Figure 7.13. The oxidized(spectrum B) form of $LuPc_2$ was observed with red shifted Q-band. Reduced(spectrum C) $LuPc_2$ however showed a blue shifted Q-band. Electrochemical oxidation also produced similar results to the chemical oxidation.

The spectroelectrochemical analysis of a 18 nm evaporated film of $LuPc_2$ on an indium tin oxide(ITO) working electrode is shown in Figure 7.14. The counter electrode was a Pt wire and the electrolyte was 1.0 M KCl at pH 1.23. The potential difference was measured with respects to the standard calomel reference electrode. At 0 V the Q-band was positioned at ca. 640 nm. At +0.960 V the Q-band clearly showed red shifted to ca. 705 nm. Our spectroelectrochemical results were also similar to those published in the literature.[31,32]

It can be concluded that the electronic absorption band due to electrochemical oxidation of the macrocycle was the same band as in the chemical oxidation(Figure 7-13B) with NOX. The NO_2 acted as an electron acceptor in the formation of NO_2-$LnPc_2$ adduct.

Figure 7.13 Chemical oxidation and reduction of $LuPc_2$ in chloroform, green starting material (A), oxidation with NOX gas (B), reduction with hydrazine (C)

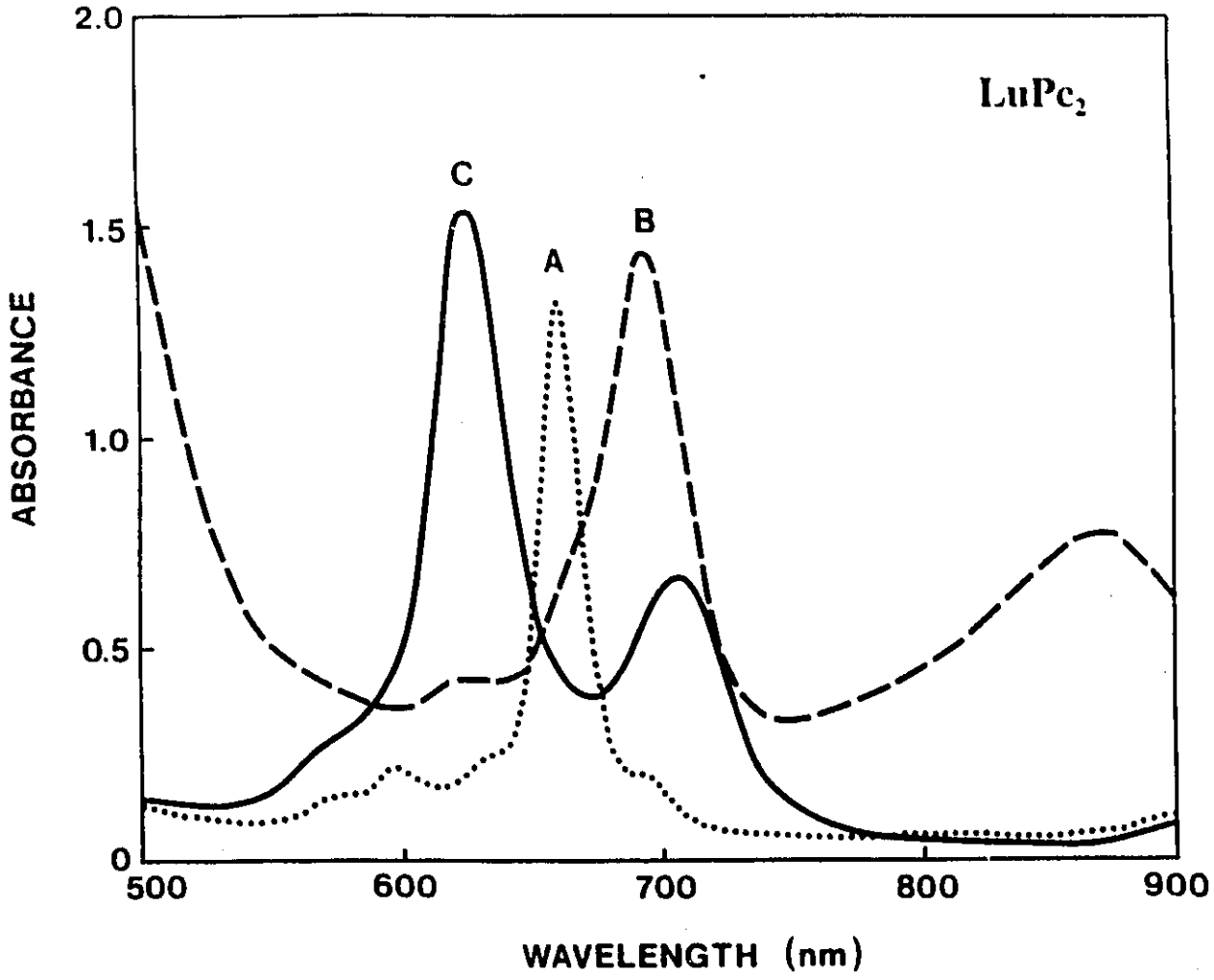
LuPc2
C
B
A
2.0
1.5
1.0
0.5
0
ABSORBANCE
500
600
700
800
900
WAVELENGTH (nm)

Figure 7.13

Figure 7.14 Absorption spectra of a 18 nm $LuPc_2$ film at (I) 0 V, (II) +0.488 V, and (III) +0.960 V. The potential are referenced against the standard calomel electrode.

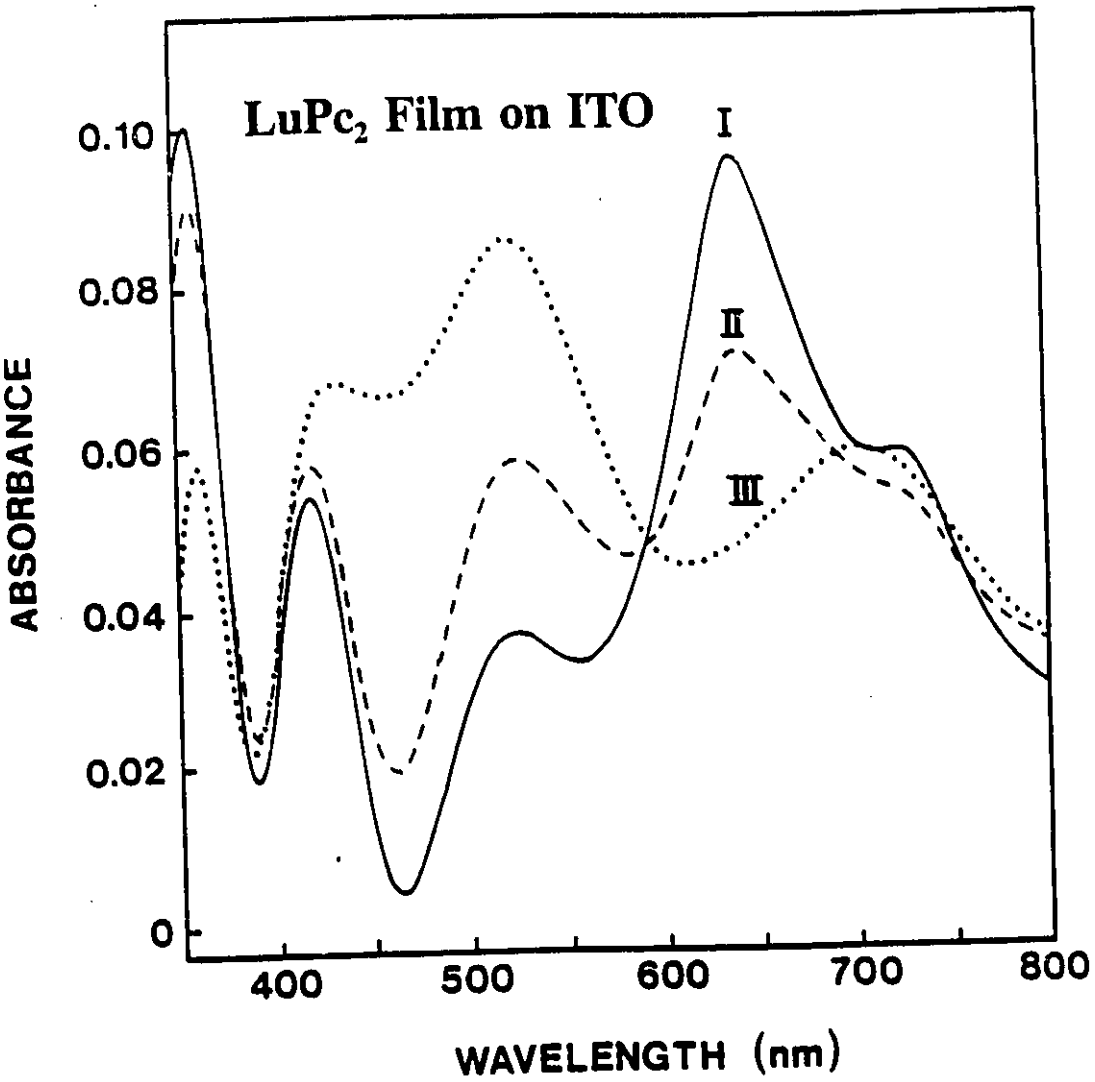
LuPc2 Film on ITO
I
II
III
ABSORBANCE
0.10
0.08
0.06
0.04
0.02
0
400
500
600
700
800
WAVELENGTH (nm)

Figure 7.14

CONCLUSIONS

In the present thesis surface enhanced {resonance} Raman scattering(SE{R}RS) was reported for various phthalocyanine derivatives. SERS and SERRS were reported for VOPc evaporated onto a Ag substrate. The IR spectrum of a thin film of VOPc sublimed onto KBr crystal showed preferred molecular orientation. The Raman data were complemented with the infrared data and the symmetry assignment of bands in VOPc was attempted. Favourable excitation with P-polarized light was observed for ultrathin films of VOPc adsorbed onto highly reflecting surfaces. Davydov splitting was also seen in the Raman spectra of these samples.

SERRS was used to characterize one Langmuir-Blodgett monolayer of VOPcTTb and ZnPcTTb. The SERS and SERRS of VOPcTTb and ZnPcTTb(or any of the Pcs in this thesis) showed no spectral evidence of strong interaction between Pc and the SERS substrate. The SERS spectra showed no shift in the molecular frequencies of Pc and the Pc molecules were therefore considered to be *physisorbed* onto the substrate. The SERRS spectra were depolarized in that the SS, SP, PP,and PS components gave identical spectra. The vibrational characterization of VOPcTTb and ZnPcTTb was also given.

Enhanced absorption was observed in the energy transfer experiments of one LB of ZnPcTTb(acceptor layer) and one LB of PBDC(donor layer) on Ag-Sn spheres. Only when the acceptor layer was directly adjacent to the Ag-Sn spheres was the excimer emission of PBDC totally quenched(i.e., there was complete energy transfer). Spectroscopic tuning was also identified in the energy transfer experiments. Selecting

a laser line in resonance with either ZnPcTTb or PBDC exclusively produced SERRS of either the donor or acceptor layer.

The LB technique was used to control surface coverage. The coverage dependence on the SERRS intensity using mixed LB films of(VOPcTTB and arachidic acid) showed a maximum at submonolayer coverage. The negative dependence of SERRS with increasing surface coverage was rationalized in terms of de-exication or quenching of the surface plasmons.

SERRS, IR, and uv-vis were used to investigate the spectral features of the green and blue form of rare earth bisphthalocyanines. The differences observed in the IR and SERRS spectra of the green and blue species could be attributed to differences in molecular symmetry.

The reversible adsorption of NO_2 on a single LB of H_2Pc, CuPcTTb and $YbPc_2$(or $LuPc_2$) was monitored by the highly sensitive SERRS technique. The changes in the SERRS spectra were attributed to NO_2 interacting with the metal in CuPcTTb, $YbPc_2$ or $LuPc_2$ and polarizing the macrocycle vibrations. The data in the electronic spectra showed that NO_2 acted as an oxidant to lanthanide bisphthalocyanine complexes.

REFERENCES-Chapter 1

1. Linstead R. P. *J. Chem. Soc.* 1016, (1934)
2. Dent, C. E.; Linstead, R. P.; Lowe, A. R. *J. Chem. Soc.* 1017, (1934)
3. Linstead, R.P.; Lowe, A. R. *J. Chem. Soc.* 1022, (1934)
4. Linstead, R.P.; Lowe, A. R. *J. Chem. Soc.* 1031, (1934)
5. Braun, A.; Tcherniac, J. *Ann Ber.* **40**, 2709, (1907)
6. Robertson, J. M. *J. Chem. Soc.* 615, (1935)
7. Robertson, J. M. *J. Chem. Soc.* 1195, (1936)
8. Roberston, J. M.; Woodward, I. *J. Chem. Soc.* 219, (1937)
9. Roberston, J. M.; Woodward, I. *J. Chem. Soc.* 36, (1940)
10. Simon. J.; André J.J., in *Molecular Semiconductors, Photoelectrical Properties and Solar Cells*(Lehn, J. M., Rees, Ch. W., eds.) Springer-Verlag, Berlin, 1985
11. Thomas, A. L., *Phthalocyanine Research and Application*, CRC Press, Boca Ralton Florida, 1990
12. Rosenthal, I.; Ben-Hur, E., in *Phthalocyanines Properties and Applications*, (Leznoff C. C.; A. P. Lever eds), VCH Publishers, New York, 1990
13. Dautartas, M. F.; Suh, S.Y.; Forrest, S. R.; Kaplan, M. L.; Lovinger A. J.; Schmidt P. H. *Appl. Phys. A.* **36**, 71, (1985)
14. Kivits, P.; de Bont, R.; van der Venn, J. *J. Appl. Phys. A.* **26**, 101, (1981)

15. Morel, D. L.; Stogryn, E. L.; Ghosh, A. K.; Feng, T.; Purwin, P. E.; Shaw, R. F.; Fishman, C.; Bird, G. R.; Piechowski, A. P. *J. Phys. Chem.* **88**, 923 (1984)

16. Fan, F.; Faulkner, L. R. *J. Chem. Phys.* **69**, 3334, (1978)

17. Loutfy, R. O.; McIntyre, L. F. *Can. J. Chem.* **61**, 72, (1982)

18. Lawrence, M. F.; Dodelet, J. P.; Dao, L. H. *J. Electrochem. Soc.* **131**, 2977, (1984)

19. Tang, C. W. *Appl. Phys. Lett.*, **48**, 183, (1986)

20. Law, K. *J. Phys. Chem.* **92**, 4226, (1988)

21. Klofta, T. J.; Danziger, P. L.; Pankow, J.; Nebesny, K. W.; Armstrong, N. R. *J. Phys. Chem.* **91**, 5646, (1987)

22. Hempstead, M. R. Ph.D. Thesis, York University, 1987

23. Hon, A. H.; Bahnemann, D. W.; Hoffmann, R. M. *J. Phys. Chem.* **91**, 2109, (1987)

24. Santos, L. M.; Baldwin R. P. *Anal. Chem.* **58**, 848, (1986)

25. Santos, L. M.; Baldwin R. P. *Anal. Chem.* **59**, 1766, (1987)

26. Moser, F H.; Thomas, A. L., *The Phthalocyanines Vol.I*, CRC Press Boca Ralton, Florida, 1983

27. Moser, F H.; Thomas, A. L., *The Phthalocyanines Vol.II*, CRC Press Boca Ralton, Florida, 1983

28. *Phthalocyanines Properties and Application* (Leznoff C. C.; Lever, A. P. eds.), VCH Publishers, New York, 1990

29. Leznoff, C. C., in *Phthalocyanines Properties and Applications*, (Leznoff C. C.; A. P. Lever eds), VCH Publishers, New York, 1990

30. Louati, A.; EL Meray, M.; André, J. J.; Simon, J.; Kadish, K. M.; Gross, M. *Inorg. Chem.* **24**, 1175, (1985)

31. Brown, C. J. *J. Chem. Soc.* 2488, (1968)

32. Ukei, K. *Acta Cryst.* **B29**, 2290, (1973)

33. Iyechika, Y.; Yakushi, K.; Ikemoto, K.; Kuroda, H. *Acta Crst.* **B32**, 766, (1982)

34. Wynne, K. J. *Inorg. Chem.* **23**, 4658, (1984)

35. Ziolo, R. F.; Griffiths, C. H.; Troup, J. M. *J. C. S. Dalton* 2300, (1980)

36. Rogers, D.; Osborn, R.S. *J. C. S. Chem. Comm.* 840, (1971)

37. Cariati, F.; Morazzoni, F.; Zocchi, M. *Inorg. Chimica. Acta* **14**, L31, (1975)

38. Day, V. W.; Marks, T. J.; Wachter, W. A. *J. Am. Chem. Soc.* **97**, 4519, (1975)

39. Bennett, W. E.; Broberg, D. E.; Baeniziger, N. C. *Inorg. Chem.* **12**, 930, (1973)

40. Gieren, A.; Hoppe, W. *J. C. S. Chem. Comm.* 413, (1971)

41. Kasuga, K.; Tsutsui, M.; Petterson, R. C.; Tatsumi, K.; Van Opdenbosh, N.; Meyer, E. F. *J. Am. Chem. Soc.* **102**, 4835, (1980)

42. Ashida, M.; Uyeda, N.; Suito C. *Bull. Chem. Soc. Jpn.* **47**, 2616, (1966)

43. Karasek, F. W.; Decius, J. C. *J. Am. Chem. Soc.* **74**, 4716, (1952)

44. Simon. J.; André J.J., in *Molecular Semiconductors, Photoelectrical Properties and Solar Cells*, (Lehn, J. M., Rees, Ch. W., eds.), Springer-Verlag, Berlin, 1985

45. Mindorff, M.S.; Brodie. D. E. *Can. J. Phys.* **59**, 249, (1981)

46. Iwatsu, F.; Koboyashi, T.; Uyeda, N. *J. Phys. Chem.* **84**, 3223, 1980

47. Sidorov, A. N.; Kotlyar, I. P. *Opt. Spectrosc.* **11**, 92, (1961)

48. Sharp, J. H.; Lardon, M. *J. Phys. Chem.* **72**, 3230, (1968)

49. Stillman, M. J.; Nyookong T., in *Phthalocyanines Properties and Applications*, (Leznoff, C. C.; Lever, A. P., eds.), VCH Publishers, New York, 1990

50. Edwards L.; Gouterman, M. *J. Mol. Spectrosc.* **33**, 292, (1970)

51. Dahlberg S. C.; Musser M. E. *J. Chem. Phys.* **70**, 6706, (1980)

52. McHugh, A.; Gouterman, M. *Theoret. Chim. Acta* **24**, 346, (1972)

53. Schaffer, A.; Gouterman, M.; Davidson, E. *Theoret. Chim. Acta* **30**, 9, (1973)

54. Dodsworth, E. S.; Lever, A. B. P.; Seymour, P.; Leznoff C. C. *J. Phys. Chem.* **89**, 5698, (1985)

55. Lyons, L. E.; Walsh, J. R.; White, J. W. *J. Chem. Soc.* 167, (1960)

56. Stillman, M. J.; Thomson, A. J. *J. Chem. Soc. Faraday Trans.II* **70**, 790, (1973)

57. Moahan, A. R.; Brado, J. A.; DeLuca A, F. *J Phys. Chem.* **76**, 446, (1972)

58. Abkowitz, M.; Monohan, A. R. *J. Chem. Phys.* **58**, 2281, (1973)

59. Snow, A. W.; Jarvis, N, L. *J. Am. Chem. Soc.* **106**, 4706, (1984)

60. Hush, N. S.; Woolsey, I. S. *Mol. Phys.* **21**, 465, (1971)

61. H. C. Wolf *Solid State Physics* **9**, 1, (1959)

62. Kasha, M.; Rawls, H. R.; Ashraf El-Bayoumi, *M. Pure Appl. Chem.* **11**, 371, (1965)

63. Davidson, A. T. *J. Chem. Phys.* **77**, 168, (1982)

64. Sims, T. D.; Pemerton, J. E.; Armstrong, N. R. *Chem. Mat.* **1**, 26, (1989)

REFERENCES-Chapter 2

1. *Handbook of Thin Film Technology* (Maissel, L. I; Glang, R. eds.), MaGraw-Hill Book Company, New York, 1970
2. Eckertová L. *Physics of Thin Films*, Plenum Press, New York, 1977
3. Langmuir, I. *J. Am. Chem. Soc.* **39**, 1848, (1917)
4. Blodgett, K. B. *J. Am. Chem Soc.* **56**, 496, (1934)
5. Blodgett, K. B. *J. Am. Chem Soc.* **57**, 1007, (1935)
6. Gaines, G. L., Jr. *Insoluble Monolayers at Liquid-Gas Interface*, Wiley-Interscience, New York, 1966
7. Möbius, M.; Bücher H., in *Physical Methods of Chemistry* (Weissberger, A.; Rossiter, B eds.) Wiley, New York, 1972
8. Sugi, M. *J. Mol. Electron.* **1**, 3, (1985)
9. Roberts, G. *Adv. Phys.* **34**, 475, (1985)
10. Agarwal, V. V. *Physics Today* 40, (1988)
11. Levine, M. J.; Schwarz J. A.. *J. Chem. Educ.* **65**, 638, (1988)
12. Richardson, T. *Chem. Br.* **25**, 1218, (1989)
13. *Langmuir-Blodgett Films* (Roberts G. ed.) Plenum Press, New York, 1990
14. Kuhn, H.,in *Physical Methods of Chemistry* (Weissberger, A.; Rossiter, B., eds.) Wiley, New York, 1972
15. Tieke, B. *Adv. Mater.* **2**, 222, (1990)
16. Bohn, P. W.; Walls., D. J. *Mikrochim. Acta* **1**, 3, (1991)

17. Swalen, J. D. *J. Mol. Electron.* **2**, 155 (1986)

18. Swalen, J. D. *Thin Solid Films* **152**, 151 (1987)

19. Egusa, S.; Gemma, N.; Azuma, M. *J. Phys. Chem.* **94**, 2512, (1990)

20 Hansma, H. G.; Gould, S. A.; Hansma P. K.; Gaub, H. E.; Longo, M. L.; Zasadzinski J. A. N. *Langmuir* **7**, 1051 (1991)

21. Lesieur, P.; Barraud, A.; Vandevyver M. *Thin Solid Films* **152**, 155 (1987)

22. Steitz, R.; Mitchell, E. E.; Peterson, I. R. *Thin Solid Films* **205**,124 (1991)

23. Shih, M. C.; Bohannon, T. M.; Mikrut, J. M.; Zschack P.; Dutta, P. *J. Chem. Phys.* **92**, 1556, (1992)

24. Bettarini, S.; Bonosi, F.; Gabrielli, G.; Martini, G. *Langmuir* **7**, 1082 (1991)

25. Knobler C. N. *Adv. Chem. Phys.* **77**, 397 (1990)

26. Tippmann-Krayer; Möhwald H. *Langmuir* **7**, 2303, (1991)

27. Hann, R. A., in *Langmuir-Blodgett Films* (Roberts, G. ed.) Plenum Press, New York, (1990)

28. Aroca, R.; Kovacs, G. J. *J. Mol. Structure* **174**, 53, (1988)

29. Murr. L. E. *Thin Solid Films* **20**, 81, (1974)

30. Aroca. R.; Cook, P. *Am. Lab* **16**, 138, (1984)

31. Damen, T. C.; Porto, S. P. S.; Tell, B. *Phys. Rev.* **142**, 570, (1966)

32. Wilson, E. B.; Decius, J. C.; Cross, P. C. in *Molecular Vibrations The Theory of Infrared and Raman Vibrational Spectra* Dover, New York, 1955

33. Carey, P. R. in *Laboratory Methods in Vibrational Spectroscopy 3rd ed.*(Willis, H. A.; van der Maas, J. H.; Miller, R. G. J. eds.) John Wiley & Sons, Chichester, 1987

REFERENCES-Chapter 3

1. Wilson, E. B.; Decius, J. C., Cross; P. C. *Molecular Vibrations*, Dover, New York, 1955
2. Woodward, L. A. *Introduction to the Theory of Molecular Vibrations and Vibrational Spectroscopy*, Oxford University Press, Oxford, 1972
3. Guillory, W. A. *Introduction to Molecular Structure and Spectroscopy*, Allyn and Bacon, Boston, 1977
4. Ferraro, J. R.; Ziomek, J. S. *Introductory Group Theory and Its Application to Molecular Structure*, Plenum, New York, 1969
5. Cotton, F. A. *Chemical Applications of Group Theory Second Edition*, Wiley-Interscience, New York, 1971
6. Morris., M. D.; Wallen, D. *Anal. Chem.* **51**, 182A, (1979)
7. Strommen, D. P.; Nakamoto, K. *J. Chem. Educ.* **54**, 474, (1977)
8. Behringer, J., in *Molecular Spectrscopy Vol. 2*, Billing & Sons, Great Britain, 1974
9. Rousseau, D. L.; Friedman, J. M.; Williams, P. M. in *Topics in Current Physics, Vol.11*, Springer, Berlin, 1979
10. Campion, A. in *Vibrational Spectroscopy of Molecules on Surfaces*, (Yates, J. T.; Madey, E. E. eds.), Plenum, New York, 1987
11. Chase, B. *Anal. Chem.* **59**, 881A, (1987)
12. Wang, Y.; McCreery, R. L. *Anal. Chem.* **61**, 2647,(1989)

13. Kawai, T.; Umemura, J.; Takenaka, T. *Chem. Phys. Lett.* **162**, 243, (1989)

14. Greenler, R.; G., Slager; T. L. *Spectrochim. Acta* **29A**, 193, (1973)

15. Fleischmann, M.; Hendra, P. J.; McQuillan, A. J. *Chem. Phys. Lett.* **26**, 163, (1974)

16. DiLella, D. P.; Lipson, R. H.; McBree, P.; Moskovits, M. *J. Chem. Phys.* **73**, 4282, (1980)

17. Hexter, R. M.; Albrecht M. G. *Spectrochim. Acta.* **35A**, 233, (1979)

18. Murray, C. A. in *Advances in Laser Spectroscopy, Vol.3* (Garetz, B. A.; Lombardi, J. R. eds.) John Wiley & Sons, New York, 1986

19. Gadzuk, J. W. in *Vibrational Spectroscopy of Molecules on Surfaces*, (Yates, J. T.; Madey, E. E., eds.) Plenum, New York, 1987

20. Gu, X, J.; Akers, K, L.; Moskovits, M. *J. Phys. Chem.* **96**, 383, (1992)

21 Xue, G.; Dai, Q.; Jiang, S. *J. Am. Chem. Soc.* **110**, 2393, (1988)

22. Cotton, T. M.; Kim, J.; Chumanov, G. D. *J. Raman Spectrosc.* **22**, 729 (1991)

23. Albrecht, M. G.; Creighton, J. A. *J. Amer. Chem. Soc.* **99**, 5215, (1977)

24. Jeanmaire, D. L.; Van Duyne, R. P. *J. Electroanal. Chem.* **84**, 1, (1977)

25. *Surface Enhanced Raman Scattering*(Chang, R. K.; Furtak, T. E., eds.), Plenum, New York, 1982

26. Seki, H. *J. Electron. Spectroscop. Relat. Phenom.* **39**, 289, (1986)

27. Otto, A. *J. Raman Spectrosc.* **22**, 743, (1991)

28 Ueba, H. *Surface Sci.* **129**, L267, (1983)

29. Ueba, H.; Ichimura, S.; Yamada, H. *Surface Sci.* **119**, 433, (1982)

30. Pettennkofer, C.; Eickmans, J.; Erturk, U.; Otto, A. *Surf. Sci.* **151**, 9, (1985).

31. Yamada, H. in *Vibrational Spectra and Structure, Vol.17A* (Bist, H. D.; During, J. R.; Sullivan, J. F. eds), Elsevier, Amsterdam, 1989

32. Pockrand, O.; Otto, A. *Solid State Comm.* **35**, 861, (1980).

33. Moskovits, M. *Rev. Mod. Phys.* **57**, 783, (1985)

34. Aroca, R.; Kovacs, G. in *Vibrational Spectra and Structure Vol.19* (Durig, J. R. ed.), Elsevier, Amsterdam, 1991

35. Chang, R.; Laube, B. L.; *CRC Cri. Rev. Solid State Mater. Sci.* **12**, 1, (1984)

36. Debe, M. K. *Progress in Surface Science* **24**, (1987)

37. Krasser, W.; Kojnok, J.; Geurts, J. *J. Raman Spectrosc.* **22**, 777, (1991)

38. Wokaun, A. *Solid State Phys.* **38**, 223, (1984)

39. Murry, C. A. in *Surface Enhanced Raman Scattering*(Chang, R. K.; Furtak, T. E. eds.), Plenum, New York, 1982

40. Cotton, T. M.; Uphaus, R. A.; Möbius, D. *J. Phys. Chem.* **90**, 6071, (1986)

41. Kovacs,G. J.; Loutfy, R. O.; Vincett, P. S.; Jennings, C.; Aroca, R. *Langmuir* **2**, 689, (1986)

42. Liao, P. F.; Bergman, J. G.; Chemla, D. S.; Wokaun, A.; Melngailis J.; Hawryluk, A. M. *Chem. Phys. Lett.* **82**, 355 (1981)

43. Moskovits, M.; DiLella, D. P. in *Surface Enhanced Raman Scattering*(Chang, R. K.; Furtak, T. E. eds.), Plenum, New York, 1982

44. Aroca, P. Jr.; Aroca, R.; Kovacs, G. J.; Loutfy, R., O. *Langmuir* **6**, 1050, (1990)

45. Walls, D. J.; Bohn, P. W. *J. Phys. Chem.* **94**, 2039, (1990)

46. Koh, R.; Hayashi, S.; Yamamoto, K. *Solid State Comm.* **64**, 375, (1987)

47. Schlegel V. L.; Cotton, T. M. *Anal. Chem.* **63**, 241, (1991)

48. Ackers, K. M.Sc Thesis, Windsor, 1987

49. Aroca, R.; Jennings, C.; Kovacs, G. J.; Loutfy, R. O.; Vincett, P. S. *J. Phys. Chem.* **89**, 4051, (1985)

50. Garrof, S.; Weitz, D. A.; Gramila, T. J.; Hanson, C. D. *Opt. Lett.* **6**, 245, (1981)

51. Bennet, R. S.; Scott, G. D. *J. Opt. Soc. Am.* **40**, 203, (1950)

52. Jennings, C. A.; Kovacs, G. J.; Aroca, R. *J. Phys. Chem.* **96**, 1340 (1992)

53. Moskovits, M. *J. Chem. Phys.* **77**, 4408, (1982)

54. Moskovits, M.; Suh, J. S. *J. Phys. Chem.* **88**, 5526, (1984)

55. Zajac, A.; Hecht, E. *Optics*, Addison-Weseley, California, 1976

REFERENCES-Chapter 4

1. Aroca, R.; Zeng, Z., Q. *J. Phys. Chem. Solids* **51**, 135, (1990)
2. Shimanouchi, T.; Matsura, H.; Ogawa, Y.; Harada, I. *J. Phys. Chem.* **94**, 1149, (1981)
3. Lautie, A.; Lautie, M. F.; Gruger, A.; Fakhri, A. *Spectrochim. Acta* **24A**, 252, (1980)
4. Lautie, A.; Novak, A.; *J. Chim. Phys. Physiochim. Biol.* **69**, 1332, (1972)
5. Kitagawa, T.; Abe, M.; Kyogoku, Y.; Ososhi, H.; Watanabe, E.; Yoshida, Z. *J. Phys. Chem.* **80**, 1181, (1976)
6. Jennings, C., M.Sc, Thesis, Windsor, (1987)
7. Aroca, R.; DiLella, D. P.; Loutfy, R. O. *Phys. Chem. Solids* **43**, 707, (1982)
8. Aroca, R.; Loutfy, R. O. *Spectrochim. Acta* **39A**, 847, (1983)
9. Jennings, C.; Aroca, R.; Hor, A.; Loutfy, R. O. *J. Raman Spectrosc.* **15**, 3, (1985)
10. Aroca, R.; Jennings, C.; Kovacs, G. J.; Loutfy, R. O.; Vincett, P. S. *J. Phys. Chem.* **89**, 4051, (1985)
11. Aroca, R.; Loutfy, R. O. *Spectrochim. Acta* **39A**, 847, (1983)
12. Jennings, C.; Aroca, R.; Hor, A. M.; Loutfy, R. O. *J. Raman Spectrosc.* **15**, 34 (1984)

13. Jennings, C.; Aroca, R.; Hor, A.; Loutfy, R. O. *Spectrochim. Acta* **41A**, 1095, (1985)

14. Jennings, C.; Aroca, R.; Hor, A.; Loutfy R. O. *Spectrochim. Acta* **43A**, 725, (1987)

15. Aroca, R.; Martin, F. *J. Raman Spectrosc.* **17**, 243, (1986)

16. Aroca, R.; Clavijo, R. E.; Jennings, C. A.; Kovacs, G. J.; Duff, J. M.; Loutfy, R. O. *Spectrochim. Acta* **45A**, 957, (1989)

17. Huang, T.; Rieckhoff, K. E.; Voight, E. *Can. J. Chem.* **56**, 976, (1978)

18. Huang, T.; Chen, W.; Rieckhoff, K. E.; Voight, E. *Can. J. Chem.* **80**, 4051, (1984)

19. DiLella, D. P.; Barger, W. R.; Snow, A. W.; Smardzewski, R. R. *Thin Solid Films* **133**, 207, (1985)

20. Kobaysahi, T. *Spectrochim. Acta* **26A**, 1313, (1970)

21. Hutchinson, B.; Spencer, B.; Thompson, R.; Neill, P. *Spectrochim. Acta* **43A**, 631, (1987)

22. Rousseau, D. L.; Friedman, J. M.; Williams, P. F. in *Topics in Current Physics Vol. 11.*, Springer, Berlin, 1979

23. Brotman, A.; Burstein, E. *Physica Scripta.* **32**, 385, (1985)

24. Debe, M. K. *Progress in Surface Science* **24**, (1987)

25. Davydov, A. S. in *Theory of Molecular Excitons*, McGraw-Hill, Toronto, 1962

26. R. F., Ziolo; Griffiths, C. H.; Troup, J. M. *J. Chem. Soc. Dalton Trans.* 2300, (1980)

27. Moskovits, M. *J. Chem. Phys.* **77**, 4408, (1982)

28. Kovacs, G. J.; Vincett, P. C.; Sharp, J. H. *Can. J. Phys.* **63**, 346, (1985)

29. Hann, R. A.; Gupta, S. K.; Fryer, J. R.; Eyres, B. L. *Thin Solid Films* **134**, 35, (1985)

30. Roberts, G. G.; Petty, M. C.; Baker, S.; Fowler, M. T.; Thomas, N. J. *Thin Solid Films* **132**, 113, (1985)

31. Brynda, E.; Koropecky, K.; Nespurek, S. *Thin Solid Films* **375**, 384, (1991)

32. Snow, A.; Jarvis, N. L. *J. Am. Chem. Soc.* **106**, 4706, (1984)

REFERENCES-Chapter 5

1. Rowe, J. E.; Shank, C. V.; Murray, C. A. *Phys. Rev. Lett.* **44**, 1770, (1980)
2. Seki, H.; Philpott, M. R. *J. Chem. Phys.* **77**, 5376, (1980)
3. Sanda, P. N.; Demuth, J. E.; Tsang, J. C.; Warlaumont, J. M. in *Surface Enhanced Raman Scattering* (Chang, R. K.; Furtak, T. E. eds.) Plenun, New York, 1982
4. Murray, C. A.; Bodoff, S. *Phys. Rev.* **B32**, 671, (1985)
5. Murray, C. A.; Bodoff, S. *Phys. Rev. Lett.* **52**, 2273, (1984)
6. Zeman, E. J.; Carron, K. T.; Schatz, G. C.; Van Duyne, R. P. *J. Chem. Phys.* **87**, 4189, (1987)
7. Kim, J.; Cotton, T. M.; Uphaus, R. A.; Möbius, D. *J. Phys. Chem.* **93**, 3713, (1989)
8. Aroca, R.; Battisti, D. *Langmuir* **6**, 250, (1990)
9. Knoll, C . M. *Science* **249**, 870, (1990)
10. Chew, H.; Wang, D. S.; Kerker, M. *Phys. Rev.* **28B**, 4169, (1983)
11. Aroca, R.; Kovacs, G. J. in *Vibrational Spectra and Structure Vol. 19* (During, J. R. ed.) Elsevier, Amsterdam, 1991
12. Garoff, S.; Weitz, D. A.; Gramila, T. J.; Hanson, C. D. *Opt. Lett.* **6**, 245, (1981)
13. Clavijo, R. E.; Battisti, D.; Aroca, R.; Kovacs, G. J.; Jennings, C. A. *Langmuir* **8**, 113, (1992)

14. Aroca, R.; Clavijo, R. E.; Jennings, C. A.; Kovacs, G. J.; Duff, J. M.; Loutfy, R. O. *Spectrochim. Acta* **9**, 957, 1989.

15. Kovacs, G. J.; Loutfy, R. O.; Vincett, P. S.; Jennings, C.; Aroca, R. *Langmuir* **2**, 689, (1986)

16. Cotton, T. M.; Uphaus, R. A.; Möbius, D. *J. Phys. Chem.* **90**, 6071, (1986)

REFERENCES-Chapter 6

1. Kasuga, K.; Tsutsui, M.; Petterson, R. C.; Tatsumi, K.; Van Opdenbosch, N.; Pepe, G.; Meyer, E. F. *J. Am. Chem. Soc.* **102**, 4836, (1980)
2. Kirin, I. S.; Moskalev, P. N.; Makashev, Yu, A. *Russ. J. Inorg. Chem.* **10**, 1065, (1965)
3. Kirin, I. S.; Moskalev, P. N.; Makashev, Yu A. *Russ. J. Inorg. Chem.* **12**, 369, (1967)
4. MacKay, A. G.; Boas, J. F.; Troup, G. J. *Aust. J. Chem.* **27**, 955, (1974)
5. Kasuga, K.; Ando, M.; Morimoto, H. *Inorg. Chim. Acta* **112**, 99, (1986)
6. Sugimoto, H.; Hiagahi, T.; Mori, M. *Chem. Lett.* 1167, (1983)
7. Sugimoto, H.; Hiagahi, T.; Mori, M. *J. Chem. Soc. Chem. Commun.* 662, (1983)
8. Corker, G. A.; Grant, B.; Clecak, N. J. *J. Electrochem. Soc.* **126**, 1339, (1979)
9. Andre, J. J.; Holczer, K.; Petit, P.; Riou, M. T.; Clarisse, C.; Even, R.; Fourmigue, M.; Simon, J. *Chem. Phys. Letters* **115**, 463, (1985)
10. Chang, A. T., Marchon, J. C., *Inorg. Chim. Acta* **53**, L241, (1981)
11. Markovitsi, D.; Tran-Thi, T. H.; Even, R.; Simon, J. *Chem. Phys. Lett.* **137**, 107, (1987)

12. Moussavi, M.; DeCian, A.; Fisher, J.; Weiss, R. *Inorg. Chem.* **27**, 1287, (1988)

13. Collins, G. C. S.; Schiffrin, D. J. *J. Electrochem. Soc.* **139**, 334, (1982)

14. M'Sadak, M.; Rooncali, J.; Garnier, F. *J. Electroanal. Chem.* **189**, 99, (1985)

15. Casataneda, F.; Plichon, V. *J. Electroanal. Chem.* **236**, 163, (1987)

16. Besbes, S.; Plichon, V.; Simon, J.; Vaxiviere *J. Electroanal. Chem.* **237**, 61, (1987)

17. Petty, M.; Lovett, D. R.; O'Connor, J. M.; Silver, J. *Thin Solid Films* **179**, 387, (1989)

18. Liu, Y.; Shigehara, K.; Hara, M.; Yamada, A. *J. Am. Chem. Soc.* **113**, 440, (1991)

19. Liu, Y.; Shigehara, K.; Yamada, A. *Thin Solid Films* **179**, 303, (1989)

20. Tomilova, L. G.; Chernykh, E. V.; Ioffe, N. T.; Luk'yanets E. A. *Zh. Obshch. Khim.* **53**, 2339, (1984)

21. Tomilova, L. G.; Chernykh, E. V.; Luk'yanets E. A. *Zh. Obshch. Khim.* **57**, 2119, (1988)

22. Konami, H.; Hatano, M.; Tajiri, A. *Chem. Phys. Lett.* **160**, 163, (1989)

23. Tomilova, L. G.; Ovchinnikova, N. A.; Luk'yanets, E. A. *Zh. Obshch. Khim.* **57**, 1880, (1988)

24. Sidorov, A. N.; Kotlyar, I. P. *Opt. Spectrosc.* **11**, 92, (1961)

25. Sharp, H. J.; Lardon, M. *J. Phys. Chem.* **72**, 3230, (1968)

26. Clarisse, C.; Riou, M. T. *Inorg. Chim. Acta* **130**, 139, (1987)

27. M'Sadak, M.; Roncali, R.; Garnier, F. *J. Chim. Phys.* **83**, 211, (1986)

28. Aroca, R.; Zeng, Z. Q.; Mink, J. *J. Phys. Chem. Solids* **51**, 135, (1990)

29. Jennings, C.; Aroca, R.; Hor, A. H.; Loutfy, R. *Spectrochim. Acta* **41**, 1095, (1985)

30. Aroca, R.; Clavijo, R. E.; Jennings, C. A.; Kovacs, G. J.; Duff, J. M.; Loutfy, R. O. *Spectrochim. Acta* **45A**, 957, (1989)

31. Walton, D.; Ely, B.; Elliot, G. *J. Electrochem. Soc.* **128**, 2479, (1981)

REFERENCES-Chapter 7

1. Wright, J. D. *Progress in Surface Science* **31**, 1, (1989)
2. Snow, A. W.; Barger, W. R. in *Phthalocyanines Properties and Applications* (Leznoff, C. C.; Lever, A. B. P., eds.) VCH Publishers, New York, 1989
3. Honeybourne, C. L.; Ewen, R. J. *J. Phs. Chem. Solids* **44**, 215, (1983)
4. Honeybourne, C. L.; Ewen, R. J. *J. Phs. Chem. Solids* **44**, 833, (1983)
5. van Ewyk, R. L.; Chadwick, A. W.; Wright, J. D. *J. Chem. Soc. Faraday Trans.I* **82**, 1117, (1986)
6. Temofonte, T. A.; Schoch, K. F. *J. Appl. Phys.* **65**, 1350, (1989)
7. Bott, B.; Jones, T. A. *Sensors and Actuators* **5**, 43, (1984)
8. Sadaoka, Y.; Jones, T. A.; Revell, G. S. *J. Mater. Sci.* **25**, 5257, (1990)
9. Sadaoka, Y.; Jones, T. A.; Gopel, W. *Sensors and Actuators* **B1**, 148 (1990)
10. Jones, T. A.; Bott, B. *Sensors and Actuators* **9**, 27, (1986)
11. Sadaoka, Y.; Jones, T. A.; Gopel, W. *J. Mater. Sci.* **8**, 1288, (1989)
12. Szczurek, A.; Lorenz, K., Int. *J. Environ. Anal. Chem.* **41**, 57, (1990)
13. Moriizumi, T. *Thin Solid Films* **160**, 413, (1988)
14. Li. J. P.; Tredgold R. H.; Jones, R. *Thin Solid Films* **186**, 167, (1990)

15. Baker, S.; Roberts, G. G.; Petty, M. C. *Proc. IEEE Part 1*, **130**, 260 (1983)

16. LLoyd, J. P.; Pearson, C.; Petty, M. C. *Thin Solid Films* **160**, 431, (1988)

17. Zhu, D. G.; Petty, M. C. *Sensors and Actuators B* **2**, 265, (1990)

18. Schoch, K. F.; Temofonte, T. A. *Thin Solid Films* **165**, 83, (1988)

19. Harikumar, P. S.; Sivasankara, V. N. *J. Mat. Sci. Lett.* **8**, 969, (1989)

20. Steinbach, F.; Joswig, H. J. *J. of Catalysis* **55**, 272, (1978)

21. Aroca, R.; Clavijo, R. E.; Jennings, C. A.; Kovacs, G. J.; Duff, J. M.; Loutfy, R. O. *Spectrochim. Acta* **45A**, 9, (1989)

22. Petty, M.; Lovett, D. R.; O'Connor, J. M.; Silver, J. *Thin Solid Films* **179**, 387, (1989)

23. Kovacs, G. J.; Vincett, P. S.; Sharp, J. H. *Can. J. Phys.* **63**, 346, (1985)

24. Von Raben, K. U.; Dorain, P. B.; Chen, T. T.; Chang, R. K. *Chem. Phys. Lett.* **96**, 269, (1983)

25. Matsuta, H.; Hirokawa, K. *Appl. Surface Sci.* **35**, 10,(1988)

26. Baker, S.; Petty, M. C.; Roberts, G. G.; Twigg, M. V. *Thin Solid Films* **99**, 53, (1983)

27. Roberts, G. G.; Petty, M. C.; Baker, S.; Fowler, M. T.; Tomas, N. J. *Thin Solid Films* **132**, 113, (1985)

28. Brynda, E.; Koropecky, I.; Kalnoda, L.; Nespurek, S. *Thin Solid Films* **199**, 375, (1991)

29. Stillman, M. J.; Nyokong, T. in *Phthalocyanines Properties and Applications*(Leznoff, C. C.; Lever, A. B. P. eds.) VCH Publishers, New York, 1989

30. Lyons, L. E.; Walsh, J. R.; White, J. W. *J. Chem. Soc.* 167, (1960)

31. Moskalev, P. N.; Kirin, I. S. *J. Phys. Chem.* **46**, 1019, (1972)

32. Liu, Y.; Shigehara K.; Yamada, A. *Thin Solid Films* **179**, 303, (1989)

Vita Auctoris

Name: Doriano Battisti

Birthdate: December 11, 1962 Italy(Caprineto, Rome)

Married: August 24, 1991 to Carmela Sullo

In 1967 Doriano and his family immigrated to Sault Ste. Marie Ontario where he was raised and attended St. Mary's College before coming to the University of Windsor. He recieved his Bachelor of Science with a major in chemistry in 1987. His graduate[Sept.(1987)-June(1992)] studies were also undertaken at the University of Windsor in the Department of Chemistry and Biochemistry.

Publications

9. Battisti, D.; Aroca, R.; Tomilova, L., *Spectroscopic Characterization of Rare Earth Octa-tert-Butyl Bisphthalocyanine Complexes*, Chem. Mater.(publication submitted)

8. Battisti, D.; Aroca, R., *Reversible Adsorption on a Single Langmuir-Blodgett Monolayer*, J. Am. Chem. Soc. **114**, 1201, (1992)

7. Aroca, R.; Clavijo, R. E.; Battisti, D.; Kovacs, G. J.; Jennings, C. A., *Surface Enhanced Raman Spectra and Gas Chemisorption of Langmuir-Blodgett Layers of Lu and Yb Bis-Phthalocyanines*, Langmuir **8**, 113, (1992)

6. Battisti, D.; Aroca, R.; Tomilova, L.; Luk'yanets E., *Surface Enhanced Raman Scattering of Green and Blue Forms of Lutetium Diphthalocyanine*, J. Mol. Liquids, (in press)

5. Battisti, D.; Aroca, R., *Selective Spectroscopic Characterization of Langmuir-Blodgett Monolayers Using SERRS*, J. Mol. Stuct. **218**, 351, (1990)

4. Aroca, R.; Battisti, D., *SERS of Langmuir-Blodgett Monolayers: Coverage Dependence*, Langmuir **6** 250, (1990)

3. Aroca, R.; Battisti, D., *SERS of Langmuir-Blodgett Monolayers*, in Recent Developments in Molecular Spectroscopy, (Jordanov, B.; Kirov, N.; Simova, P. eds.), World Scientific, Singapore, p.213 (1989)

2. Battisti, D.; Aroca, R.; Loutfy R. O., *From Molecules to Thin Solid Films: Vibrational Characterization of Evaporated Organic Films*, Chem. Mater. **1**, 124, (1989)

1. Aroca,R.; Battisti, D.; Loutfy, R. O.; Kovacs G. J., *Surface Enhanced Raman Scattering of Molecular Dyes Adsorbed on Metal Surfaces*, J. Electrochem. Soc. **136**, 2902, (1989)